CALCULATIONS OF QUASIELASTIC ELECTRON SCATTERING
FROM NUCLEI
AT HIGH MOMENTUM TRANSFERS

Thesis by

Anne Allder

In Partial Fulfillment of the Requirements

for the Degree of

Doctor of Philosophy

California Institute of Technology

Pasadena, California

1992

(Submitted 7 August 1991)

Abstract

I perform calculations of high momentum-transfer, quasielastic electron scattering from nuclei using a relativistic, microscopic model of the reaction that includes the effects of final-state interactions via an eikonal approximation and the effects of color transparency via a cross-section that varies along the exit path of the proton. The results of this microscopic calculation agree to 5% with a semiclassical estimate based on the mean free path of the proton in the nuclear medium. The overall uncertainty in the calculation is on the order of 10%; this figure is dominated by uncertainties in the potential that describes the final state interaction. Color transparency effects an enhancement on the order of a few percent (in total cross-section) for $Q^2 = 1$ GeV^2, and ten percent for $Q^2 = 10$ GeV^2. The predictions of various specific transparency models differ by approximately 20%, and thus are probably not experimentally distinguishable for $Q^2 < 10$ GeV^2.

Acknowledgments

I would like to thank my advisor, Professor Steven Koonin, for giving me this project and resources to pursue it. I also acknowledge contributions from Dr. Ryoichi Seki. D.A. Wasson and R.G. Furnstahl provided me with computer codes that generated the relativistic nuclear wavefunctions I used in my calculations.

My deepest gratitude is to David, whose love and support support wrote this thesis as much as I did. I also want to thank my whole wonderful family and many good friends, especially at Jacob Maarse, who made the time I spent working on this thesis enjoyable. My last acknowledgment is in the form of an inscription, borrowed from J.S. Bach. *SDG*

Table of Contents

List of Figures

Dedicated To
Evelyn Gall Allder

Chapter 1
Introduction

This thesis describes calculations of quasielastic electron scattering from nuclei at high momentum transfers. In this introduction, I discuss two ways of modeling the interaction between the outgoing proton and the residual nucleus: first, using the conventional nucleon-nucleus interaction; and second, using a model that includes "color transparency" effects, which modify the usual final state interaction. I then briefly discuss some important aspects of perturbative quantum chromodynamics, present a physical motivation for color transparency, and discuss the relationship between the two. Finally, I give an outline of the rest of this thesis.

1.1 Final State Interactions in Quasielastic Electron Scattering

The subject of this thesis is the quasielastic (QE) nuclear reaction, which is depicted schematically in Figure 1.1. An incident electron emits a virtual photon in the electromagnetic field of a target nucleus. The photon is absorbed by a proton which subsequently exits the nucleus into a detector. No other particles are measured in the final state, neither is there enough missing energy that one may have been produced. This investigation concerns processes in which the momentum transferred to the nucleus by the electron is large—on the order of several GeV.

In my calculations, I consider only single-photon exchange between the electron and the nucleus, because higher-order corrections due to quantum electrodynamics (on the order of $\alpha^2 \approx 1/137^2$) are negligible compared to the uncertainty in the
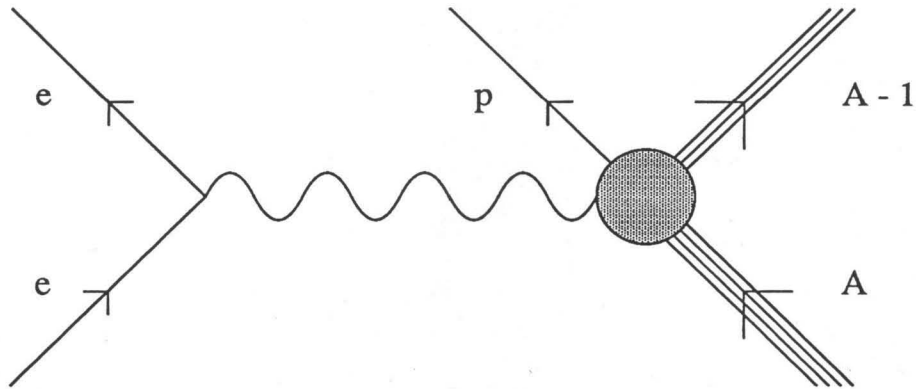
Figure 1.1 − Schematic diagram for the (e, e′p) reaction. An incident electron scatters from a target composed of A nucleons, knocking out a proton and leaving A − 1 nucleons in a (possibly excited) residual nucleus. The momentum transfers relevant to this thesis are on the order of a few GeV.

description of the hadronic interactions (on the order of 5 to 10%) [1]. Furthermore, at the electron energies I study, electromagnetic distortions of the outgoing electron due to either the residual nucleus or the the ejected proton are unimportant [2]. However, I do wish to treat the interaction between the outgoing proton and the rest of the nucleus: these interactions are the focus of this thesis.

In the semiclassical calculation presented in Chapter 2, the final state interaction (FSI) is modeled semiclassically as absorption governed by the mean free path of the proton as it travels through the nuclear medium. In the microscopic calculation described in Chapters 3 and 4, the FSI is described by an optical potential. This

potential is determined by fitting a parameterized potential form to proton-nucleus scattering data or by using free nucleon-nucleon amplitudes together with a nuclear density distribution to construct a phenomenological nucleon-nucleus interaction. An eikonal approximation (rather than a partial wave analysis, which is tractable only at lower energies), is used to calculate the distortions of the final state wavefunction. In both these calculations, the physical mechanism responsible for the FSI is the ordinary interaction between the struck proton and the rest of the nucleus.

In Chapter 5, I consider an extension of the microscopic model that includes the effects of color transparency (CT); these investigations of the color transparency phenomenon are the primary new results in this thesis. Color transparency causes protons that have been scattered with high momentum transfer to be less strongly absorbed by the nuclear medium than would otherwise be expected [3,4]. Therefore, an understanding of nuclear color transparency requires an accurate model of the conventional final state interaction, because the signature of CT is an enhancement in the observed flux of QE protons relative to the expected flux, and the expected flux clearly depends upon the details of the final state interaction.

1.2 Perturbative Quantum Chromodynamics and Color Transparency

Because the color transparency hypothesis is a prediction of perturbative quantum chromodynamics (PQCD), I briefly sketch some of the important ideas of PQCD.

Consider elastic electron-proton scattering. At low energies, the virtual photon scatters from the proton coherently and its quark substructure is not apparent; at higher energies, the photon may resolve the quark constituents and most likely will cause a change in the internal degrees of freedom of the proton. In a high-energy elastic scattering process, however, the internal degrees of freedom of the final state must be identical to those of the initial state; hence, the struck quark must *distribute*

its momentum by (hard) rescattering with the other quarks. Since, to leading order, the coupling constant of QCD varies with the momentum transfer Q^2 according to

$$\alpha_s(Q^2) = \frac{\alpha_s(\Lambda^2)}{1 + \frac{\alpha_s(\Lambda^2)}{12\pi}\left(33 - 2N_f\right)\log\frac{Q^2}{\Lambda^2}} \tag{1.1}$$

(where N_f is the number of quark flavors and Λ is the QCD scale parameter [5]), these hard rescatterings among quarks can be treated perturbatively when $\left(Q^2/\Lambda^2\right)$ is large enough to make $\alpha_s(Q^2)$ small compared to one. Using the factorization hypothesis, the matrix element for the process is written as a product of three pieces: a form factor (or wavefunction) describing the nonperturbative initial state of the proton, a hard scattering amplitude which is calculated perturbatively, and another form factor describing the final state [6].

1.2.1 Scaling Law for High-Energy Exclusive Hadronic Processes

A major prediction of PQCD is the high energy, fixed center-of-mass angle scaling law for high-energy exclusive hadronic or semi-hadronic processes [7]. The scaling law can be written

$$\frac{d\sigma}{dt} \to \frac{1}{s^{n-2}} f\left(\frac{t}{s}\right) \qquad \text{high } s, t; \quad \frac{t}{s} \text{ fixed}, \tag{1.2}$$

where s and t are Mandelstam variables and n is the total number of pointlike constituents (valence quarks, leptons, or photons) in the initial and final states. A heuristic derivation of the scaling law for exclusive (semi–) hadronic processes follows.

Consider a generic quark level diagram for such a process, depicted in Figure 1.2, and perform dimensional analysis on the matrix element for this diagram. External fermion lines contribute a dimension $E^{\frac{1}{2}}$, gluon and photon propagators contribute $1/E^2$, and quark propagators contribute $1/E$. Only those diagrams that have the
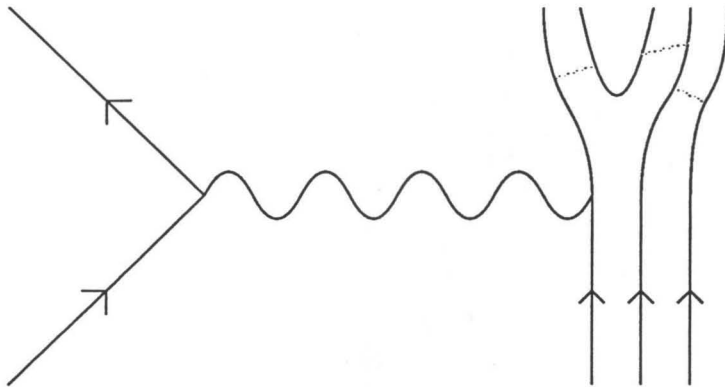
Figure 1.2 – Schematic diagram of an exclusive semi-hadronic scattering process, for example, ep → epπ. The virtual photon strikes the leftmost quark, which then shares its momentum with the other parton that composes the final pion.

fewest number of intermediate gluon and photon lines contribute at high energy because of the extra factor of E^2 in the denominator for each additional propagator. However, since the reaction is exclusive, only diagrams in which all the quarks that belong to a given particle in the final state are connected are physical. These constraints require that the lowest order matrix element for the process have dimension

$$[\mathcal{M}] = \frac{1}{E^{n-4}}, \tag{1.3}$$

where n is the total number of external lines. The differential cross-section then has dimension

$$\left[\frac{d\sigma}{dt}\right] = \left(\frac{1}{E^{n-4}}\right)^2 \frac{1}{E^4} = \left(\frac{1}{E^2}\right)^{n-2}. \tag{1.4}$$

At high energies (those large relative to all of the masses of the particles involved), the only scale for the process is the center-of-mass energy, $\sqrt{s}$. Replacing E^2 with s gives the scaling result

$$\frac{d\sigma}{dt} \propto \frac{1}{s^{n-2}}. \tag{1.5}$$

This scaling prediction has been tested experimentally by by measuring the electromagnetic form factors of various hadrons and found to be reasonably accurate for Q^2 on the order of 5 GeV^2 [8]; however, the agreement is not exact and further experimental investigation of PQCD is desirable.

1.2.2 Color Transparency

Like the scaling law, color transparency is a prediction of PQCD that applies to exclusive hadronic processes. Consider elastic electron-proton scattering again. At momentum transfers on the order of several GeV, the wavelength of the virtual photon is short compared to the characteristic radius of the proton

$$\lambda = \frac{h}{|\mathbf{q}|} \approx \frac{1}{2 \text{ GeV}} = 0.1 \text{ fm} \ll r_{\text{proton}} = 0.81 \text{ fm}. \tag{1.6}$$

Of course, the proton "radius" is only an average quantity: while the QCD proton is most likely to be observed in a configuration of radius approximately 1 fm, there exist configurations (Fock space components) in which the separation distance between quarks is significantly smaller. When a proton is struck by a short-wavelength photon, it is most likely that the photon will interact with a single quark incoherently (since the other quarks are probably at least several wavelengths distant); thus, at high energies, inelastic processes like fragmentation dominate.

In elastic processes, however, the final state must remain bound as a proton; hence, if a short-wavelength photon strikes a quark, the other quarks must be sufficiently "close" to the struck quark that a coherent response is possible. Heuristically, elastic processes can be regarded as sampling only those Fock space components with a size on the order of the wavelength of the virtual photon. Because the amplitude for observing these small components is small, elastic reactions are unlikely at high energies; however, in the rare cases in which high momentum-transfer elastic reactions do take place, it can be inferred that the initial proton occupied a space with a dimension on the order of the wavelength of the virtual photon. Since that wavelength is inversely proportional to $|\mathbf{q}|$, the initial size of the struck proton vanishes with increasing momentum transfer.

After undergoing a high-energy exclusive scattering, the proton relaxes by expanding back to its equilibrium size. Several models exist for how this "hadronization" occurs [9], but for now it is sufficient to say that the quarks expand at approximately the speed of light until they reach their normal separation distance and then remain in that state; and that the "hadronization length", or the distance the proton travels while this process occurs, is on the order of $\gamma = E/M$, where E is the energy of the proton and M is its mass.

Now consider elastic electron-proton scattering carried out in a nuclear environment. The above argument about the size of a proton following a high momentum-transfer exclusive reaction still applies; however, in this case the small configuration interacts with the residual nucleus as it is returning to its equilibrium size. In the normal proton-nucleus interaction, the proton scatters from the other nucleons with a cross-section that is determined primarily by its size [10]; therefore, it is plausible that the cross-section for the interaction of the "small" proton with the other nucleons will

be small. For instance, at $|\mathbf{q}| = 2$ GeV, the "geometrical" cross-section (obtained by evaluating $\pi r_\perp^2$ where $r_\perp = 1/|\mathbf{q}|$) is 0.3 mb, much less than the free value of 40 mb. Furthermore, the hadronization length for such a proton is of the same order as a typical nuclear radius; again using $|\mathbf{q}| = 2$ GeV, $l_h \approx \gamma = 2.4$ fm. Hence the recoiling proton interacts only weakly with the medium along its much of its exit path, and the residual nucleus can be regarded as becoming "transparent" to it. By varying the ratio of the hadronization length to the nuclear radius (i.e. by varying A at fixed Q^2 or *vice versa*), the CT mechanism can be investigated [3,4].

That a proton of reduced size has a correspondingly reduced nuclear absorption cross-section is actually a necessary consequence of QCD. Since the proton, like all QCD-allowed states, is a color singlet, a multipole expansion of its color field has only terms which are dipole or higher in order. Moreover, since dipole (and higher order) fields are proportional to the separation distance between the (color) charges, the color field of the struck proton tends toward zero as its size becomes small. Because the FSI between the proton and the rest of the nucleus is due to the strong force acting between their respective color fields, the strength of the final state interactions must be diminished for protons of reduced size.

Bearing in mind the above argument, I now clarify the semiclassical color transparency picture of a small proton, modeled as a black disk, interacting with the nucleons in the residual nucleus. The interaction between two normal nucleons is almost perfectly absorptive: their cross-section is nearly equal to the sum of their projected areas. When a small proton interacts with a normal nucleon, however, the relevant area is that of the small particle; this is because the large nucleon, rather than itself being absorbing, is transparent to a color singlet of a much smaller size. Physically, the small configuration "passes through" the larger one without interaction.

Neither the fixed-angle scaling prediction nor the color transparency hypothesis relies on any specific property of QCD beyond the fact that in QCD, hadrons are composed of pointlike fermions that are asymptotically free [7]. Indeed, both are necessary consequences of QCD but are not sufficient to rule out other nonabeliean gauge theories, which share these essential properties; hence, observation of either one of these phenomena can provide only indirect support for the correctness of QCD. However, because no exact calculation of electron-proton or electron-nucleus scattering exists, even indirect evidence is worth considering.

1.3 Organization of this Thesis

In Chapter 2, I give a description of a semiclassical calculation of proton absorption in QE scattering. In Chapter 3, I present a relativistic, microscopic formalism for the QE reaction. Detailed algebra is deferred to Appendix A, and Appendices B and C contain derivations of a density-dependent optical model and a general optical potential satisfying incoming-wave boundary conditions, respectively. In Chapter 4, I present results of numerical calculations based on the formalism of Chapter 3, both for plane-wave final states and distorted-wave final states without color transparency. The effects of color transparency are included in the calculations presented in Chapter 5. For completeness, Appendix D contains a listing of the code used in these calculations. Chapter 6 contains a summary and conclusions.

Chapter 2
Semiclassical Calculations

I describe a semiclassical model of the interaction between a high-energy proton and a target nucleus, and use this model to calculate the probability that a quasielastically scattered proton will be absorbed on its way out of the residual nucleus. Results of this calculation indicate that nearly all of the escaping particles originate in the nuclear surface; moreover, the escape probability displays a keen sensitivity to the surface thickness of the nuclear density distribution. I discuss a similar calculation by Farrar *et al* that includes color transparency effects.

2.1 Formalism

I seek to derive a formula for the probability of absorption of an incident particle by a target medium. My approach is purely semiclassical: I neglect any wave properties of the projectile (or the target), since they should not be important for describing the behavior of a few-GeV proton in a nucleus. Quantitatively, the proton's deBroglie wavelength

$$\lambda = \frac{hc}{2 \text{ GeV}} \approx 0.1 \text{ fm} \tag{2.1}$$

is much smaller than both the characteristic internucleon distance

$$D_{NN} \approx \left(3\pi^2\right)^{\frac{1}{6}} r_0 = 2.1 \text{ fm} \tag{2.2}$$
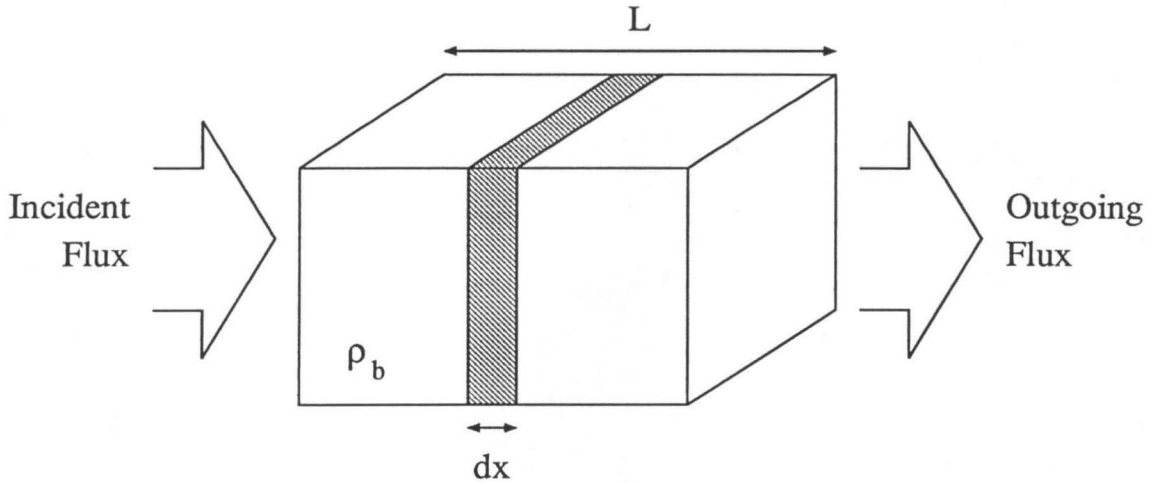
Figure 2.1 – Schematic diagram for deriving the change in flux of a particle as it traverses an absorptive medium. The incident particle is denoted a, the target particles are denoted b, and the flux of a past the point x is denoted $\mathcal{F}(x)$.

(obtained by assuming a density of $\rho = \left(\frac{4}{3}\pi r_0^3\right)^{-1}$ on a regular body-centered cubic lattice of nucleons) and the characteristic intranucleon distance

$$r_{\mathrm{rms}} = 0.81 \text{ fm.} \qquad (2.3)$$

Thus, a semiclassical approximation (equivalent to averaging over many proton wavelengths) is justified.

Consider a particle a incident upon a medium composed of particles b with density ρ_b, and let σ_{ab} be the total cross-section for interaction between the incident and target particles. Define x to be a coordinate in the direction of a's motion, and let $\mathcal{F}(x)$ be the flux of a past x, schematically shown in Figure 2.1.

Upon traversing a small distance, Δx, the change in the flux of a is

$$\mathcal{F}(x) - \mathcal{F}(x + \Delta x) = \mathcal{F}(x)\,\sigma_{ab}\,\rho_b\,\Delta x, \qquad (2.4)$$

since by definition the cross-section is

$$\sigma_{ab} \equiv \frac{\text{Scattered Flux of } a \text{ Particles}}{(\text{Incident Flux of } a \text{ Particles})\,(\text{Incident Flux of } b \text{ Particles})}. \qquad (2.5)$$

Rewriting the finite difference as a differential, and integrating from $x = 0$ to $x = L$ gives

$$\frac{\mathcal{F}(L)}{\mathcal{F}(0)} = e^{-\sigma_{ab}\,\rho_b\,L}, \qquad (2.6)$$

where the left side of the equation can be interpreted as the probability that a will exit the material unscattered.

Equation 2.6 can be used to calculate the probability that a quasielastically scattered proton will be absorbed on its way out of the residual nucleus. Let $\mathbf{r_0} \equiv (z_0, \mathbf{b_0})$ denote the intial position of the proton in the nucleus, and let $\hat{\mathbf{z}}$ be the direction of its final momentum. The exit trajectory is taken to be a straight line because only those protons which follow such a trajectory will exit the nucleus with the desired quasielastic kinematics. The probability that the proton will travel through a small element dz of its path without being scattered is

$$P(dz) = \exp\left[-\sigma_{pN}\,\rho_N(z)\,dz\right], \qquad (2.7)$$

where $\rho_N(z)$ is the total nucleon density at $(z, \mathbf{b})$ and σ_{pN} is the proton-nucleon cross-section. Multiplying together the escape probabilities associated with each element of the exit path then gives the probability that a proton originating at $\mathbf{r_0}$ will escape the

nucleus unscattered. This product of exponentials can be rewritten as the exponential of a sum, and the sum over infinitesimal path elements can in turn be written as an integral

$$P(\mathbf{r_0}) = \exp\left[-\int_{z_0}^{\infty} dz'\, \sigma_{pN}\, \rho_N(z')\right], \tag{2.8}$$

where the direction of the (straight-line) exit path might still depend upon the initial position of the proton.

Assuming that all of the momentum of the virtual photon is transferred to the struck proton, the final momentum is $(\mathbf{k_b} + \mathbf{q})$, where $\mathbf{k_b}$ is the momentum of the initial bound proton and $\mathbf{q}$ is the three-momentum transfer of the reaction. Since the values of $|\mathbf{q}|$ relevant to this calculation are on the order of a few GeV, and $|\mathbf{k_b}|$ is at most a few hundred MeV [11], neglecting $\mathbf{k_b}$ in their sum is not unreasonable. With this approximation, the exit path is in the direction of $\hat{\mathbf{q}}$, independent of the particular bound state (hence also the position) from which the proton was emitted.

The total escape probability is the density-weighted average of the expression in Equation 2.8; explicitly,

$$P_{\text{esc}} = \int_V d^3\mathbf{r}\, \rho_p(\mathbf{r}) \exp\left[-\int_z^{\infty} dz'\, \sigma_{pN}\, \rho_N(z')\right], \tag{2.9}$$

where the densities ρ_p and ρ_N are normalized to 1 and A, respectively. The cross-section does not depend strongly on either the energy of the proton or the isospin of the target nucleon; approximating σ_{pN} as a constant 40 mb is reasonably accurate for energies above 1 GeV [10]. The escape probability can then be evaluated analytically for a uniform nuclear density or computed numerically for a more realistic distribution

like the Fermi distribution. A rough estimate of the A dependence of P_{esc} can be made as follows: the average mean free path of a proton through nuclear matter is

$$\lambda_{\text{mfp}} = \frac{1}{\overline{\rho}\,\sigma_{pN}} = 1.5 \text{ fm}; \tag{2.10}$$

therefore, for a nucleus with a radius larger than a few fermis (i.e. for $A > 20$), only particles on the surface have a significant probability for escape. Thus, P_{esc} should scale as the ratio of the surface area of a nucleus to its volume, or as $A^{-\frac{1}{3}}$.

2.2 Results of Semiclassical Calculations

Equation 2.9 requires two pieces of input; as usual, these contain the important physics. The first is the cross-section, which I take to be 40 mb; the second is the nuclear density, which I investigate below.

The nuclear density distributions of Barrett and Jackson [12] are determined by fitting parameterized distributions to low-energy elastic electron-nucleus scattering data. They assume that the neutron distribution (and hence also the total nucleon distribution) is proportional to the proton (charge) distribution: $\rho_N \propto \rho_n \propto \rho_p$, where $\rho_N = Z\rho_p + N\rho_n$. For most larger nuclei, they use the two-parameter Fermi distribution

$$\rho_p(r) = \frac{C_p}{1 + \exp\left(\frac{r-R}{a}\right)} \tag{2.11}$$

to parameterize the density, where C_p is chosen so that ρ_p is normalized to 1. In lighter nuclei, surface effects are more significant. Some require three parameters for an accurate description of their surfaces:

$$\rho_p(r) = \frac{C_p}{1 + \exp\left(\frac{r-R}{a}\right)}\left(1 + \omega\frac{r^2}{R^2}\right). \tag{2.12}$$
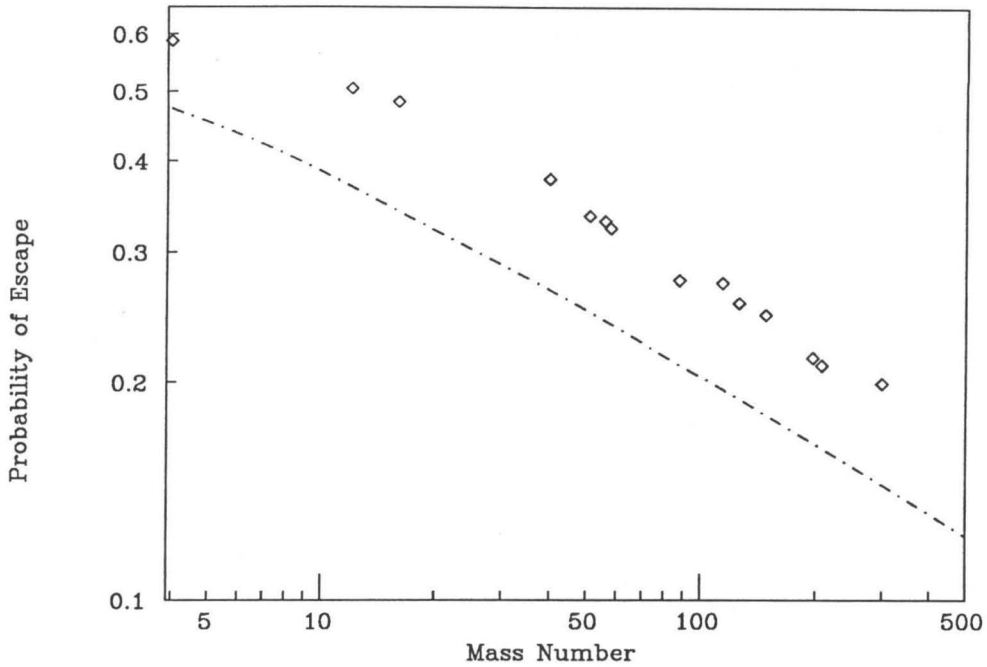
Figure 2.2 − Probability that the ejected proton of an (e, e′p) reaction will escape the nucleus unscattered. The dotdashed line was calculated analytically for a uniform nuclear distribution of radius $1.2A^{\frac{1}{3}}$ fm and the diamonds were evaluated numerically with the experimental distributions of Reference [12].

The modified Gaussian distribution

$$\rho_p(r) = C_p \left(1 + \alpha k^2 \frac{r^2}{R^2}\right) \exp\left(-\frac{k^2 r^2}{R^2}\right) \qquad (2.13)$$

is best-suited to describing the exceptional ^{12}C nucleus. Reference [12] contains a compilation of data and parameter values for a large range of nuclei.

Figure 2.2 shows the escape probability plotted as a function of the nuclear mass number. The dotdashed line represents the escape probability calculated with a uniform density distribution of $\bar{\rho} = 0.17$ nucleons/fm^3 [11], and the diamonds are the results obtained with the experimentally-determined distributions.

The values of the escape probability obtained using realistic density distributions exceed those obtained with a uniform distribution by a constant factor of about 35%. The effects of finite surface thickness are so marked because most of the exiting protons originate in the surface and thus are particularly sensitive to its diffuseness. Mathematically, this sensitivity arises from the exponential density dependence in the expression for the escape probability: a small change in the line integral of the density results in a relatively large change in the escape probability. The slope of the dotdashed line on the log plot is -0.3 (for large A), in good agreement with the simple $A^{-\frac{1}{3}}$ mean-free-path prediction. I note that the results of this calculation agree with the predictions (also semiclassical) of Farrar *et al* [9].

2.3 Color Transparency Effects

The semiclassical formalism described above is easily extended to include the effects of color transparency [9]. The only necessary change is to replace the pN cross-section with an effective cross-section, $\sigma_{pN}^{\text{eff}}(z')$, that varies along the exit path of the proton. The modified escape probability is then

$$P_{\text{esc}}^{\text{TRANS}} = \int_V d^3\mathbf{r}\, \rho_p(\mathbf{r}) \exp\left[-\int_z^\infty dz'\, \sigma_{pN}^{\text{eff}}(z')\, \rho_N(z')\right]. \qquad (2.14)$$

The physics of transparency is embedded in the effective cross-section, more specifically, in the function of z that multiplies the free cross-section to simulate the expansion of the initially-small proton. As discussed earlier, the cross-section for a high-energy hadron in nuclear matter is primarily geometric:

$$\sigma_{hN} \approx \pi r_\perp^2, \qquad (2.15)$$

where $r_\perp$ is the characteristic transverse dimension of the hadron [13]. A hadron that has a small transverse size has a correspondingly small absorption cross-section

and conversely a large escape probability. To specify a color transparency model, it suffices to determine $r_\perp(z)$ for the expanding proton; the behavior of the cross-section is then determined via Equation 2.15.

Farrar *et al* consider two models for this expansion. In their "naive parton model", the quarks separate at the speed of light until the proton regains its normal size. Alternatively, they consider a case where the partons "diffuse" out until they reach their equilibrium separation distance. The naive model provides a simple estimate of the size of the transparency effect; the more sophisticated diffusion model is supposed to better reflect the underlying dynamics of perturbative QCD. I discuss both models below, as they will be used in the relativistic calculations of Chapter 5.

For convenience, denote the semiclassical model without transparency, the quantum diffusion model, and the naive parton model as $\tau = 0$, 1, and 2, respectively.

$\tau = 0$

The cross-section remains constant along the entire exit path; thus, the expansion function is

$$r_\perp(z) \equiv r_\perp^{\mathrm{f}}, \tag{2.16}$$

and the cross-section is

$$\sigma_{pN}^{\mathrm{eff}}(z) \equiv \sigma_{pN}, \tag{2.17}$$

where σ_{pN} is the total pN cross-section and $r_\perp^{\mathrm{f}} = \sqrt{\sigma_{pN}/\pi}$ is the free value of $r_\perp$.

$\tau = 1$

In a random-walk process, the quarks separate at a rate proportional to $\sqrt{z}$, thus the cross-section increases linearly along the exit path. The initial size of the proton

is $r_\perp^i \, (\text{fm}) \approx 1.2/\sqrt{t \; (\text{GeV})}$, where t is the usual Mandelstam variable (equal to the square of the four-momentum transfer). The hadronization length—the length over which the proton regains its normal size—is

$$l_h \; (\text{fm}) = 0.6 \, |\mathbf{k}| \; (\text{GeV}), \tag{2.18}$$

where $|\mathbf{k}|$ is the magnitude of the proton's momentum.

$\tau = 2$

In the naive parton model, the quarks are regarded as essentially free, and they separate at the speed of light. Thus $r_\perp(z)$ increases as z, and the cross-section grows quadratically along the exit path. In units where $c = 1$, the hadronization length is simply the time it takes the quarks to attain their equilibrium separation, properly boosted to the rest frame of the nucleus

$$l_h = \frac{|\mathbf{k}|}{M} \, r_\perp^{\text{f}} \, (1 - t_s), \tag{2.19}$$

where $t_s = 1 \text{ GeV}/q$ is the initial proton shrinkage, and $r_\perp^{\text{f}} = 0.81$ fm is the final size of the proton.

All three models can be succinctly combined into the single expression

$$\sigma_{pN}^{\text{eff}}(z) = \sigma_{pN} \max \left\{ \left(\frac{z - z_0}{l_h} \right)^\tau (1 - t_s) + t_s \, , \, 1 \right\}, \tag{2.20}$$

where both l_h and t_s depend on τ implicitly. These effective cross-sections are plotted together in Figure 2.3.

Of the two models, the naive parton model predicts the greater escape probability (hence the greater transparency), both because the cross-section grows more slowly and because the hadronization length is larger than in the diffusion model.
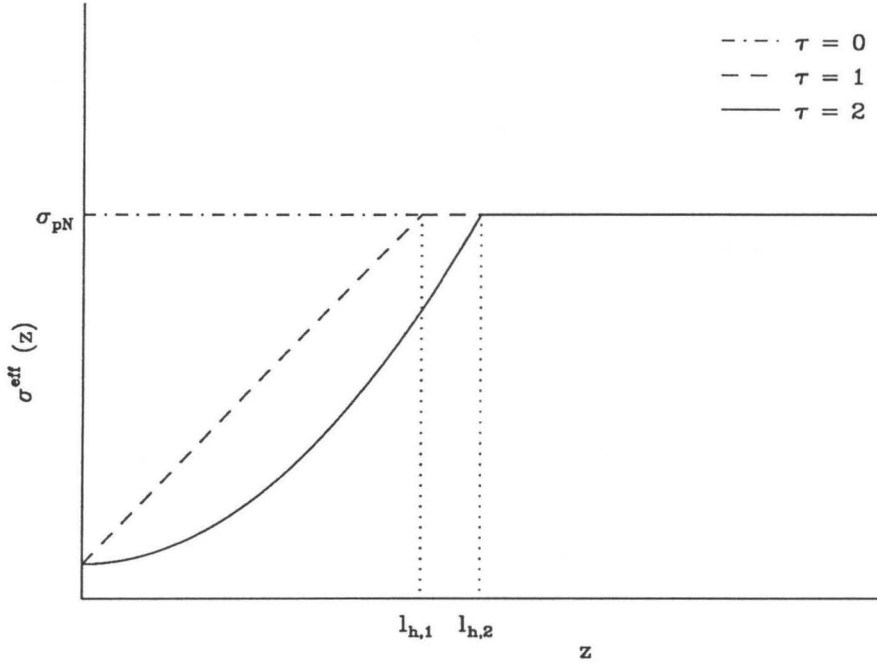
Figure 2.3 − Effective cross sections of each of the three transparency models. The effective cross-section is shown as a function of the distance from the point where the proton was struck. The dashed line corresponds to the diffusion model ($\tau = 1$), the solid line to the naive parton model ($\tau = 2$), and the dotdashed line to the model without any transparency effects ($\tau = 0$). The hadronization length depends on τ; subscripts are used to distinguish l_h for the two models.

Calculations performed using this semiclassical color transparency model are published in Reference [9]. The authors conclude that predictions of the three expansion models vary significantly, so an experimental determination of whether transparency exists, and if so, which model best describes it, appears possible. They also make a similar calculation for general exclusive hadron-nucleus scattering. The only modification to the previous discussion is that instead of one exponential attenuation factor in Equation 2.14, there are three: one each for the incident hadron to reach the interaction point and the scattered hadron to leave the nucleus unattenuated,

and the usual factor describing the attenuation of the knocked-out nucleon. In the case of quasielastic proton-nucleus (p,2p) scattering, experimental data is available. Carroll *et al* [14] measure the (p,2p) cross-section for lithium, carbon, aluminum, copper, and lead targets at incident proton momenta of 6, 10, and 12 GeV/c. To investigate transparency, they plot their measured cross-section, divided by the free proton-proton cross-section, as a function of the incident proton beam momentum. When compared to Farrar's semiclassical calculations, the measurements support the existence of some amount of transparency, however, the observed decrease in the transparency for $p_{\text{LAB}} > 10$ GeV is not predicted by any of the models. Theoretical attempts to understand this result have focussed on improved descriptions of the free proton-proton cross-section, including oscillations around the leading s^{-10} behavior of σ_{pN} [15] and postulated heavy quark resonance thresholds [16], but these are primarily speculative. Both a clearer experimental investigation of transparency (for example, using electrons as the projectile [17]) and a detailed theoretical understanding of the process (including a full relativistic and quantum mechanical description of the final state interaction) are desirable.

Chapter 3
Relativistic DWIA Calculation

In Section 1, I review the standard scattering formalism for the (e,e′p) reaction, giving the cross-section in terms of matrix elements of the nuclear electromagnetic current operator between the initial and final states of the proton. In Section 2, I derive an expression for the distorted-wave final state of the proton, using an eikonal approximation to include the effects of its interactions with the residual nucleus. Section 3 contains a brief description of the model used to generate relativistic wavefunctions for the initial bound state. Detailed formulae for the nuclear current matrix elements are given in Appendix A.

3.1 Quasielastic Electron Scattering Formalism

The quasielastic reaction under consideration is represented schematically in Figure 3.1. The incoming and outgoing electron (four-) momenta are denoted p and p'; q is the momentum of the virtual photon; and k is the momentum of the ejected proton.

I work in the distorted-wave impulse approximation (DWIA); I assume that the only physical mechanism for the scattering is one-photon exchange between the electron and a single nucleon, after which the ejectile may interact with (become distorted by) the rest of the nucleus. This approximation should become more accurate at higher energies since the probability for coherent excitation of several nucleons decreases as the wavelength of the virtual photon decreases; its use is well-justified for
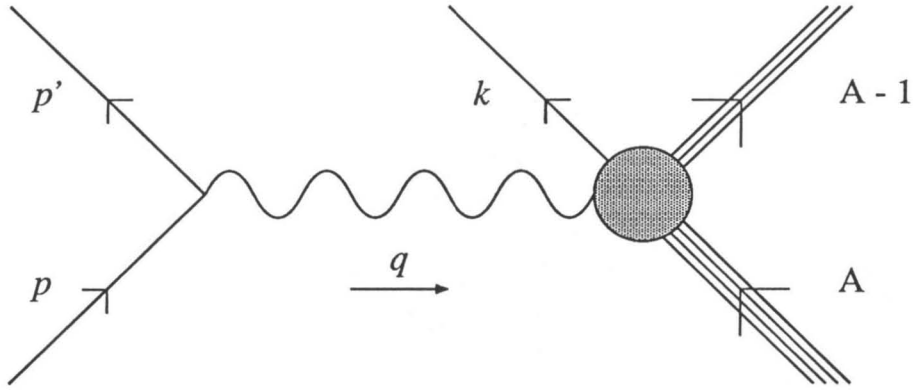
Figure 3.1 – Schematic representation of the (e, e′p) reaction. The incoming and outgoing electron (four-) momenta are denoted p and $p′$; q is the momentum of the virtual photon; and k is the momentum of the ejected proton. The recoil momentum of the nucleus is denoted P. Here and throughout this thesis, italic letters denote four-vectors and boldface letters denote three-vectors.

the energies of interest here. Throughout these calculations, the recoil momentum $P′$ of the residual nucleus, which is of order $1/A$ compared to p, $p′$, and k, is neglected.

The ejectile is knocked out of a nuclear shell state characterized by principal quantum number n, total angular momentum quantum numbers j and m, orbital angular momentum quantum number l, and isospin quantum number t. For the proton knockout reaction, t is $+\frac{1}{2}$. Since the final state proton is on mass-shell, its energy is $E_k = \sqrt{|\mathbf{k}|^2 + M^2}$.

I define coordinates such that **k** is parallel to **ẑ**, because the final-state distorted wave is most naturally expressed in the coordinate system where the ejectile exit path is along the positive z axis. This system differs from the one most often used; in "parallel kinematics" it is **q** rather than **k** that defines the positive z axis.
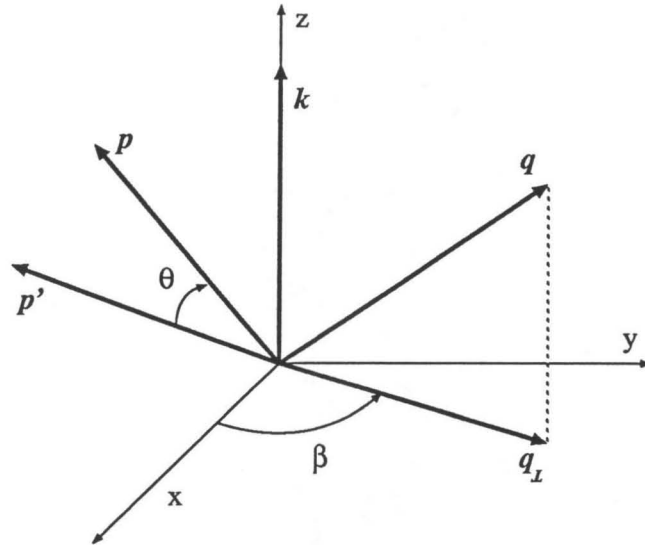
Figure 3.2 – Coordinate system used in (e, e′p) calculations. The positive z axis lies along the outgoing proton's momentum k. The angle that the perpendicular component of the momentum transfer, q⊥, makes with the positive x axis is β. The angle between the electron momenta is θ.

My coordinate system is shown in Figure 3.3. The azimuthal orientation of the coordinate system is arbitrary, subject to the constraint that the angle β is not a multiple of $\frac{\pi}{4}$, as this causes either the transverse-transverse or the longitudinal-transverse response function to become ill-defined. β is defined as the angle between **q** and the positive x axis, and θ is the angle between initial and final electron momenta.

Following a derivation in Reference [18], the cross-section for the $(e, e'p)$ reaction is

$$d\sigma = \frac{m}{|\mathbf{p}|} \frac{m \, d^3 p'}{(2\pi)^3 E_{p'}} \frac{M \, d^3 k}{(2\pi)^3 E_k} \sum_{P} \delta^4(p - p' + P - P' - k) \times$$

$$|\bar{u}_{p'}\gamma_\mu u_p \frac{e^2}{q^2} \langle \Psi_f(\mathbf{k}, P') | \hat{J}^\mu | \Psi_i(P) \rangle |^2, \tag{3.1}$$

where the P below the summation sign is an abbreviation for the usual sum over final and average over initial polarization states, and m and M are the electron and proton masses, respectively. The initial wavefunction of the target nucleus is $|\Psi_i(P)\rangle$ and the final wavefunction that describes both the ejected proton and the recoiling residual nucleus is denoted $|\Psi_f(\mathbf{k}, P')\rangle$. It is customary to separate the cross-section into an electron contribution and a nuclear contribution

$$d\sigma = \frac{m}{|\mathbf{p}|} \, d \, (\text{Phase Space}) \frac{e^4}{m^2 q^4} \eta^{\mu\nu} W_{\mu\nu}, \tag{3.2}$$

where the lepton tensor as

$$\eta_{\mu\nu} \equiv \sum_{P} m^2 \, \bar{u}_{p'}\gamma_\mu u_p u_{p'}\gamma_\nu \bar{u}_p. \tag{3.3}$$

With typical electron energies on the order of a few GeV, the electron's mass is negligible compared to its momentum. In this extreme relativistic limit, $\eta_{\mu\nu}$ is easily evaluated using trace algebra; the result is

$$\eta_{\mu\nu} = \frac{1}{2}(p'_\mu p_\nu + p'_\nu p_\mu - p' \cdot p \, g_{\mu\nu}). \tag{3.4}$$

In contrast, the nuclear tensor

$$W^{\mu\nu} \equiv \sum_{P} \delta^4(\text{Energy}) \mathcal{J}^{\mu\dagger} \mathcal{J}^\nu, \tag{3.5}$$

composed of the nuclear current matrix elements $\mathcal{J}^\mu \equiv \langle \Psi_f(\mathbf{k}, P')|\hat{J}^\mu(q)|\Psi_i(P)\rangle$, cannot be evaluated directly from a fundamental field theory, as it depends on the details of the complicated many-body (and nonperturbative) initial and final hadronic states. Clearly, additional phenomenological assumptions about these states are required; they will be addressed shortly.

Substituting the expression for $\eta_{\mu\nu}$ in Equation 3.4 into the formula for the cross-section yields

$$
\frac{d^3\sigma}{dE_{p'}\,d\Omega_{p'}\,d\Omega_k} = \frac{m|\mathbf{k}|}{(2\pi)^3}\left(\frac{d\sigma}{d\Omega}\right)_{\text{Mott}} \times
$$
$$
\left[\xi^2\,R_L + \left(\tan^2\frac{\theta}{2} - \frac{1}{2}\xi\right)R_T - \frac{1}{2}\xi\cos(2\beta)\,R_{TT} + \xi\left(\tan^2\frac{\theta}{2} - \xi\right)^{\frac{1}{2}}\sin\beta R_{LT}\right], \quad (3.6)
$$

where $\xi \equiv q^2/|\mathbf{q}|^2$, and the Mott cross-section for elastic scattering from a free, pointlike, spin-$\frac{1}{2}$ particle

$$
\left(\frac{d\sigma}{d\Omega_{p'}}\right)_{\text{Mott}} = \frac{\alpha^2\cos^2(\frac{\theta}{2})}{4|\mathbf{p}|^2\sin^4(\frac{\theta}{2})}, \quad (3.7)
$$

has been factored out of the cross-section. There are four independent response functions [19]; they are defined to be the following elements of the nuclear response tensor:

$$
R_L \equiv W^{00} = |\mathcal{J}^0|^2
$$
$$
R_T \equiv W^{22} + W^{11} = |\mathcal{J}^2|^2 + |\mathcal{J}^1|^2
$$
$$
\cos(2\beta)\,R_{TT} \equiv W^{22} - W^{11} = |\mathcal{J}^2|^2 - |\mathcal{J}^1|^2 \quad (3.8)
$$
$$
\sin\beta\,R_{LT} \equiv W^{02} - W^{20} = 2\,\text{Re}\,[\mathcal{J}^{0*}\mathcal{J}^2].
$$

Together with kinematics, these completely determine the behavior of the cross-section; the problem is then reduced to calculating the nuclear current matrix elements $\mathcal{J}^\mu$. I note that Equations 3.7 and 3.10 are taken from the derivation in

Reference [18], which is performed in parallel kinematics; thus, the matrix elements I calculate in the coordinate system shown in Figure 3.2 must be rotated into parallel coordinates before the cross-section may be evaluated.

The nuclear current matrix elements consist of three ingredients: the initial bound state, the current, and the final state of the outgoing proton. For the present discussion, the current is taken to be that of a free nucleon

$$\hat{J}^{\mu}\gamma^0 = F_1\gamma^{\mu} + \frac{F_2}{2M}i\sigma^{\mu\nu}q_{\nu}. \tag{3.9}$$

In the next two sections, I treat the initial and the final states of the proton.

3.2 Distorted Wave Final State: The Relativistic Eikonal Approximation

I seek an expression for the wavefunction of the outgoing proton that accounts for final state interactions between the proton and the residual nucleus. Assume that this interaction can be described by a potential, hereafter called the optical potential. Since this potential will be used in a relativistic framework, its Dirac structure must be specified. Much work has been done recently [20] to construct an accurate relativistic description of nuclear structure; in these models, the nucleon-nucleus interaction is expressed as the sum of two large pieces of opposite sign which nearly cancel to give the relatively small nuclear binding. These are a strong, repulsive, vector interaction and a slightly stronger, attractive, scalar interaction. In this calculation, I assume that the optical potential that describes the final state interaction between the ejected proton and the rest of the nucleus can be written with the same Dirac structure as the potential which binds the nucleons inside the nucleus. Fits to p-A scattering data with potentials of this form have been performed on a variety of nuclei [21,22,23]. Both potentials are taken to be central, and are usually written in a two-parameter Fermi form.

Let $|\Psi_{\mathbf{k},s}^{(-)}\rangle$ be the wavefunction of the outgoing proton, where $\mathbf{k}$ and s are its momentum and spin. The superscript $(-)$ specifies that it obeys incoming spherical wave boundary conditions; that is, the outgoing wave consists of a plane wave of momentum $\mathbf{k}$ and spin s. Following Reference [24], let $|\Psi_{\mathbf{k},s}^{(-)}\rangle$ have Pauli upper and lower components $u_{\mathbf{k},s}^{(-)}$ and $w_{\mathbf{k},s}^{(-)}$. Then the Dirac equation which these wavefunctions obey is

$$(\alpha \cdot \mathbf{p} + \beta M + \beta V_s + V_v) \begin{pmatrix} u_{\mathbf{k},s}^{(-)} \\ w_{\mathbf{k},s}^{(-)} \end{pmatrix} = E_{\mathbf{k}} \begin{pmatrix} u_{\mathbf{k},s}^{(-)} \\ w_{\mathbf{k},s}^{(-)} \end{pmatrix}. \tag{3.10}$$

This equation can be decomposed into a system of two coupled differential equations in the (two-component) wavefunctions $u_{\mathbf{k},s}^{(-)}$ and $w_{\mathbf{k},s}^{(-)}$. Using the Dirac representation for α and β and eliminating $w_{\mathbf{k},s}^{(-)}$ from this system gives, after some algebraic manipulation, the following equation in Schrödinger form

$$\left[\frac{p^2}{2M} + V_C + V_{SO}(\sigma \cdot \mathbf{L} - i\mathbf{r} \cdot \mathbf{p}) \right] u_{\mathbf{k},s}^{(-)} = \frac{k^2}{2M} u_{\mathbf{k},s}^{(-)}, \tag{3.11}$$

where V_C and the V_{SO} are central and spin-orbit potentials, defined to be the following functions of V_s and V_v:

$$\begin{aligned} V_C &= V_s + \frac{E}{M} V_v + \frac{V_s^2 - V_v^2}{2M} \\ V_{SO} &= \frac{1}{2M[E + M + V_s - V_v]} \frac{1}{r} \frac{d}{dr}[V_v - V_s]. \end{aligned} \tag{3.12}$$

Motivated by the knowledge of its asymptotic form, the upper component of the wavefunction can be rewritten as

$$u_{\mathbf{k},s}^{(-)} = e^{i\mathbf{k}\cdot\mathbf{r}} e^{iS(\mathbf{r})} \chi_s, \tag{3.13}$$

implicitly defining a new function $S(\mathbf{r})$. The problem of solving for the wavefunction has now been recast as solving for $S(\mathbf{r})$, the "eikonal phase" [25]. This function is in

general an operator in spin space, i.e. a 2×2 matrix that acts on χ_s. Now at high enough energies, this phase is only weakly modulated by the potential. Algebraically, for

$$\frac{V_s}{E}, \frac{V_v}{E} \ll 1$$

we have

$$\frac{\partial S}{\partial z} \ll 1. \tag{3.14}$$

Therefore, the second order terms $\nabla^2 S$ and $(\nabla S)^2$ can be neglected in the expansion of the kinetic energy term of the Schroedinger equation

$$
\begin{aligned}
\frac{p^2}{2M} u_{\mathbf{k},s}^{(-)} &= -\frac{\nabla^2}{2M}(\mathrm{e}^{i\mathbf{k}\cdot\mathbf{r}}\mathrm{e}^{iS(\mathbf{r})}\chi_s) \\
&= -\frac{1}{2M}\left[(i\mathbf{k}+i\nabla S(\mathbf{r}))\cdot(i\mathbf{k}+i\nabla S(\mathbf{r}))+i\nabla^2 S(\mathbf{r})\right](\mathrm{e}^{i\mathbf{k}\cdot\mathbf{r}}\mathrm{e}^{iS(\mathbf{r})}\chi_s). \\
&\approx \left[\frac{k^2}{2M}+\frac{\mathbf{k}\cdot\nabla S}{M}\right]\left(\mathrm{e}^{i\mathbf{k}\cdot\mathbf{r}}\mathrm{e}^{iS(\mathbf{r})}\chi_s\right)
\end{aligned}
\tag{3.15}
$$

Substituting this expression for the kinetic energy back into Equation 3.11 yields

$$-\left(\frac{1}{M}\right)\mathbf{k}\cdot\nabla S = V_C + V_{SO}\left[\sigma\cdot(\mathbf{r}\times\mathbf{k})-i\mathbf{r}\cdot\mathbf{k}\right]. \tag{3.16}$$

Choosing $\hat{z} = \hat{k}$, decompose $\mathbf{r}$ into parallel and a perpendicular components, $\mathbf{r} \equiv (z, \mathbf{b})$ Then $\mathbf{k}\cdot\nabla S$ is just $|\mathbf{k}|\partial S/\partial z$. Integrating Equation 3.18 from $z' = z$ to ∞ with the boundary condition that $S(\infty, \mathbf{b}) = 0$ yields the following expression for S

$$S(z,\mathbf{b}) = \frac{M}{k}\int\limits_{z}^{\infty} dz'\left(V_C(z',\mathbf{b})+V_{SO}(z',\mathbf{b})\left[\sigma\cdot(\mathbf{b}\times\mathbf{k})-ikz'\right]\right). \tag{3.17}$$

Care must be taken when choosing a potential with which to calculate this eikonal phase [26]; the optical potential that corresponds to outgoing spherical-wave boundary

conditions—which has a negative imaginary part—would cause enhancement rather than absorption of the distorted wave in this expression. In fact, the potential appropriate for incoming wave boundary conditions is the complex conjugate of the ordinary potential; for a derivation, see Appendix C. For convenience, whenever potentials are discussed in this thesis, their "standard" form is used, and it is understood that the conjugate of the potentials must be taken in the first step of any calculations.

It is convenient to divide S into two parts on the basis of its spin structure

$$S = S_1 + S_2 \left(\sigma \cdot \mathbf{a} \right), \tag{3.18}$$

where S_1 is proportional to the unit operator in the Pauli spin space,

$$S_1(z, \mathbf{b}) \equiv \frac{M}{k} \int\limits_{z}^{\infty} dz' \left[V_C(z', \mathbf{b}) - V_{SO}(z', \mathbf{b}) i k z' \right], \tag{3.19}$$

and S_2 contains the nontrivial spin dependence,

$$S_2(z, \mathbf{b}) \left(\sigma \cdot \mathbf{a} \right) \equiv \frac{M}{k} \int\limits_{z}^{\infty} dz' \left\{ V_{SO}(z', \mathbf{b}) [\sigma \cdot (\mathbf{b} \times \mathbf{k})] \right\}. \tag{3.20}$$

These definitions are used later in Appendix A.

3.3 Relativistic Nuclear Wavefunctions: Quantum Hadrodynamics

The goal of Quantum Hadrodynamics (QHD) is to describe the nucleus by a field theory of nucleons interacting via the exchange of mesons. This is motivated theoretically by the fact that QCD, (which presumably describes the strong inter- and intra-nucleon interactions exactly) must in the limit of low energies reduce to a field theory of interacting nucleons and mesons [27] and experimentally by the fact that the two-nucleon interaction is indeed to a good approximation described by a one-pion

exchange potential at long distances [11]. While treating QHD as true field theory (for example by performing loop expansions) is dubious [28], the model, considered as a phenomenology, gives an adequate description (to within 10 percent [29])of nuclear densities and energy levels, and provides the best available nuclear wavefunctions consistent with a relativistic formalism.

In the simplest version of the model [30] (QHD-I, or the $\sigma-\omega$ model), there are only two meson fields in addition to the nucleon field. As mentioned in Section 3.2, there is an attractive scalar field, σ, which is associated with the two-pion resonance in the nucleon-nucleon amplitude, and a repulsive vector field, ω, which is identified with the physical ω meson. A more sophisticated version of the model (QHD-II) includes additional fields due to π, ρ, and γ particles. In the mean field approximation, we seek to find the ground state of a particular nucleus by replacing the meson fields with their mean values while allowing the nucleon fields to fluctuate.

Writing the Euler-Lagrange equation for the nucleon field in the presence of the meson mean-fields gives a Dirac equation

$$
\left[-i\alpha \cdot \nabla + g_v V^0 + \frac{1}{2} g_\rho \tau_3 b^0 + e\frac{1}{2}(1 + \tau_3) A^0(r) + \beta(M - g_s \phi^0(r)) \right] \Psi_a = E_a \Psi_a,
$$

(3.21)

where V, ϕ, b, and A are the ω, σ, ρ, and γ fields, respectively, which can be solved self-consistently for the nucleon wavefunctions.

The bound states of the nucleons in the potential generated by the meson fields is written as the product of angular momentum eigenstates (spin spherical harmonics) and radial wavefunctions

$$
\Psi_{n\kappa mt}(\mathbf{r}) = \frac{1}{r} \left(\begin{array}{c} iG_{n\kappa t}(r)\Psi_{\kappa m}(\Omega) \\ -F_{n\kappa t}(r)\Psi_{-\kappa m}(\Omega) \end{array} \right) \eta_t,
$$

(3.22)

where κ is a convenient way to characterize l and j simultaneously

$$j = |\kappa| - \frac{1}{2}$$

$$l = \begin{cases} \kappa, & \kappa < 0 \\ -(\kappa + 1), & \kappa > 0 \end{cases}, \tag{3.23}$$

and η_t is an isospin eigenstate, with $t = +\frac{1}{2}$ for protons and $t = -\frac{1}{2}$ for neutrons. Note that the full four-component wavefunction is not an eigenstate of the orbital angular momentum operator, $\hat{L}$; either the upper components have $l = j + \frac{1}{2}$ and the lower components have $l = j - \frac{1}{2}$ or *vice versa*. Ψ is normalized so that $\int d^3x \Psi^\dagger \Psi = 1$. Codes implementing this general formalism exist [29,31], and I use the radial wavefunctions they generate as input to my calculation.

Chapter 4
DWIA Calculations

In Section 4.1, results of relativistic calculations of quasielastic scattering from oxygen, calcium, and lead are presented. Section 4.2 contains an analysis of theoretical uncertainty in the calculation; computational and numerical accuracy are examined in Section 4.3.

4.1 DWIA Results

The previous chapter, together with Appendix A, specifies a prescription for computing the response of any nucleus to quasielastic scattering, provided the energy of the outgoing particle is high enough that the eikonal approximation is valid. The calculation requires three pieces of input: first, the kinematics, specifically the momentum transfer of the reaction and the final momentum of the proton; second, the wavefunction of the initial bound state; and third, an optical potential describing the interaction between the outgoing proton and the residual nucleus. Given these, the code implementing the formalism of the appendix returns four response functions (five if the initial electrons are polarized) that completely determine the hadronic contribution to the $(e, e'p)$ cross-section. The first of the three inputs is simple (at least for a theorist); the second is more interesting, but outside the scope of this thesis (References [29] and [31] contain the details of the relativistic nuclear wavefunctions I use). In this chapter I concentrate on the third, which embodies most of the essential physics of this calculation.

The bulk of the results shown here are for quasielastic scattering from calcium, primarily because a high energy, relativistic optical potential for calcium is available in the literature [21]. Cooper *et al* obtain relativistic scalar and vector potentials by assuming they can be described by symmetrized two-parameter Fermi distributions and then performing an energy-dependent global fit to all of the available p−^{40}Ca elastic scattering data. I convert their Dirac scalar and vector potentials into central and spin-orbit potentials via Equations 3.14, which I then use as input to my code. In their model, both the parameters that describe the shape of the potential as well as those that determine its strength have a quadratic dependence on the laboratory kinetic energy of the proton. While their parabolic fitting procedure yields a good description of the data within the range of proton kinetic energies they study (150 MeV to 1040 MeV), it makes extrapolation to higher energies dangerously unreliable. For these energies, I use the density-dependent potential model described in Appendix B. The densities I use are taken from Barrett and Jackson [12].

An example of typical output from the calculation is shown in Figure 4.1. The five response functions for the quasielastic scattering of polarized electrons from the $1p_{\frac{1}{2}}$ shell of calcium, both with and without distortion, are shown as functions of $|\mathbf{p}| \equiv |\mathbf{k} - \mathbf{q}|$, where $|\mathbf{q}| = |\mathbf{k}|$ is held fixed. Figure 3.1 defines the kinematic variables; however, the results shown in this and all following figures have been calculated by rotating the matrix elements to parallel kinematics before calculating either response functions or cross-sections. The value of the incident electron momentum used in this calculation is 1840 MeV; in general, I use $|\mathbf{p_i}| = T_f + 800$ (MeV) for these calculations. Throughout, I take the angle between initial and final electron momenta to be 0.9 radians, the electron helicity to be one half, and the angle β to be 2.0 radians.
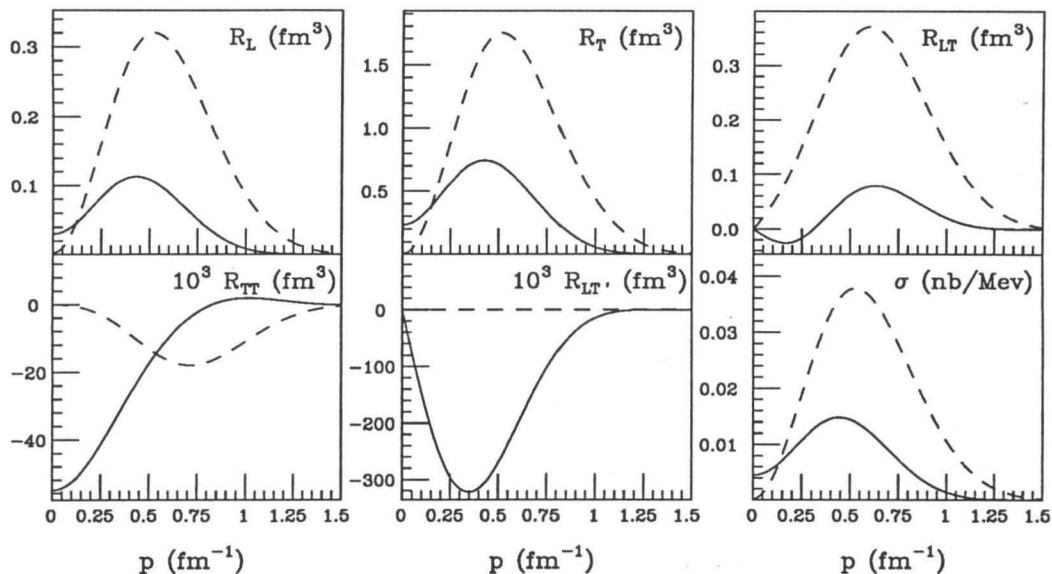
Figure 4.1 – Response functions for the quasielastic knockout of a 1040 MeV proton from the $1p_{\frac{1}{2}}$ shell of calcium. The five response functions and the cross-section are plotted as functions of $|p| \equiv |k - q|$, where $|q| = |k| = 1741$ MeV. The dashed curves represent the plane-wave calculation and the solid curves are results of the distorted-wave calculation. The electron kinematics used are given in the text.

The plane-wave results were calculated by using the full distorted-wave code and setting the distorting potentials to zero, rather than by performing the simpler plane-wave calculation independently. This procedure provides a means of checking the complex distorted-wave code, since the physical effect produced by distortion should be primarily absorption. The curves plotted in Figure 4.2 were calculated for an ejectile with 1040 MeV of kinetic energy, the highest for which the optical potential of Reference [21] is valid.

The results of the calculations show the expected behavior: the distorted-wave responses are in general smaller in magnitude than the plane-wave responses because of the absorptive effects embodied in the large negative imaginary part of the central

potential. The transverse response function is largest at this energy and dominates the cross-section. The helicity-dependent response function, $R_{LT'}$, is identically zero in the absence of distortion. At nearly-parallel kinematics (small $|\mathbf{p}|$) as well as in the smaller transverse-transverse and helicity-dependent response functions, an enhancement (in magnitude) due to the spin-orbit potential is evident. (V_{SO} and V_C have opposite signs.) While the inclusion of a spin-orbit term in the potential is necessary to achieve a good description of low and intermediate energy scattering behavior [32], its effects should decrease as energy increases. In the density-dependent potential used at higher energies, the additional factor of $1/k$ in V_{SO} relative to V_C (Equation B.10) effects this decrease, which is investigated further in Section 4.1.3.

In a real experiment, it would be difficult or impossible to determine that a proton had been ejected from a specific nuclear bound state (in this example the $1p_{\frac{1}{2}}$ shell), since the final state of the residual nucleus is difficult to measure. The calculation shown in Figure 4.2 is the same as that in Figure 4.1, except that the results have been averaged over all six of the proton states in calcium (with appropriate weights from simple angular momentum counting) and thus are more appropriate for comparison with experimental data.

These response functions show the same qualitative behavior as those for any one of the individual shells: the effect of distortion is an overall decrease in magnitude by a factor of about one half. (This factor depends of course on the energy of the proton as well as the mass number of the nucleus it traverses.) The knee apparent in each of the response functions of Figure 4.2 is due to the contribution of the $2s_{\frac{1}{2}}$ shell, which has a slightly more complex structure than the other $n = 1$ shells.
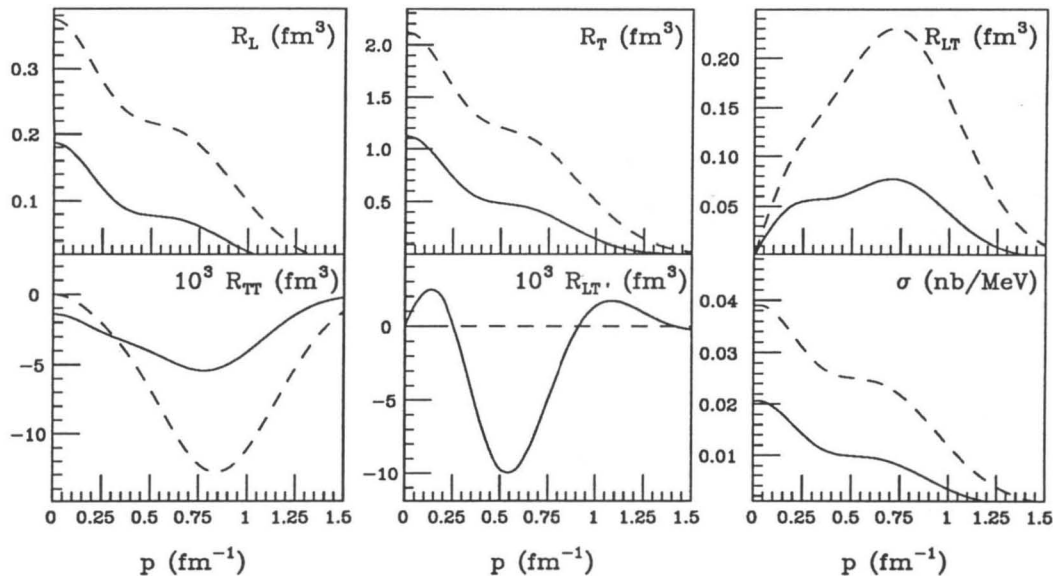
Figure 4.2 − Same as Figure 4.1 except that these results have
been averaged over all of the possible initial bound states of the
proton in calcium.

4.1.1 Initial State Dependence

While the nuclear-averaged calculation shown in Figure 4.2 is more relevant to
experiment than the single-shell calculation shown in Figure 4.1, it is interesting to
examine briefly the systematic dependence of the response functions on the quantum
numbers of the initial bound state. In the nonrelativistic, plane-wave limit, the
transverse and longitudinal response functions are essentially Fourier transforms of
the bound state radial wavefunctions. Thus the response from a particular shell
should be peaked at a value determined by the r.m.s. radius of that shell and the
magnitude of the momentum transfer. In Figure 4.3, the longitudinal responses from
each of the shells of calcium are plotted together for the same kinematics. The
progression from the s shells to the p shells to the d shells is clear. The expected

node in the response functions for scattering from the $2s_{\frac{1}{2}}$ shell is also manifest. All of the response functions shown in the figure were calculated using the distorting potential of Reference [21]. The normalizations of the response functions from the various shells appear different in the figure; however, with the correct weight of p^2 and a necessary additional factor of p in the $2s_{\frac{1}{2}}$ response, their integrals (over p) are the same.
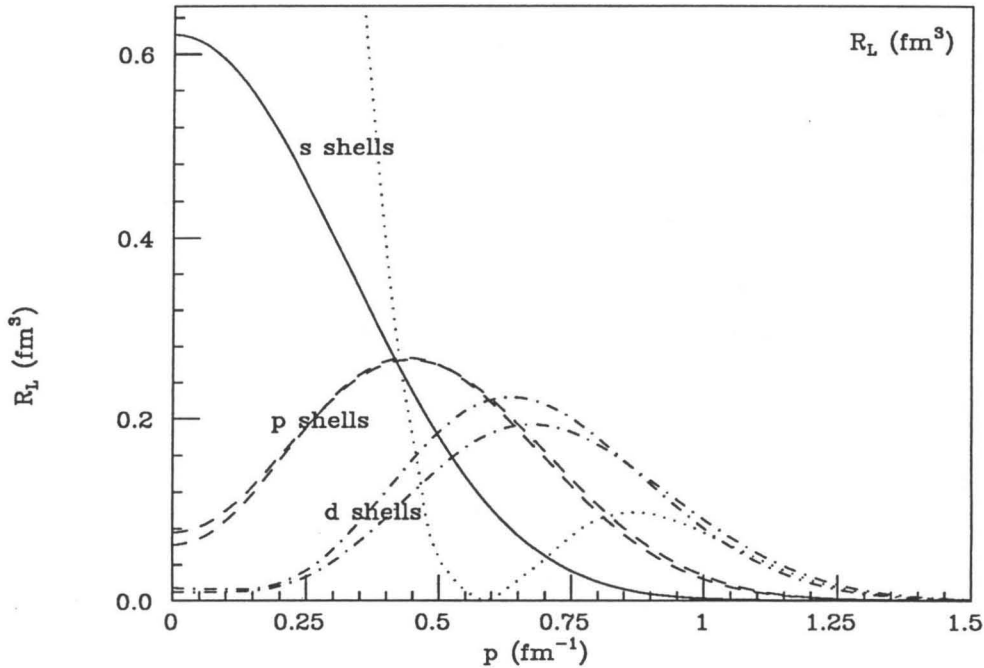
Figure 4.3 – Longitudinal response functions for knockout of an 800 MeV proton from each of the shells of ^{40}Ca. The different line types correspond to knockout from different initial shells: the solid curve to knockout from the $1s_{\frac{1}{2}}$ shell, the dotted curve to the $2s_{\frac{1}{2}}$ shell, the dashed curves to $1p_{\frac{1}{2}}$ and $1p_{\frac{3}{2}}$, and the dotdashed curves to $1d_{\frac{3}{2}}$ and $1d_{\frac{5}{2}}$.

4.1.2 Absorption Analysis

A more physically interesting quantity that can be extracted from raw results like those shown in Figures 4.1 through 4.3 is the fraction of the plane wave that is absorbed by the nuclear medium. I define the absorption, A, to be

$$A \equiv \frac{\sigma_u - \sigma_d}{\sigma_u}. \qquad (4.1)$$

In evaluating of A, I use cross-sections that have been integrated over $|\mathbf{p}|$.

Figure 4.4 shows the absorption as a function of ejectile kinetic energy for various nuclei. The values obtained for the absorption are positive: the spin-orbit enhancements (which tend to cause the absorption to be *negative*) in R_{TT} and $R_{LT'}$ are overwhelmed by the contribution of R_T to the differential cross-section, and the enhancement at small $|\mathbf{p}|$ does not survive the $|\mathbf{p}|$-integration. Results obtained using the potential of Reference [21] (plotted as solid diamonds) show a slight rise in the absorption with energy, due in part to the corresponding decrease in the relative magnitude of the spin-orbit potential. The density-dependent potential model of Appendix B, however, predicts a nearly constant absorption, with a value of about sixty percent for calcium.

It is this asymptotic value which may be compared with the results of the semiclassical calculation of Chapter 2. Indeed, the two agree quite well, indicating that for an outgoing particle of more than about one GeV of kinetic energy, the details of the interaction mechanism (relativity, spin-dependence, and even quantum mechanics) are small perturbations to the simple semiclassical picture of Chapter 2. Table 4.1 shows this comparison for oxygen, calcium, and lead.
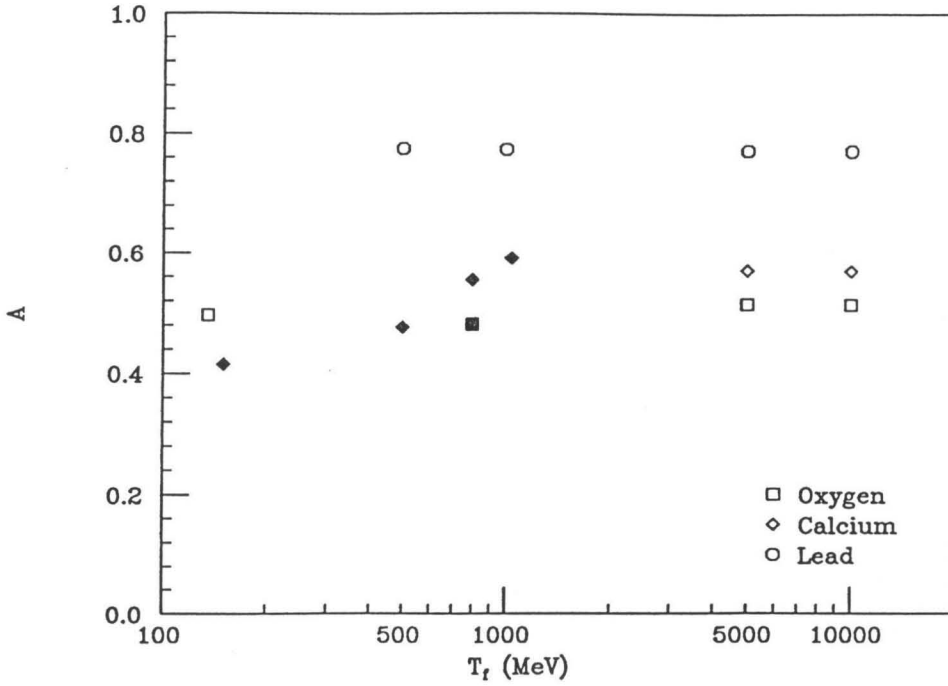
Figure 4.4 − Energy dependence of proton absorption in oxygen, calcium, and lead. The fraction of the undistorted cross-section that is absorbed by the nuclear medium is shown as a function of ejectile kinetic energy. The various symbols corresponding to different nuclei are defined in the legend. Solid symbols correspond to results obtained with the potentials [21] and [22]; open symbols were calculated using the density-dependent potential.

Nucleus	Mass	Absorption (Full)	Absorption (Semiclassical)
Oxygen	16	0.51	0.52
Calcium	40	0.57	0.63
Lead	208	0.77	0.79

4.1.3 Quenching of Longitudinal Response Function

A notable success of the relativistic description of electron-nucleus scattering is its prediction of a suppression of longitudinal (relative to transverse) response functions at intermediate and high energies [33]. While nonrelativistic approaches yield transverse and longitudinal responses of nearly equal magnitude independent of energy, calculations using a relativistic formalism exhibit a natural suppression of R_L at higher energies. Figure 4.5 shows this quenching behavior in the results of my (relativistic) calculation.
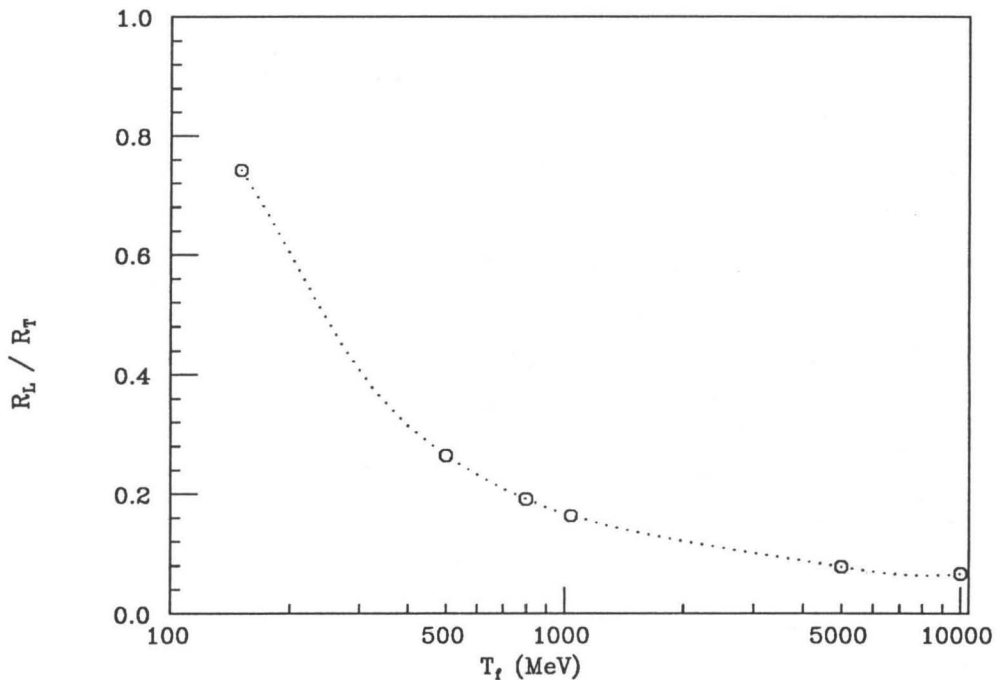
Figure 4.5 – Relative size of longitudinal and transverse response functions as a function of energy. R_L and R_T are calculated for quasielastic scattering averaged over the entire calcium nucleus and are integrated over all kinematically-allowed $|p|$; their ratio is then plotted as a function of ejectile kinetic energy. Circles represent points where the (distorted-wave) calculation was actually performed; the dotted curve connects them smoothly.

4.1.4 Effects of Spin-Orbit Potential

The last results I present before turning to uncertainty analyses are some calculations in which I examine the effects of different pieces of the optical potential separately. Of course the full potential provides the most accurate description of the final state interaction; however, it is instructive investigate how its individual components contribute to the final results. To this end, calculations were performed in which different parts of the potential were set to zero; comparisons with the full calculations then allow a determination of their effects.

Figure 4.6 shows three calculations of R_{TT} for quasielastic scattering from calcium using: (1) the full distorting potential of Reference [21], (2) only the central part of that potential, and (3) a potential that is identically zero. The transverse-transverse response function is particularly sensitive to the spin-orbit potential, which causes a large enhancement in its magnitude even at the relatively high energy of 500 MeV. Its effects are largest at small $|\mathbf{p}|$.

The dramatic effect that the spin-orbit potential has upon R_{TT} suggests that a measurement of the transverse-transverse response function might yield more accurate information about the presently ill-constrained spin-orbit term; however, the separation of R_{TT} from the other response functions requires proton spectrometry at several angles outside the electron scattering plane and would be experimentally demanding. Perhaps a more accessible effect of V_{SO} then is the slight decrease observed in the total cross-section when the spin-orbit potential is turned off. The spin-orbit distortions actually *increase* the outgoing flux of protons, thus the absorption is *greater* without the spin-orbit term than with it. The ratio of the absorption without the spin-orbit potential to the absorption with it is plotted in Figure 4.7 as a function of the initial bound state quantum numbers of the proton and its final
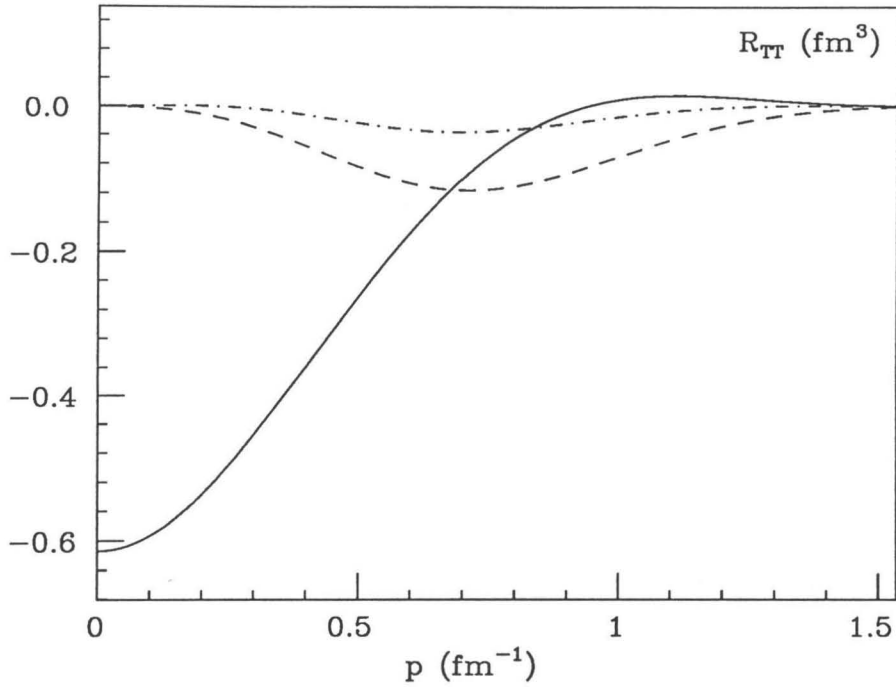
Figure 4.6 − Effects of spin-orbit potential. The transverse-transverse response function is plotted for knockout of a 500 MeV proton from the $1p_{\frac{1}{2}}$ shell of calcium. The solid curve was calculated using the full potential of Reference [21]. The dashed curve shows the plane-wave result. The dot-dashed curve represents the modified calculation in which the spin-orbit term was set to zero.

kinetic energy. As expected, the spin-orbit effects decrease with energy; they are on the order of several percent for protons with one GeV of kinetic energy. In general, those shells in which the wavefunction is concentrated further out from the center of the nucleus are affected most, since V_{SO} is itself surface-peaked.

A similar analysis was made of the effect of the real part the optical potential. It was found to be even smaller than that of V_{SO}; the real potential has negligible impact on the results of this calculation.
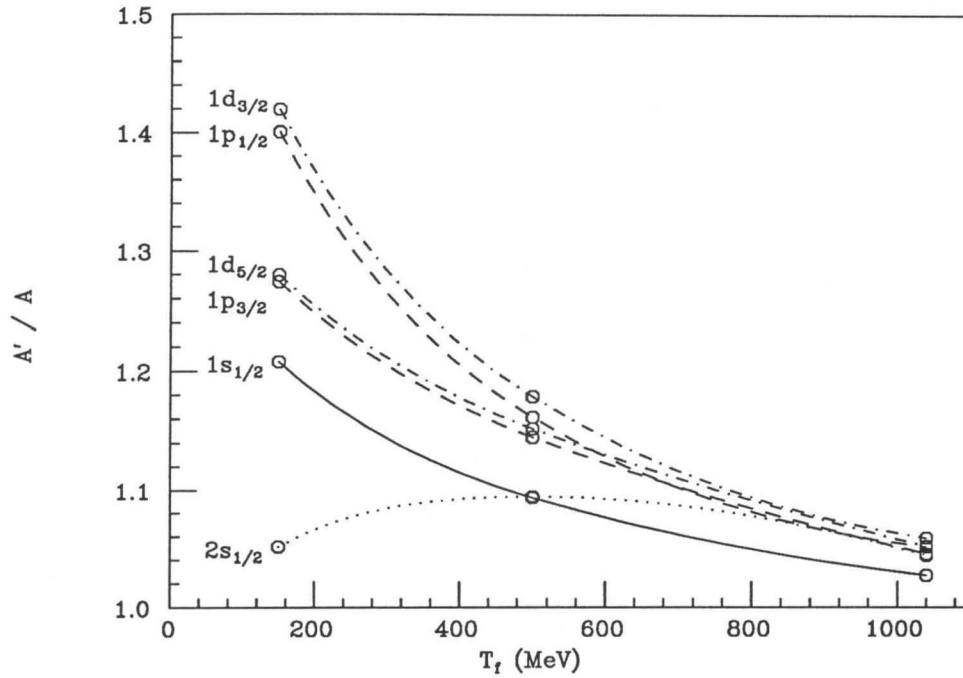
Figure 4.7 − Energy and shell dependence of enhancement due to spin-orbit potential. A modified distorted-wave calculation was performed setting the spin-orbit potential to zero. The ratio of the absorption obtained in this modified calculation to the absorption obtained in the full calculation is plotted as a function of ejectile kinetic energy separately for each of the shells in calcium.

4.2 Uncertainty Analysis—Theoretical

In order to gauge the reliability of the results in the previous sections, it is necessary to understand the sources of uncertainty in the calculation and their relative sizes. I first examine the class of uncertainties arising from theoretical ambiguities in the inputs to the calculation.

4.2.1 Choice of Optical Potential

The most immediately apparent and potentially most hazardous of these ambiguities lies in the choice of the optical potential. I use two different classes of optical model: potentials derived from parameterized fits to elastic scattering data, and potentials of the form of Equation B.10, where only the nuclear density is taken from experiment. Even within the first class, different fitting procedures yield different potentials and there is no *a priori* way of deciding which gives the best results. Only if differences of this kind have minimal impact on physical predictions can the results be considered meaningful. Figure 4.8 shows that calcium results obtained using two such optical potentials are indeed quite similar, even though the potentials themselves are very different (especially in their real and spin dependent parts).

Of course, that this should be true is not simply fortuitous. The real and spin-dependent parts of optical potentials derived from different fitting procedures vary as much as they do precisely because the data constrains $\text{Im}\,[V_C]$ most strongly. Indeed, high energy elastic scattering data can be explained to a great degree by a single quantity characterizing the mean free path of the proton in the nuclear medium, which corresponds roughly to the depth of the well in the imaginary part of the central potential [34]. The degree to which predictions of two such potentials do differ is a measure of the uncertainty in the results that arises from the choice of an optical potential—in this case on the order of ten percent.

Another similar question that must be addressed arises from the fact that the optical potential of Reference [21] can only be used to describe the interaction between the proton and the calcium nucleus when the proton has less than one GeV of kinetic energy. At higher energies (which are most relevant to the investigation of color transparency) I use the density-dependent model of Appendix B. Like Cooper's, this
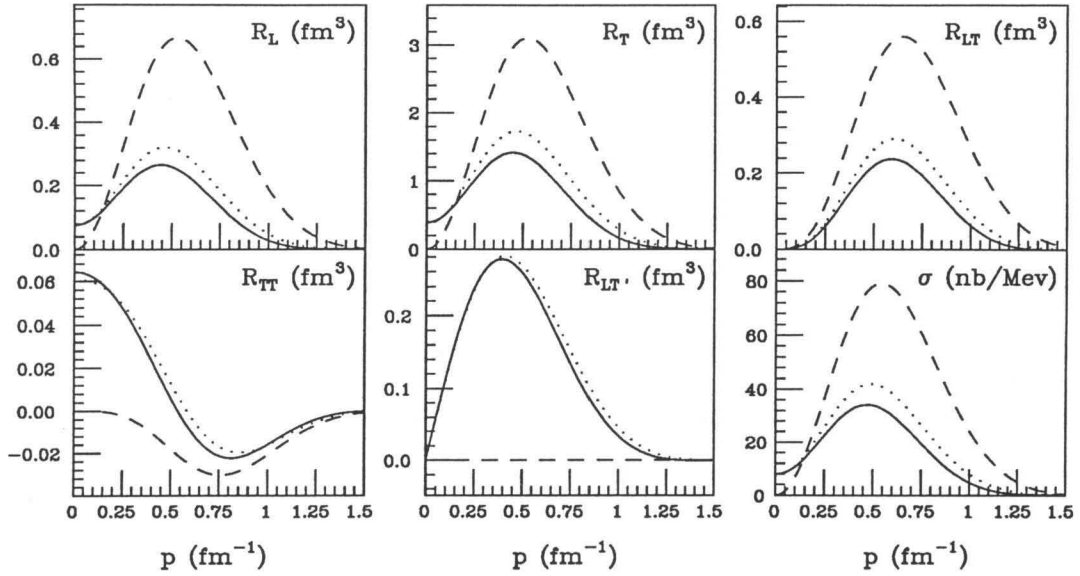
Figure 4.8 − Sensitivity of DWIA results to uncertainties in the optical potential. All three of the curves represent calculations of knockout from the $1p_{\frac{3}{2}}$ shell of calcium at 800 MeV, differing only in the optical potential used. The solid curve was calculated using the potential defined by Parameter Set I of Reference [21]; the dotted curve was calculated using Parameter Set II. For comparison, the plane-wave results are shown as a dashed curve.

potential is both complex and spin-dependent. It should become more accurate with increasing energy, since its formulation depends upon the assumption that the outgoing proton interacts with each particle in the medium independently—an assumption that becomes more correct as the wavelength of the proton becomes short compared to the mean separation distance between particles in the medium. Algebraically, this condition can be expressed as

$$\lambda_{\text{proton}} \ll r_{\text{sep}}, \tag{4.2}$$

where $\lambda_{proton} = 1/|\mathrm{k}|$ and $r_{sep} \simeq (\sqrt{3}/2)(2/\rho)^{\frac{1}{3}}$, yielding

$$k \gg \rho^{\frac{1}{3}}. \qquad (4.3)$$

For a typical nuclear density of $0.16\,\mathrm{fm}^{-3}$, the momentum constraint becomes $k \gg 100$ MeV. Clearly, for a proton with 800 MeV of kinetic energy, this inequality is satisfied, thus both Cooper's potential and the density-dependent potential are applicable. Figure 4.9 shows the two potentials plotted together for comparison. While they have roughly the same shape and magnitude, their differences are not *a priori* negligible.
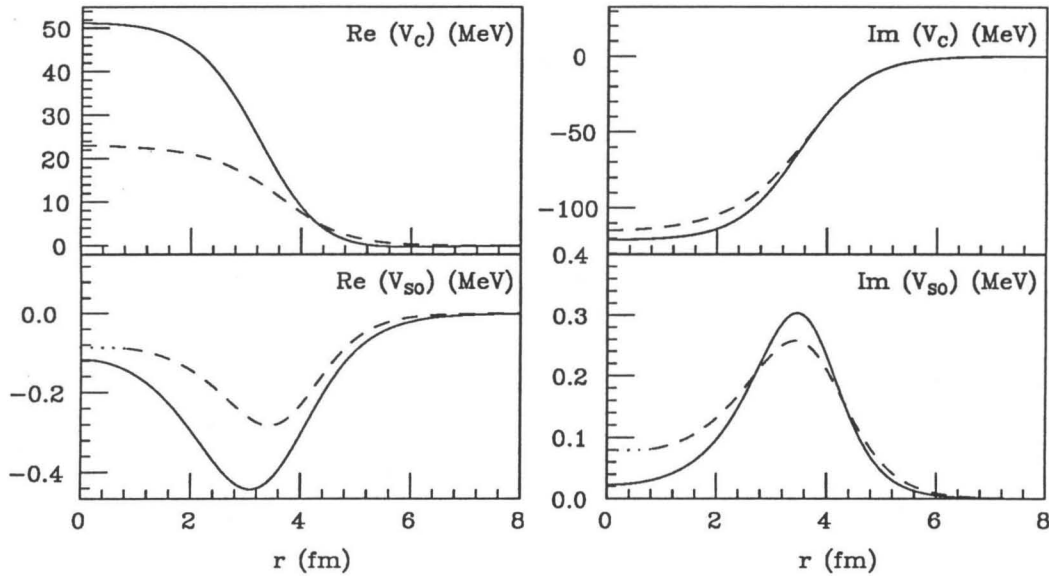
Figure 4.9 – Comparison of two different calcium optical potentials. The solid curve is the optical potential defined by Parameter Set I of Reference [21], and the dashed curve density-dependent potential of Appendix B. Both potentials are energy-dependent and are shown here for a particle with 800 MeV of lab kinetic energy. The spin-orbit part of the density-dependent potential must be smoothed out near the origin; the domain over which the function has been smoothed is indicated by dotted lines.

Figure 4.10 shows a comparison of the results obtained with the two potentials plotted in Figure 4.9. As before, the differences in physical quantities (i.e., cross-sections, absorptions) are much smaller than the differences between the potentials themselves.
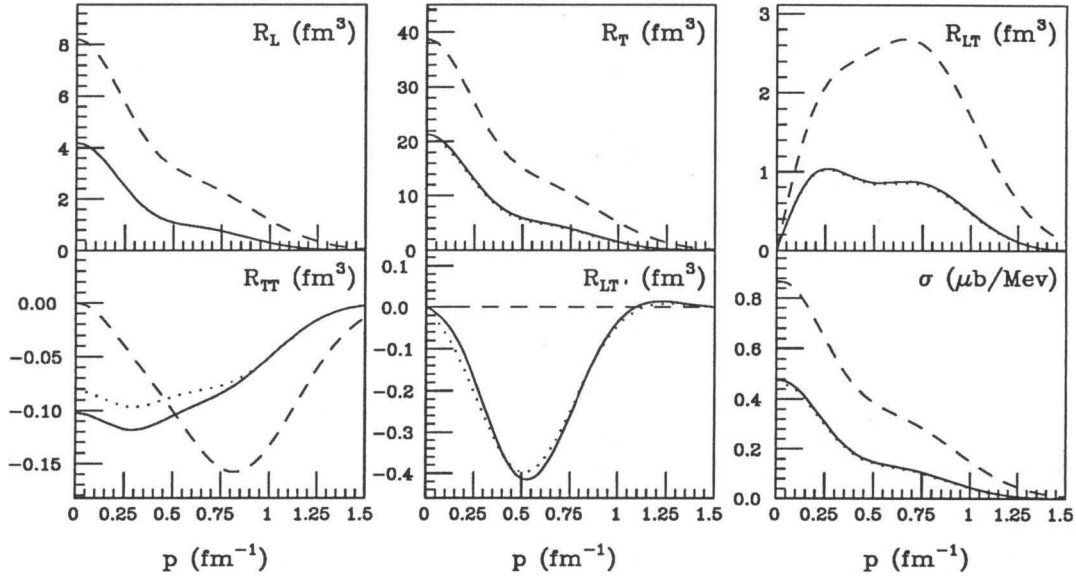
Figure 4.10 − **Comparison of results using the two potentials in Figure 4.9. The results obtained with the potential of Reference [21] are shown with solid curves, those obtained with the density-dependent potential are shown with dotted curves. The undistorted results are shown with dashed lines. Note that in some plots the dotted and solid lines are almost superimposed.**

The same analysis was performed for oxygen; results obtained with the phenomenological potential of Reference [22] were compared with those obtained using the density-dependent potential model. As for calcium, physical quantities are relatively insensitive to differences in the optical potentials. I conclude that despite the ambiguity inherent in choosing a particular optical model, or even a particular scheme

for fitting the parameters of that model to the data, the results of the calculation do not depend greatly on the details of the model and are therefore unambiguous.

4.2.2 Bound State Wavefunction Model Dependence

Another potential source of uncertainty is the uncertainty in the wavefunction describing the initial bound state of the proton. In order to estimate how this uncertainty affects my predictions, I performed calculations with two different initial state wavefunctions and examined the differences between the results. These are shown in Figure 4.11. I found that the differences in the response functions are of the same magnitude as the differences in the wavefunctions themselves, usually a few percent. The figure shows results for knockout from the $1p_{\frac{1}{2}}$ shell of oxygen, for which the two different relativistic wavefunctions show a particularly large disagreement. In the other shells, as well as in the oxygen nucleus as a whole, the differences between the response functions calculated with the two different kinds of wavefunctions are several times smaller.

4.2.3 Summary of Theoretical Uncertainty

Compiling the uncertainty discussed in the previous section together in one table, I have

Source	Magnitude
Fitting Procedure	9%
Potential Model	2%
Bound State Wavefunction	4%
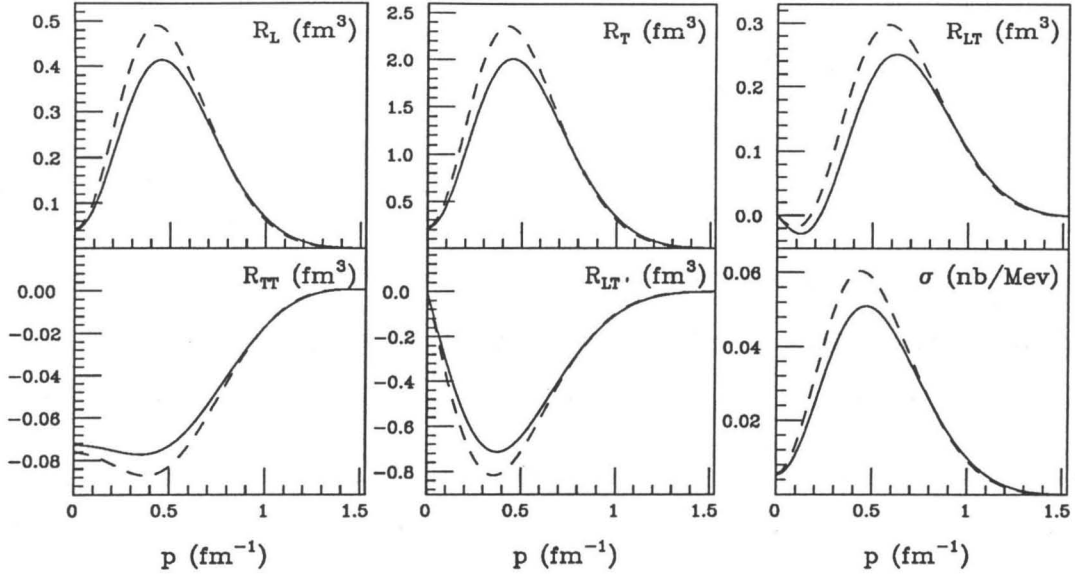
Figure 4.11 – Effect of varying the initial bound state wavefunc-tion. Two different relativistic $1p_{\frac{1}{2}}$ bound states, one calculated using a linearized Hartree solution of QHD-II (solid curve) [31], and the other using a nonlinear Hartree solution (dashed curve) [29] of the same nuclear field theory, are used as input and the output is compared.

Thus, there is a total uncertainty in the calculation on the order of fifteen percent.

It is curious that the variance in the results due to different fitting procedures ap-plied to the same potential is over four times as large as the variance between results obtained using completely disparate potential models. I suspect that a realistic num-ber for the overall uncertainty arising from a reasonable choice of an optical potential lies somewhere in between, thus making the total uncertainty in the calculation closer to ten percent.

4.3 Constraints on Computational and Numerical Error

Turning now to more prosaic aspects of the calculation, I discuss first some calculations made to test that the code faithfully implements the formalism laid out in the appendix.

The first such check was to compare with another calculation of the same process. Van Orden *et al* [18] have calculated quasielastic scattering using a relativistic distorted-wave model, but instead employ a partial-wave analysis of the distortion. Their calculation is performed entirely in momentum space, and thus bears very little resemblance to mine at a computational level. That the two calculations yield similar results is therefore convincing evidence that they are both free of computational errors. Figure 4.12 shows a comparison of our plane-wave results. The differences between the plane-wave calculations can be attributed to differences in the bound state wavefunctions used.

Figure 4.13 shows a comparison of our distorted-wave calculations. Since the calculations were done for protons of only 135 MeV kinetic energy, the eikonal approximation could well introduce significant errors into my calculation. However, the two calculations agree quite well, even at this low energy.

A second check I performed on the calculation was to compare with analytical expressions for nonrelativistic, undistorted knockout from harmonic oscillator bound states. The results generated by the code with these simplified inputs agree with the analytic results to within numerical accuracy.

These numerical effects were investigated thoroughly in a third set of tests performed on the code. All of the purely numerical parameters of the calculation, such as integration and differentiation step sizes, were halved until the results remained
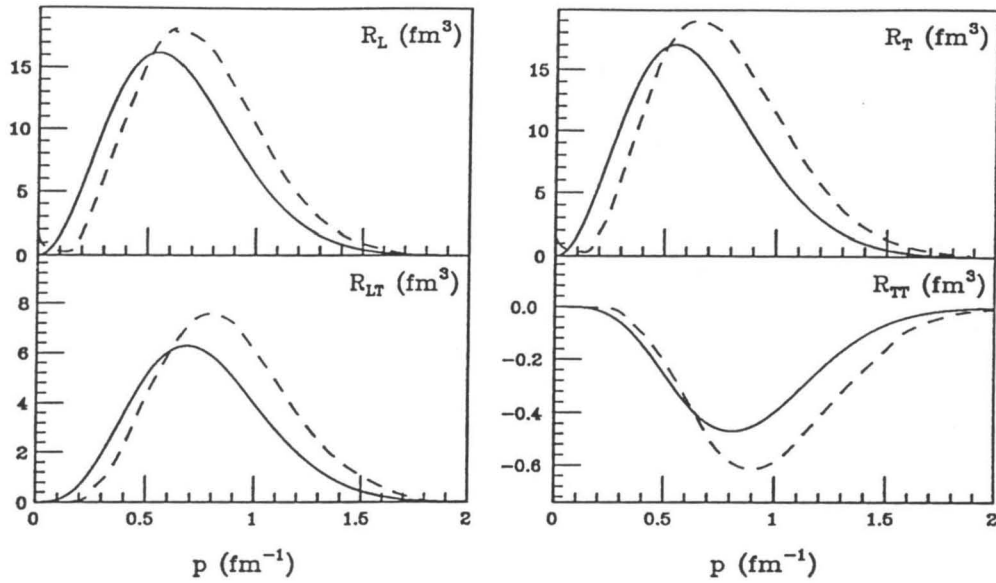
Figure 4.12 – Comparison of plane-wave calculations of knock-out of a 135 MeV proton from the $1p_{\frac{3}{2}}$ shell of oxygen. The solid curves are my calculations; the dashed curves were taken from Reference [18]. They follow a slightly different angular momentum convention; I have divided their results by $(2J + 1)$ for the comparison.

invariant to within one part in 10^{-6}. I determined a set of numerical parameters that yielded sufficient numerical accuracy and reasonable run times, and used these in the production runs of the code. "Sufficient" numerical accuracy was taken to be 10^{-3}, an order of magnitude smaller than any of the other effects studied.
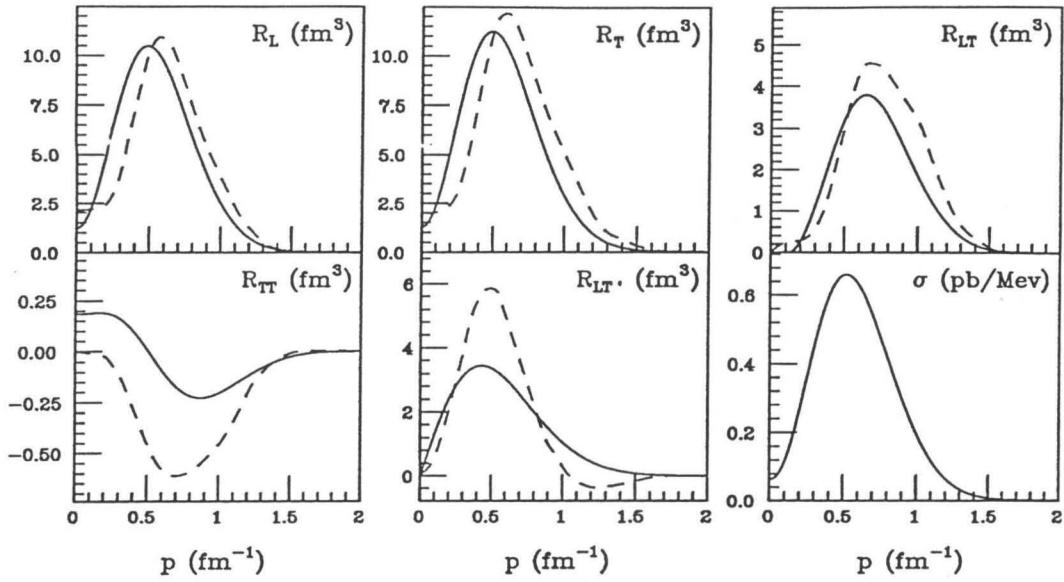
Figure 4.13 − Same as Figure 4.12, except with distortion effects included. No dashed line appears in the lower right-hand window of the plot, since Van Orden *et al* do not publish a total cross-section.

Chapter 5
Color Transparency Results

This chapter contains results of $(e, e'p)$ calculations that include color transparency effects. In Section 5.1, I outline a prescription for incorporating the color transparency mechanism into the DWIA calculation of Chapter 4. I present results, and discuss their uncertainty, in Section 5.2.

5.1 Transparency Formalism

In their semiclassical calculation, Farrar *et al* [9] model color transparency via an effective proton-nucleon interaction cross-section that varies along the exit path of the proton. This cross-section, initially very small, grows monotonically until its magnitude equals the usual free value of σ_{NN}. In my (quantum mechanical) calculation, there is no well-defined proton exit path; however, the eikonal formulation of the distorted wave that I use does allow a fairly straightforward translation of their basic idea into the language of quantum mechanics. The final state wavefunction at any point in the nucleus depends on the integral of the interaction potential along a line in the direction of the final momentum from the point in question to the nuclear surface; thus, the appropriate generalization of Farrar's effective cross-section is an effective potential that varies along the eikonal integration path.

This general strategy is not without several subtleties that warrant careful examination. The first such issue to be resolved arises because of the relativistic nature

of my calculation. Recall that the nuclear interaction can be characterized relativistically either by its Dirac components, V_S and V_V, or by its central and spin-orbit components, V_C and V_{SO}. A prescription for computing the effective potential must specify which of these pairs is to be scaled along the integration path. The choice is not arbitrary, since the transformation between the two sets of potentials is nonlinear (Equations 3.14) and thus a multiplicative factor applied to V_S and V_V does not correspond to the same function of V_C and V_{SO}. Since the latter appear in the eikonal integral (in this sense they are more physical quantities), it would be convenient to choose them as the basis for the effective potential that describes color transparency. Equations B.17 provide further motivation for this selection: V_C—which is an order of magnitude larger than V_{SO}—depends linearly on σ_{NN}. A linear (quadratic) growth of V_C and V_{SO} in the full calculation reduces to a linear (quadratic) growth of σ_{NN} in the nonrelativistic, non-spin-dependent limit. For these reasons, I use effective central and spin-orbit potentials that scale with distance along the eikonal path to describe color transparency.

Before addressing the final technical question of how to eliminate V_S and V_V from the calculation entirely, I complete the color transparency prescription by specifying the function used to scale V_C and V_{SO}. Guided by the expression for the effective cross-section in Reference [9], I seek a function that has a value proportional to $1/|\mathbf{q}|$ at the origin and grows linearly at the rate determined by the final momentum of the proton until it reaches one. The initial size of the proton is of the order of the wavelength of the virtual photon, and is

$$t_s = \frac{1}{|\mathbf{k}\,(\text{GeV})|^2}. \tag{5.1}$$

The quarks in the proton separate at a speed on the order of c, and, in the frame of the nucleus, the distance the proton travels during that time is

$$l_h = \frac{|\mathbf{k}|}{M} r_0 (1 - t_s),$$

(5.2)

where $r_0 = 0.81$ fm is the proton's final size, and the finite initial size of the proton has been treated exactly. The scaling function I seek is then

$$R(z; z_0) = \max \left\{ \left(\frac{z - z_0}{l_h} \right) (1 - t_s) + t_s \, , \, 1 \right\},$$

(5.3)

and color transparency is introduced into the distorted-wave calculation via the substitutions

$$\int\limits_z^\infty V_C(z', \mathbf{b}) \, z' \, dz' \to \int\limits_z^\infty R(z'; z) V_C(z', \mathbf{b}) \, z' \, dz'$$
$$\int\limits_z^\infty V_{SO}(z', \mathbf{b}) \, z' \, dz' \to \int\limits_z^\infty R(z'; z) V_{SO}(z', \mathbf{b}) \, z' \, dz'.$$

(5.4)

The generalization of the scaling function to include Farrar's quadratic expansion model is

$$R(z; z_0) = \max \left\{ \left(\frac{z - z_0}{l_h} \right)^\tau (1 - t_s) + t_s \, , \, 1 \right\},$$

(5.5)

where $\tau = 0$, 1, and 2 are defined in Section 2.3.

I return now to the remaining technical problem of eliminating the Dirac components of the potential from the calculation completely, in favor of a central/spin-orbit description of the interaction. The potentials that appear as integrands in the distorted wavefunction have already been converted into effective, transparency-inducing potentials; however, this eikonal term is not the only potential-dependent term in the

matrix elements. The function $D(r) = E + M + V_s(r) + V_v(r)$ appears in the lower spinor components of the distorted wavefunction—see for example Equation A.18. Not only do these potentials fail to enter in the form of an integral over the proton's exit path (which facilitated the analogy with the effective cross-section of the semiclassical calculation), but they are also the wrong pair of potentials for the formulation of color transparency altogether. If the transformation between scalar/vector potentials and central/spin-orbit potentials were invertible there would be no problem, but unfortunately it is not. Closer inspection shows, however, that full invertability is not actually required. An expression for D in terms of V_C and V_{SO} suffices, and is derived below.

From Equations 3.14, I have

$$V_{SO}(r) = -\left(\frac{1}{2M}\right) \frac{1}{E + M + V_s(r) - V_v(r)} \frac{1}{r} \left(V_s'(r) - V_v'(r)\right). \qquad (5.6)$$

The desired function, $D(r)$, is conveniently embedded in the expression for V_{SO}. Rearranging the differentials as

$$V_{SO}(r)\, r\, dr = -\left(\frac{1}{2M}\right) \frac{d\left[V_s(r) - V_v(r)\right]}{E + M + V_s(r) - V_v(r)} \qquad (5.7)$$

suggests a solution by integration. At fixed **b**, I have

$$r\, dr = z\, dz. \qquad (5.8)$$

Changing the variable of the integral on the left side and performing the right-hand integral analytically yields

$$\int_z^\infty V_{SO}(z', \mathbf{b})\, z'\, dz' = -\frac{1}{2M} \ln\left[E + M + V_s(z', \mathbf{b}) + V_v(z', \mathbf{b})\right]\Big|_z^\infty. \qquad (5.9)$$

The potentials vanish at infinity, so

$$D(r) = (E + M) \exp\left[2M \int\limits_{z}^{\infty} V_{SO}(z', \mathbf{b}) \, z' \, dz'\right], \tag{5.10}$$

eliminating not only V_s and V_v but also V_C from the expression for D. It also has the desirable form of an integral along the eikonal path, which is, moreover, one that is already computed in the DWIA calculation.

5.2 Transparency Results

Figure 5.1 shows the effect color transparency has on the results of the DWIA calculations that were presented in Section 4.1. This figure is the same as Figure 4.2, except that a third (dotted) curve shows the transparency results. Unless otherwise specified, the transparency model used in the calculations presented here is the diffusion model ($\tau = 1$) discussed in Chapter 2. In addition, the outgoing proton's kinetic energy is five times higher in this figure than in the earlier one, since the color transparency effect is nearly negligible for protons with less than one GeV of kinetic energy. Transparency effects are strictly zero for protons with $k < 1$ GeV ($T_f = 433$ MeV), because the wavelength of the virtual photon is then larger than the proton and no shrinkage occurs.

While increasing the proton energy makes the color transparency effect more pronounced, it has disadvantages too: the magnitudes of both the response functions and the total cross-section drop steeply with increasing energy. (Note the additional overall factors of 10^{-3}.) In calcium at 5 GeV, about one third of the absorptive effects of distortion are nullified by transparency.
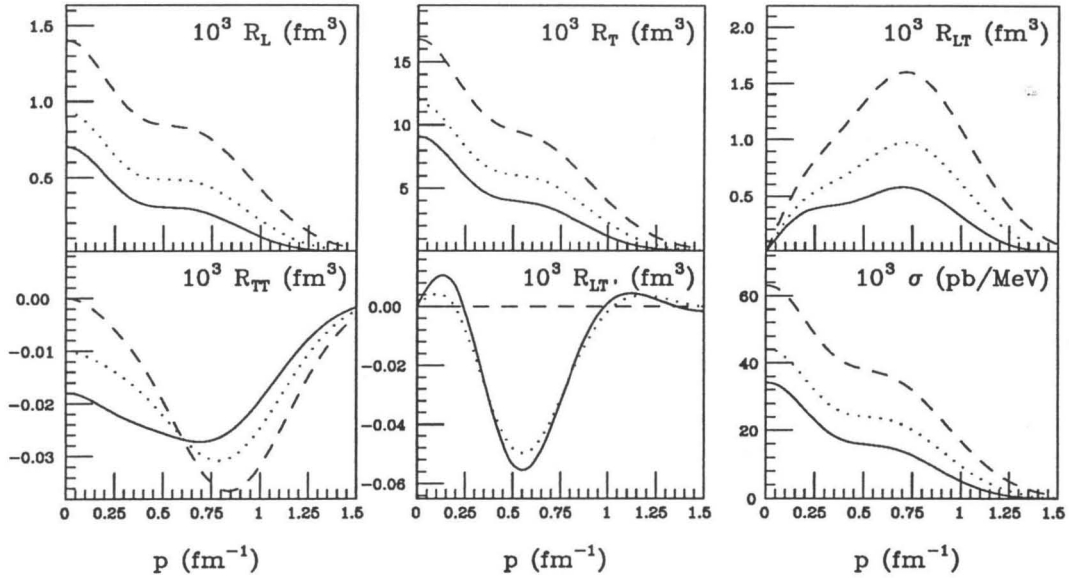
Figure 5.1 – Response functions for the quasielastic knockout of a 5 GeV proton from calcium. This plot represents the same calculation as the one in Figure 4.2, only at $T_f = 5$ GeV. The solid curve corresponds to the distorted-wave calculation, and the dotted curve corresponds to a calculation that includes transparency effects. The undistorted results are plotted as dashed curves for comparison.

The amount of the distortion that is negated in this way is an interesting quantity which characterizes the transparency. I define the transparency, T, to be

$$T \equiv \frac{\sigma_t - \sigma_d}{\sigma_u - \sigma_d}, \tag{5.11}$$

where σ_t, σ_d, and σ_u are the transparent, distorted, and undistorted cross-sections, respectively. Note that my definition of transparency is quite different from the quantity of the same name often quoted in the literature [9, 14]. According to my definition, a transparency of one implies that the transparent cross-section is identical to the undistorted cross-section (i.e., that the distortion is entirely thwarted by

transparency). Likewise, a transparency of zero corresponds to the case where the transparent cross-section is equal to the distorted cross-section. This definition of the transparency is reminiscent of the definition given to the absorption in Equation 4.1; indeed, the two are related simply by

$$T = 1 - \frac{A_t}{A_d},$$ (5.12)

where A_t and A_d are the absorption with and without transparency effects.
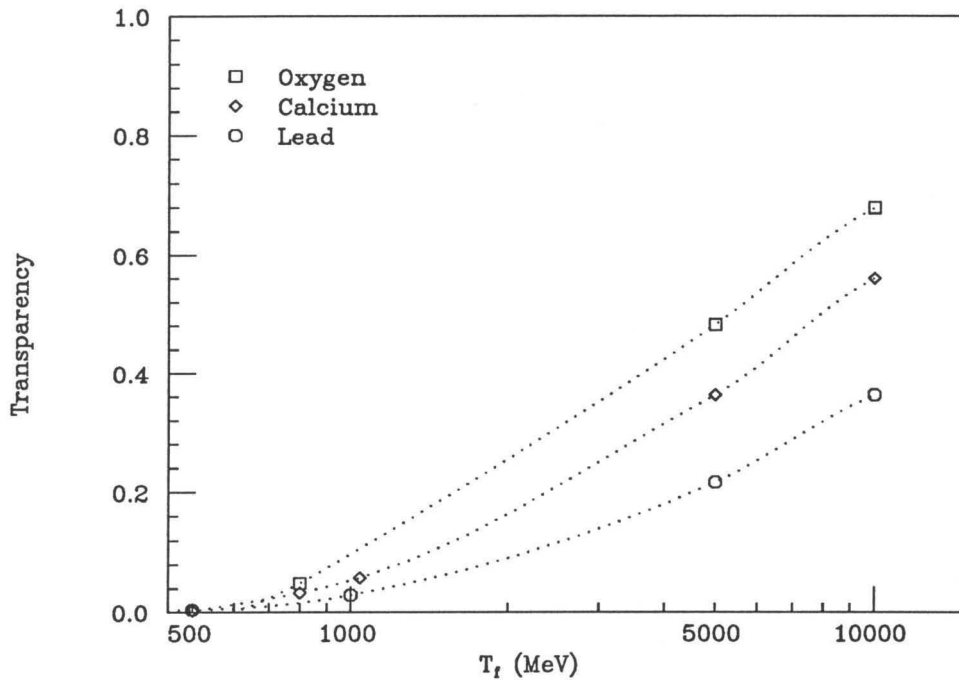
Figure 5.2 – Transparency as a function of energy and nucleus. The transparency, T, is plotted as a function of the kinetic energy of the outgoing proton for oxygen, calcium, and lead. Note that, using the definition of Equation 5.11, the transparency observed in oxygen at a fixed energy is actually greater than the transparency observed in lead at the same energy.

Transparency is plotted as a function of energy and nucleus in Figure 5.3. The transparency rises monotonically with energy as it should, becoming appreciable for $T_f \simeq 1$ GeV. By 10 GeV, it is an important effect. At a fixed energy, the transparency increases for decreasing A, because the hadronization length is a larger fraction of the smaller nuclear radius.

Another quantity of interest is the absolute size of the color transparency effect. Whereas T is defined to be the enhancement due to transparency *normalized to the distortion*, I define the "raw" enhancement to be

$$E \equiv \frac{\sigma_t}{\sigma_d}. \tag{5.13}$$

While the relative sizes of distortion and transparency are of theoretical interest, the enhancement is the quantity that is significant in determining whether color transparency is experimentally observable. Figure 5.3 shows E as a function of $|q|^2$ for the usual three nuclei.

Note that, at fixed energy, the vertical ordering of the symbols in Figure 5.3 is reversed relative to that found in Figure 5.2. Figure 5.4, which illustrates the proton expansion at several energies, provides a graphical explanation of this behavior. For concreteness, the figure is drawn using the naive parton model for the expansion. Since a greater fraction of the distortion is cancelled out by transparency in oxygen, I have

$$T_{\mathrm{Ox}} > T_{\mathrm{Pb}}; \tag{5.14}$$

however, since the *integrated* effect is larger in lead, I have

$$E_{\mathrm{Ox}} < E_{\mathrm{Pb}}. \tag{5.15}$$
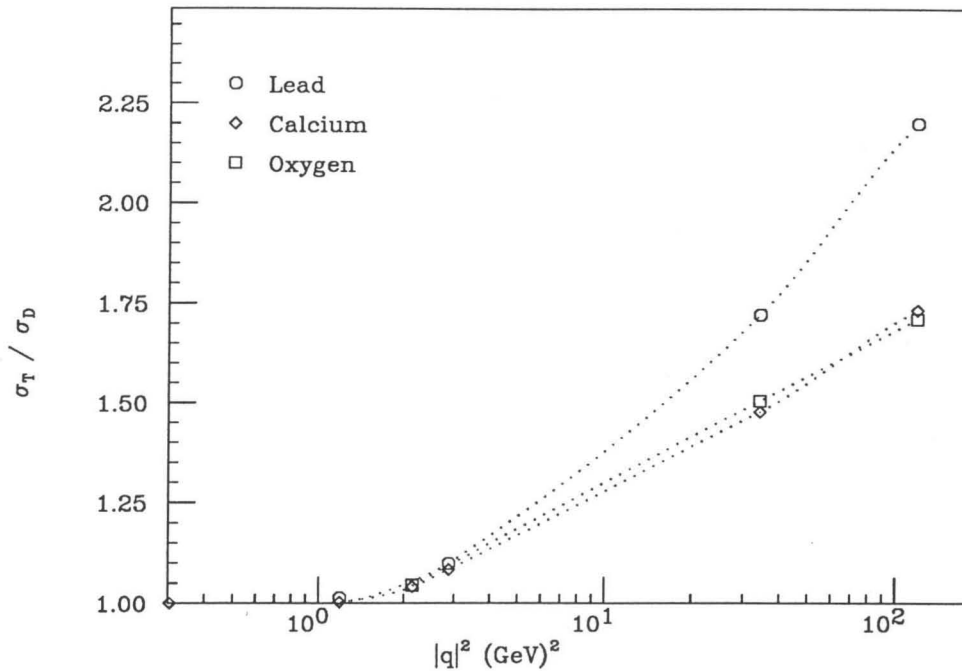
Figure 5.3 − Magnitude of transparency enhancement. The ratio of the total cross-section with transparency effects included to that without any such effects is plotted as a function of the square of the magnitude of the (three-) momentum transfer.

Since the effects of color transparency are of a measurable magnitude, it is interesting to examine whether the details of a particular transparency model are observable. In Figure 5.5, I compare three such models. The solid curve represents the nominal transparency model, the dashed curve represents this same model with the hadronization length parameter artificially doubled, and the dotted curve represents the $\tau = 2$ model. The nominal transparency model, in which the partons separate as fast as physically possible, presents a lower bound on the observable transparency, if the geometric arguments about the initial size of the proton and its interaction cross-section are to be believed.
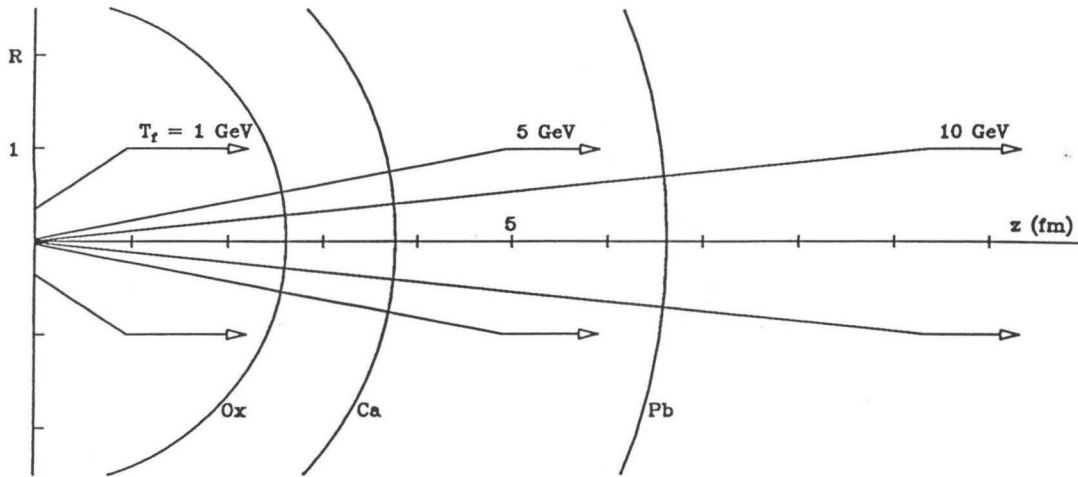
Figure 5.4 – Geometry of (naive parton) expansion at 1, 5, and
10 GeV. The circles represent the nuclear radii, and the scal-
ing function, $R(z)$, is plotted along the vertical axis at several
different proton kinetic energies.

The transparency is fairly sensitive to both l_h and τ. Doubling l_h or setting τ
equal to two each cause an increase of approximately fifty percent T.
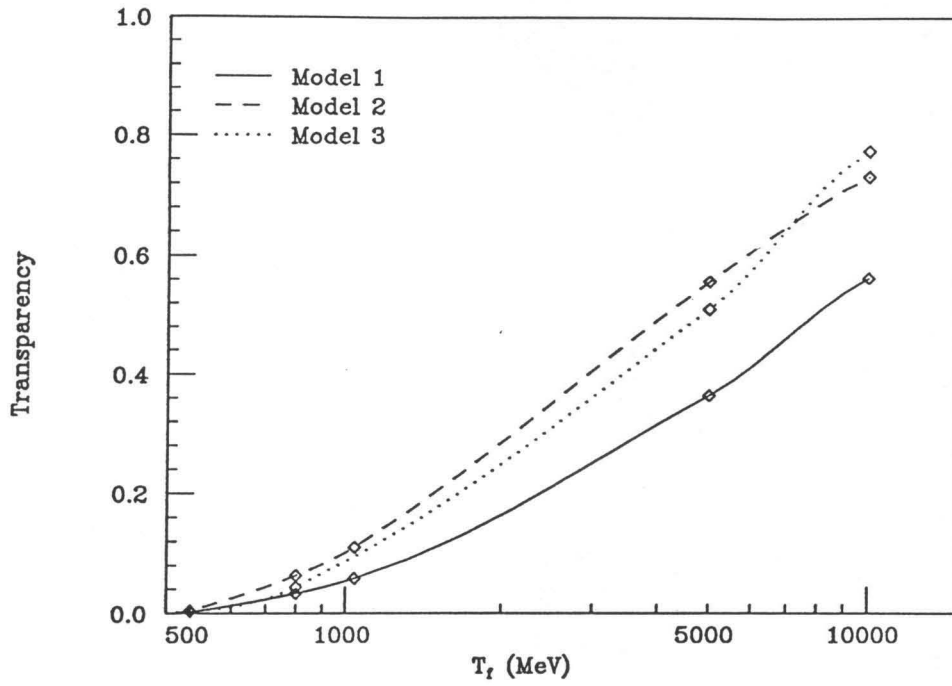
Figure 5.5 − Model dependence of transparency effect. Transparencies are plotted for the Calcium nucleus using three different models: the solid curve is the result of the nominal transparency model. The dashed curve is the result of doubling the hadronization length parameter. The dotted curve was calculated by considering quadratic, rather than linear, expansion.

Chapter 6
Summary

I performed calculations of high momentum-transfer, quasielastic electron scattering from nuclei using three theoretical models. The first of these is a semiclassical model based on a simple picture of absorption governed by the mean free path of the proton in the nuclear medium; the primary physics input to this calculation is the nuclear density distribution. The second is a fully relativistic, quantum mechanical model of the reaction that includes the effects of final-state interactions via an eikonal approximation; its essential inputs are an initial bound state wavefunction, a nuclear current, and an optical potential describing the distortion of the final-state wavefunction. The third model is an extension of the second, and includes color transparency effects.

The results of the microscopic calculation and those of the semiclassical calculation agree very well—to within five percent—in their predictions of the magnitude of the attenuation suffered by the outgoing proton. Since the uncertainty in the microscopic calculation itself is of this same size, I conclude that the essential physics is semiclassical. Surface diffuseness alone causes a 30% decrease in absorption, an effect much larger than the effects of quantum mechanics and relativity combined. The proton escape probability displays the expected $A^{-\frac{1}{3}}$ behavior in both models.

Conclusions that can be drawn from the microscopic calculations beyond the semiclassical results include: (1) The eikonal approximation used to calculate the

distortion of the final state is accurate for outgoing kinetic energies as low as several hundred MeV, (2) The response of the nucleus to the reaction is unexpectedly sensitive to the small spin-dependent part of the distorting potential. This potential causes an overall decrease in the absorption (as much as 50% at very low energies) and a radical enhancement of the transverse-transverse response function, (3) The longitudinal response function is increasingly suppressed relative to the transverse response function at high energies; nonrelativistic approaches have failed to account for this experimentally-observed behavior.

An analysis of the variance in the results of distorted-wave calculations performed with different inputs shows that most of their uncertainty arises from the choice of an optical potential, and relatively little from the bound-state wavefunction. The overall magnitude of the uncertainty is less than 10%; results of the calculation were not greatly sensitive to large changes in the more poorly-constrained parts of the distorting potentials.

Color transparency effects are of the order of a few percent for $Q^2 = 1$ GeV^2 and ten percent for $Q^2 = 10$ GeV^2. For a Q^2 of 100, the (albeit tiny) cross-section is increased by a factor of two in the presence of transparency. The experiment running presently at SLAC with Q^2 up to 7 can thus be expected to see a small amount of transparency. The various transparency models differ in their predictions by approximately 20%, and thus are probably not distinguishable for Q^2 below 10.

Appendix A
Nuclear Current Matrix Elements

Complete detailed expressions for the nuclear current matrix elements are derived.

I begin with the general nuclear current matrix element for the $(e, e'p)$reaction

$$\mathcal{J}^\mu \equiv \langle \Psi_F \,|\, \widehat{J}^\mu \,|\, \Psi_I \rangle. \qquad (A.1)$$

In the distorted wave impulse approximation (DWIA), the initial state consists of a bound proton, whose wavefunction is characterized by i, and $(A-1)$ "spectator" nucleons, properly antisymmetrized; the final state consists of an outgoing proton of momentum $\mathbf{k}$ and spin s, and the $(A-1)$ other nucleons in some final configuration

$$\mathcal{J}^\mu(q) = \langle \psi_{\mathbf{k},s}^{(-)} \, \psi_F^{A-1} \,|\, \widehat{J}^\mu(q) \,|\, \psi_i \, \psi_I^{A-1} \rangle. \qquad (A.2)$$

The index, i, is an abbreviation for the complete set quantum numbers which describe the bound state

$$i \equiv (n, j, l, m, t). \qquad (A.3)$$

The DWIA allows the matrix element to be factored into spectator degrees of freedom, which obey the closure approximation, and ejectile degrees of freedom

$$\mathcal{J}^\mu(q) = \langle \psi_F^{A-1} \,|\, \psi_I^{A-1} \rangle \, \langle \psi_{\mathbf{k},s}^{(-)} \,|\, \widehat{J}^\mu(q) \,|\, \psi_i \rangle = \langle \psi_{\mathbf{k},s}^{(-)} \,|\, \widehat{J}^\mu(q) \,|\, \psi_i \rangle. \qquad (A.4)$$

Since the scattered state wavefunction in position space contains differential operators which are simplest when they can be regarded as operating on everything lying to their right, I take the complex conjugate of the matrix element

$$\mathcal{J}^{\mu*}(q) = \langle \psi_i \, | \, \widehat{J}^{\mu \, \dagger}(q) \, | \, \psi_{\mathbf{k},s}^{(-)} \rangle. \qquad (A.5)$$

Using the normalization conventions

$$\langle \, p \, \alpha \, | \, p' \, \beta \, \rangle = (2\pi)^3 \delta^3(\mathbf{p}' - \mathbf{p}) \, \delta_{\alpha\beta} \qquad \text{and}$$

$$\langle \, r \, \alpha \, | \, r' \, \beta \, \rangle = \delta^3(\mathbf{r}' - \mathbf{r}) \, \delta_{\alpha\beta}, \qquad (A.6)$$

the matrix element is expanded by inserting (position space) identity operators before and after the current operator. Assuming that $\widehat{J}^\mu(q)$ is just the current of a free nucleon, (i.e. that the nuclear environment does not change the properties of a nucleon too much), the (adjoint) current operator has as its position space representation

$$\langle \, r \, \alpha \, | \, \widehat{J}^{\mu \, \dagger}(q) \, | \, r' \, \beta \, \rangle = e^{-i\mathbf{q}\cdot\mathbf{r}} \delta^3(\mathbf{r}' - \mathbf{r}) \left[J^{\mu \, \dagger}(q) \right]_{\alpha\beta}, \qquad (A.7)$$

where the matrices J^μ are

$$J^\mu(q) = \gamma^0 \left[F_1(q^2)\gamma^\mu + i\frac{F_2(q^2)}{2M}\sigma^{\mu\nu}q_\nu \right]. \qquad (A.8)$$

F_1 and F_2 are the usual nucleon form factors and are computed using a parameterization of their experimental values. The delta function in the current operator cancels one of the space integrals, leaving

$$\mathcal{J}^{\mu*}(q) = \int d^3r \, \psi_i^{\dagger}(\mathbf{r}) \, e^{-i\mathbf{q}\cdot\mathbf{r}} \, J^{\mu \, \dagger}(q) \, \psi_{\mathbf{k},s}^{(-)}(\mathbf{r}). \qquad (A.9)$$

All spinor algebra is performed in the Dirac-Pauli representation

$$\gamma^0 = \begin{bmatrix} I & 0 \\ 0 & -I \end{bmatrix} \qquad (A.10)$$

and

$$\gamma^a = \begin{bmatrix} 0 & \sigma^a \\ -\sigma^a & 0 \end{bmatrix}. \qquad (A.11)$$

From Section 3.4, the bound state wavefunction is

$$\psi_i(\mathbf{r}) = \frac{1}{r} \begin{bmatrix} i\,G_{n\kappa t}(r)\,\Phi_{+\kappa,m}(\Omega) \\ -\,F_{n\kappa t}(r)\,\Phi_{-\kappa,m}(\Omega) \end{bmatrix} \eta_t. \qquad (A.12)$$

The notation κ is discussed in that section. For the remainder of this appendix, the quantum numbers n, κ, m, and t will be dropped; all subsequent equations implicitly refer to proton knockout from a *single* nuclear shell. In this notation, $\Phi_{\pm\kappa,m}$ will be denoted simply $\Phi_\pm$. This bound state wavefunction is normalized to unity.

The scattered wavefunction (Section 3.2) is

$$\psi_{\mathbf{k},s}^{(-)}(\mathbf{r}) = N_S \left[D\,(r)^{-\frac{1}{1}}\,(\boldsymbol{\sigma}\cdot\mathbf{p}) \right] e^{i\mathbf{k}\cdot\mathbf{r}} e^{iS(\mathbf{r})}\chi_s, \qquad (A.13)$$

where $D(r) = E + M + V_s(r) - V_v(r)$.

The crucial quantity to be evaluated is the integrand in equation A.9

$$\mathcal{I}^\mu \equiv \psi_i^\dagger(\mathbf{r})\,e^{-i\mathbf{q}\cdot\mathbf{r}}\,J^{\mu\,\dagger}(q)\,\psi_{\mathbf{k},s}^{(-)}(\mathbf{r}). \qquad (A.14)$$

Consider first the time component of the 4-vector integrand. In so doing, I sacrifice the manifest covariance of the formalism to derive an expression that is amenable to

actual computation. In the Dirac-Pauli representation, the time component of the current matrix is

$$\mathcal{J}^{0\,\dagger}(q) = F_1(q^2) \begin{bmatrix} I & 0 \\ 0 & I \end{bmatrix} - \widetilde{F}_2(q^2) \sum_{a=x,y,z} q^a \begin{bmatrix} 0 & \sigma^a \\ -\sigma^a & 0 \end{bmatrix}, \qquad (A.15)$$

where the spacetime indices of the momentum transfer have been raised according to

$$q_a = -q^a \qquad \text{and} \qquad q_0 = q^0, \qquad (A.16)$$

thus leaving an expression involving (non-lorentz) sums over repeated (upper) space indices, which are indicated by small roman letters. The nucleon mass has been absorbed into the second form factor via

$$\widetilde{F}_2(q^2) \equiv \frac{F_2(q^2)}{2M}. \qquad (A.17)$$

The general approach is to first decompose Dirac 4-component spinors and 4x4 matrix operators into Pauli 2-component "spinors" and 2x2 matrix operators, and then to express the full nuclear current matrix element as an integral of (scalar) matrix elements in the two-dimensional Pauli spin space. Performing the first of these reductions on $\mathcal{I}^0$ yields

$$\begin{aligned}
\mathcal{I}^0 = N_S\, F_1\, \frac{1}{r}\, e^{-i\mathbf{q}\cdot\mathbf{r}} &\left[-i\, G(r)\, \Phi_+^\dagger\, e^{i\mathbf{k}\cdot\mathbf{r}}\, e^{iS(\mathbf{r})}\chi_s - \right. \\
&\left. \frac{F(r)}{D(r)}\Phi_-^\dagger\, (\boldsymbol{\sigma}\cdot\mathbf{p})\, e^{i\mathbf{k}\cdot\mathbf{r}}\, e^{iS(\mathbf{r})}\chi_s \right] + \\
N_S\, \widetilde{F}_2\, \frac{1}{r}\, e^{-i\mathbf{q}\cdot\mathbf{r}} &\left[\; i\frac{G(r)}{D(r)}\Phi_+^\dagger\, \sigma^a\, (\boldsymbol{\sigma}\cdot\mathbf{p})\, e^{i\mathbf{k}\cdot\mathbf{r}}\, e^{iS(\mathbf{r})}\chi_s - \right. \\
&\left. F(r)\, \Phi_-^\dagger\, \sigma^a\, e^{i\mathbf{k}\cdot\mathbf{r}}\, e^{iS(\mathbf{r})}\chi_s \right] q^a.
\end{aligned} \qquad (A.18)$$

The angular momentum eigenstates of the bound proton, $\Phi_\pm$, are just projections of the states of total angular momentum j and orbital angular momentum $l^\pm$ onto states of definite m

$$\Phi_\pm(\Omega) = \begin{pmatrix} \langle l^\pm \, (m - \tfrac{1}{2}) \, \tfrac{1}{2} \; \tfrac{1}{2} | jm \rangle \, Y_{l^\pm}^{m - \frac{1}{2}}(\Omega) \\ \langle l^\pm \, (m + \tfrac{1}{2}) \, \tfrac{1}{2} \; -\tfrac{1}{2} | jm \rangle \, Y_{l^\pm}^{m + \frac{1}{2}}(\Omega) \end{pmatrix}, \tag{A.19}$$

where $l^\pm$ is defined to be $l(\pm\kappa)$. These spin spherical harmonics can be written compactly as

$$\Phi_\pm(\Omega) = \sum_{\alpha=1}^{2} \mathcal{C}_\alpha^\pm \, Y_{l^\pm}^{m_\alpha}(\Omega) \, \chi_\alpha, \tag{A.20}$$

with $m_1 = m - \tfrac{1}{2}$ and $m_2 = m + \tfrac{1}{2}$. The Clebsch-Gordan coefficients

$$\begin{aligned} \mathcal{C}_1^\pm &\equiv \langle l^\pm \, m_1 \, \tfrac{1}{2} \; \tfrac{1}{2} | jm \rangle \qquad \text{and} \\ \mathcal{C}_2^\pm &\equiv \langle l^\pm \, m_2 \, \tfrac{1}{2} \; -\tfrac{1}{2} | jm \rangle, \end{aligned} \tag{A.21}$$

can be evaluated algebraically; they are

$$\mathcal{C}_1^\pm = \begin{cases} -\sqrt{\dfrac{l^\pm - m_1}{2l^\pm + 1}}, & \kappa > 0 \\ \sqrt{\dfrac{l^\pm + m_1 + 1}{2l^\pm + 1}}, & \kappa < 0 \end{cases} \qquad \text{and} \qquad \mathcal{C}_2^\pm = \begin{cases} \sqrt{\dfrac{l^\pm + m_2}{2l^\pm + 1}}, & \kappa > 0 \\ \sqrt{\dfrac{l^\pm - m_2 - 1}{2l^\pm + 1}}, & \kappa < 0. \end{cases} \tag{A.22}$$

The vectors χ_1 and χ_2 are the (two-dimensional) basis spin states. It is the adjoint of this spin spherical harmonic that appears in $\mathcal{I}^\mu$; in addition, it is convenient to make explicit its azimuthal dependence. Thus I recast equation A.20 as

$$\Phi_\pm^\dagger(\Omega) = \sum_{\alpha=1}^{2} \mathcal{C}_\alpha^\pm \, f_\alpha^\pm(\theta) \, e^{-im_\alpha \phi} \chi_\alpha^\dagger, \tag{A.23}$$

where f is the ϕ-independent part of the spherical harmonic

$$f_\alpha^\pm(\theta) = e^{im_\alpha \phi} Y_{l^\pm}^{m_\alpha}(\Omega)^* = \sqrt{\frac{2l^\pm + 1}{4\pi} \frac{(l^\pm - m_\alpha)!}{(l^\pm + m_\alpha)!}} P_{l^\pm}^{m_\alpha}(\cos\theta). \tag{A.24}$$

The sign convention for the associated Legendre polynomial is that of Jackson [35].

With these expressions in hand, I define azimuthally-averaged Pauli matrix elements. These must must include the factors $e^{iS(\mathbf{r})}$ and $e^{i\mathbf{q}\cdot\mathbf{r}}$ as well since they depend on ϕ

$$
\mathcal{P}_\alpha^1 \equiv \int_0^{2\pi} d\phi\, e^{-i\mathbf{q}\cdot\mathbf{r}}\, e^{-im_\alpha\phi} \left[\chi_\alpha^\dagger e^{i\mathbf{k}\cdot\mathbf{r}}\, e^{iS(\mathbf{r})} \chi_s \right]
$$

$$
\mathcal{P}_\alpha^2 \equiv \int_0^{2\pi} d\phi\, e^{-i\mathbf{q}\cdot\mathbf{r}}\, e^{-im_\alpha\phi} \left[\chi_\alpha^\dagger (\boldsymbol{\sigma}\cdot\mathbf{p})\, e^{i\mathbf{k}\cdot\mathbf{r}}\, e^{iS(\mathbf{r})} \chi_s \right]
$$

$$
\mathcal{P}_\alpha^{3,a} \equiv \int_0^{2\pi} d\phi\, e^{-i\mathbf{q}\cdot\mathbf{r}}\, e^{-im_\alpha\phi} \left[\chi_\alpha^\dagger \sigma^a (\boldsymbol{\sigma}\cdot\mathbf{p})\, e^{i\mathbf{k}\cdot\mathbf{r}}\, e^{iS(\mathbf{r})} \chi_s \right]
$$

$$
\mathcal{P}_\alpha^{4,a} \equiv \int_0^{2\pi} d\phi\, e^{-i\mathbf{q}\cdot\mathbf{r}}\, e^{-im_\alpha\phi} \left[\chi_\alpha^\dagger \sigma^a e^{i\mathbf{k}\cdot\mathbf{r}}\, e^{iS(\mathbf{r})} \chi_s \right].
$$

$$(A.25)$$

In terms of these (still not completely specified) functions, the ϕ-integrated matrix element is

$$
\int_0^{2\pi} d\phi\, \mathcal{I}^0 = N_S\, F_1\, \frac{1}{r} \left[-i\, G(r)\, \mathcal{C}_\alpha^+ f_\alpha^+(\theta)\, \mathcal{P}_\alpha^1(r,\theta) - \frac{F(r)}{D(r)} \mathcal{C}_\alpha^- f_\alpha^-(\theta)\, \mathcal{P}_\alpha^2(r,\theta) \right] +
$$
$$
N_S\, \widetilde{F}_2\, \frac{1}{r} \left[i\frac{G(r)}{D(r)} \mathcal{C}_\alpha^+ f_\alpha^+(\theta)\, \mathcal{P}_\alpha^{3,a}(r,\theta) - F(r)\, \mathcal{C}_\alpha^- f_\alpha^-(\theta)\, \mathcal{P}_\alpha^{4,a}(r,\theta) \right] q^a,
$$

$$(A.26)$$

where sums over α and repeated upper roman indices are implied. Finally, the integral over the remaining two space coordinates, r and $x \equiv \cos\theta$, is carried out. It is shown only symbolically here since in practice it must be evaluated numerically

$$
\mathcal{J}^{0*} = \int_{x=-1}^{1} \int_{r=0}^{\infty} r^2\, dr\, dx \left[\int_{\phi=0}^{2\pi} d\phi\, \mathcal{I}^0 \right](r,x).
$$

$$(A.27)$$

A similar expression can be derived for the spacelike components of the nuclear current. Only the nuclear current matrix differs; in this case it is

$$J^{a\,\dagger}(q) = F_1 \begin{bmatrix} 0 & \sigma^a \\ \sigma^a & 0 \end{bmatrix} + \widetilde{F}_2 \begin{bmatrix} 0 & -\sigma^a \\ \sigma^a & 0 \end{bmatrix} q^0 + i\widetilde{F}_2 \begin{bmatrix} \sigma^c & 0 \\ 0 & -\sigma^c \end{bmatrix} \epsilon^{abc} q^b. \qquad (A.28)$$

Substituting this matrix into equation A.14 and performing the azimuthal integration as before yields

$$\int_0^{2\pi} d\phi\, \mathcal{I}^a = N_S\, F_1\, \frac{1}{r}\left[-i\frac{G(r)}{D(r)}\mathcal{C}_\alpha^+ f_\alpha^+(\theta)\, \mathcal{P}_\alpha^{3,a}(r,\theta) - F(r)\mathcal{C}_\alpha^- f_\alpha^-(\theta)\, \mathcal{P}_\alpha^{4,a}(r,\theta) \right] +$$

$$N_S\, \widetilde{F}_2\, \frac{1}{r}\left[i\frac{G(r)}{D(r)}\mathcal{C}_\alpha^+ f_\alpha^+(\theta)\, \mathcal{P}_\alpha^{3,a}(r,\theta) - F(r)\mathcal{C}_\alpha^- f_\alpha^-(\theta)\, \mathcal{P}_\alpha^{4,a}(r,\theta) \right] q^0 +$$

$$N_S\, \widetilde{F}_2\, \frac{1}{r}\left[G(r)\mathcal{C}_\alpha^+ f_\alpha^+(\theta)\, \mathcal{P}_\alpha^{4,c}(r,\theta) + i\frac{F(r)}{D(r)}\mathcal{C}_\alpha^- f_\alpha^-(\theta)\, \mathcal{P}_\alpha^{3,c}(r,\theta) \right] \epsilon^{abc} q^b.$$
$$(A.29)$$

This expression is also integrated over r and θ numerically

$$\mathcal{J}^{a*} = \int_{x=-1}^{1} \int_{r=0}^{\infty} r^2\, dr\, dx \left[\int_{\phi=0}^{2\pi} d\phi\, \mathcal{I}^a \right] (r,x). \qquad (A.30)$$

The $\cos\theta$-integration is done using a 20- or 32-point Gauss-Legendre quadrature formula [36], and the r-integration is performed using Simpson's rule, also with 20 to 30 integration points. Equations A.26 through A.30 complete the prescription for calculating the nuclear current matrix elements except for the evaluation of the azimuthally-averaged Pauli matrix elements. I conclude the appendix with that evaluation.

All eight of the Pauli matrix elements (equation A.25) depend on the exponential of the eikonal phase,

$$S(\mathbf{r}) = S_1(\mathbf{r}) + S_2(\mathbf{r})\, \boldsymbol{\sigma}\cdot\hat{\mathbf{n}}, \qquad (A.31)$$

and on its derivatives and its products with other Pauli matrices. An application of the relation

$$\exp\left[ia + ib\boldsymbol{\sigma}\cdot\mathbf{c}\right] = e^{ia}\left[\cos bc + i\,\boldsymbol{\sigma}\cdot\hat{\mathbf{c}}\,\sin bc\right] \qquad (A.32)$$

yields

$$
\begin{aligned}
e^{iS(\mathbf{r})} &= e^{iS_1(\mathbf{r})}\left[\cos S_2(\mathbf{r}) + i\,\boldsymbol{\sigma}\cdot\hat{\mathbf{n}}\sin S_2(\mathbf{r})\right] \\
&= \mathcal{C}(r,\theta)\,I + i\,\mathcal{S}(r,\theta)\,\boldsymbol{\sigma}\cdot\hat{\mathbf{n}}.
\end{aligned}
\qquad (A.33)
$$

The sole azimuthal dependence of this operator is contained in the vector $\hat{\mathbf{n}}$,

$$\hat{\mathbf{n}} = (\sin\phi, \cos\phi, 0). \qquad (A.34)$$

Using the coordinate system defined in Section 3.1, the vector dot products are

$$
\begin{aligned}
\mathbf{k}\cdot\mathbf{r} &= kr\cos\theta \qquad \text{and} \\
\mathbf{q}\cdot\mathbf{r} &= q^x b\cos\phi + q^z z,
\end{aligned}
\qquad (A.35)
$$

where

$$
\begin{aligned}
\mathbf{k} &= (\mathbf{0}, k) = (0, 0, k)\,, \\
\mathbf{q} &= (\mathbf{q}_\perp, q^z) = (q^x, 0, q^z) \qquad \text{and} \\
\mathbf{r} &= (\mathbf{b}, z) = (b\cos\phi, b\sin\phi, z).
\end{aligned}
\qquad (A.36)
$$

There are five azimuthal integrals which appear in the matrix elements; they are

$$A_n(m, z) \equiv \int_0^{2\pi} d\phi\, e^{-im\phi} e^{iz\cos\phi} f_n(\phi), \qquad (A.37)$$

where the functions $f_n(\phi)$ are

$$
\begin{aligned}
f_1(\phi) &= 1, \qquad f_2(\phi) = \sin\phi, \qquad f_3(\phi) = \cos\phi, \\
&f_4(\phi) = \sin 2\phi, \qquad f_5(\phi) = \cos 2\phi.
\end{aligned}
\qquad (A.38)
$$

These can be evaluated analytically in terms of ordinary Bessel functions to be

$$A_1(m, z) = 2\pi i^m J_m(z)$$

$$A_2(m, z) = -\pi i^m \left[J_{m-1}(z) + J_{m+1}(z) \right]$$

$$A_3(m, z) = \pi i^{m-1} \left[J_{m-1}(z) - J_{m+1}(z) \right] \qquad (A.39)$$

$$A_4(m, z) = \pi i^{m-1} \left[-J_{m-2}(z) + J_{m+2}(z) \right]$$

$$A_5(m, z) = -\pi i^m \left[J_{m-2}(z) + J_{m+2}(z) \right].$$

I use $\mathcal{C}_r$ and $\mathcal{S}_r$ to denote derivatives with respect to r of the functions $\mathcal{C}$ and $\mathcal{S}$, and similarly define $\mathcal{C}_\theta$ and $\mathcal{S}_\theta$. The matrix elements of σ^a and of the identity matrix between the initial states of spin α and the final state of spin s are denoted S^a and S^0, respectively. Finally, the Pauli spin algebra (which is straightforward, but long) was performed using *Mathematica*. The result is

$$r\mathcal{P}_\alpha^1 = r\mathcal{C}A_1 S^0 + ir\mathcal{S}S^p$$

$$(A.40)$$

$$r\mathcal{P}_\alpha^2 = \mathcal{S} \left[-A_4 S^0 - iA_5 S^z \right] \frac{1}{\sin\theta} + \mathcal{C}_\theta \left[-i\cos\theta S^q + i\sin\theta A_1 S^z \right] +$$
$$\mathcal{S}_\theta \left[\cos\theta A_4 S^0 + i\sin\theta A_3 S^x + -i\sin\theta A_2 S^y + i\cos\theta A_5 S^z \right] +$$
$$\mathcal{C}_r \left[-ir\sin\theta S^q + -ir\cos\theta A_1 S^z \right] +$$
$$\mathcal{S}_r \left[r\sin\theta A_4 S^0 + -ir\cos\theta A_3 S^x + ir\cos\theta A_2 S^y + ir\sin\theta A_5 S^z \right]$$

$$(A.41)$$

$$r\mathcal{P}_\alpha^{3,x} = \mathcal{S} \left[-A_4 S^x - A_5 S^y \right] \frac{1}{\sin\theta} + \mathcal{C}_\theta \left[-\cos\theta S^r + \sin\theta A_1 S^y \right] +$$
$$\mathcal{S}_\theta \left[i\sin\theta A_3 S^0 + \cos\theta A_4 S^x + \cos\theta A_5 S^y + \sin\theta A_2 S^z \right] +$$
$$\mathcal{C}_r \left[-r\sin\theta S^r - r\cos\theta A_1 S^y \right] +$$
$$\mathcal{S}_r \left[-ir\cos\theta A_3 S^0 + r\sin\theta A_4 S^x + r\sin\theta A_5 S^y - r\cos\theta A_2 S^z \right]$$

$$(A.42)$$

$$rP_\alpha^{3,y} = S\left[A_5 S^x - A_4 S^y\right]\frac{1}{\sin\theta} + C_\theta\left[-\cos\theta S^s - \sin\theta A_1 S^x\right] +$$

$$S_\theta\left[-i\sin\theta A_2 S^0 - \cos\theta A_5 S^x + \cos\theta A_4 S^y + \sin\theta A_3 S^z\right] +$$

$$C_r\left[-r\sin\theta S^s + r\cos\theta A_1 S^x\right] +$$

$$S_r\left[ir\cos\theta A_2 S^0 - r\sin\theta A_5 S^x + r\sin\theta A_4 S^y - r\cos\theta A_3 S^z\right]$$

$$(A.43)$$

$$rP_\alpha^{3,z} = S\left[-iA_5 S^0 - A_4 S^z\right]\frac{1}{\sin\theta} + C_\theta\left[\cos\theta S^t + i\sin\theta A_1 S^0\right] +$$

$$S_\theta\left[-\sin\theta S^p + i\cos\theta A_5 S^0 + \cos\theta A_4 S^z\right] + C_r\left[-ir\cos\theta A_1 S^0 + r\sin\theta S^t\right] +$$

$$S_r\left[r\cos\theta S^p + ir\sin\theta A_5 S^0 + r\sin\theta A_4 S^z\right]$$

$$(A.44)$$

$$rP_\alpha^{4,x} = rCA_1 S^x + S\left[irA_2 S^0 - rA_3 S^z\right]$$

$$rP_\alpha^{4,y} = rCA_1 S^y + S\left[irA_3 S^0 + rA_2 S^z\right]$$

$$rP_\alpha^{4,z} = rCA_1 S^z + S\left[rA_3 S^x - rA_2 S^y\right],$$

$$(A.45)$$

where each of the matrix elements has been multiplied by r (the product of r^2 from the Jacobian and $\frac{1}{r}$ from the bound state wavefunction). The following definitions have been used to simplify the final results

$$S^p \equiv A_2 S^x + A_3 S^y \qquad S^q \equiv A_3 S^x + A_2 S^y \qquad S^r \equiv iA_3 S^0 - A_2 S^z$$

$$S^s \equiv iA_2 S^0 + A_3 S^z \qquad S^t \equiv A_3 S^y - A_2 S^x.$$

Appendix B
Density-Dependent Optical Potential

I present a relativistic, density-dependent optical model of the interaction between a high-energy proton and a nucleus.

Glauber [25] derives an approximate potential to describe the interaction between an incident particle and the nucleons that comprise a target nucleus: the effective (or "optical") potential due to the collection of nucleons in the target is expressed as a function of the density of target nucleons and empirical two-body scattering amplitudes. I give a brief sketch of that derivation here, paying particular attention to the assumptions employed and the modifications necessary for relativistic kinematics. There remain some technical questions concerning the use of quasielastic- rather than elastic-scattering boundary conditions; these are addressed in Appendix C for an arbitrary complex optical potential.

Glauber begins with the underlying two-body process: the scattering amplitude is related to the phase-shift that the incident particle suffers as a result of its interaction with a target particle by

$$f(\mathbf{k}', \mathbf{k}) = \frac{ik}{2\pi} \int e^{i(\mathbf{k}'-\mathbf{k})\cdot\mathbf{r}} \left[1 - e^{i\chi(\mathbf{b})} \right] d^2\mathbf{b}, \qquad (B.1)$$

where $\mathbf{b}$ is a two-component projection of $\mathbf{r}$ onto a plane perpendicular to $\mathbf{k}$, i.e., an impact parameter. In the eikonal approximation, this phase-shift is a function of the

line integral of the (two-body) potential along k

$$\chi(\mathbf{b}) = -\frac{M}{\hbar^2 k} \int\limits_{-\infty}^{\infty} V(\mathbf{b}, z') \, dz' \, . \tag{B.2}$$

I have written the phase-shift as a function of the incident momentum rather than the incident velocity; this change is the only one needed to obtain a relativistic generalization of Glauber's derivation.

The phase-shift for scattering from a collection of particles is just the density-weighted average of the individual phase-shifts

$$e^{i\chi_{\text{opt}}(\mathbf{b})} = \int |\Psi_0|^2 \prod_{j=1}^{A} e^{i\chi_j(\mathbf{b}-\mathbf{s}_j)} \, d^3 \mathbf{q}_j, \tag{B.3}$$

where $\Psi_0(\mathbf{q}_1, \mathbf{q}_2 \cdots \mathbf{q}_A)$ is the ground-state wavefunction of the target and $\mathbf{q}_j = (\mathbf{s}_j, z_j)$ are the coordinates of the jth particle perpendicular to, and parallel to, k. In the independent-particle approximation, the square of the wavefunction can be factored into a product of single-particle densities

$$|\Psi_0(\mathbf{q}_i)|^2 = \prod_{j=1}^{A} \rho_j(\mathbf{q}_j), \tag{B.4}$$

and the collective phase-shift can then be written

$$e^{i\chi_{\text{opt}}(\mathbf{b})} = \prod_{j=1}^{A} \int \rho_j(\mathbf{q}_j) \, e^{i\chi_j(\mathbf{b}-\mathbf{s}_j)} \, d^3 \mathbf{q}_j. \tag{B.5}$$

After taking logarithms of both sides, it is useful to introduce the functions   .

$$\Gamma_j(\mathbf{b}) \equiv 1 - e^{i\chi_j(\mathbf{b})}. \tag{B.6}$$

Since the single-particle densities are normalized,

$$\int \rho_j(\mathbf{q}_j) \, d^3\mathbf{q}_j = 1, \tag{B.7}$$

the phase-shift is

$$\chi_{\text{opt}}(\mathbf{b}) = -i \sum_{j=1}^{A} \log \left[1 - \int \rho_j(\mathbf{q}_j) \, \Gamma_j(\mathbf{b} - \mathbf{s}_j) \, d^3\mathbf{q}_j \right]. \tag{B.8}$$

The integrals $\int \rho_j \Gamma_j$ are small: by the optical theorem, $\int \Gamma_j d^2\mathbf{b} = \frac{\sigma}{2} = 20$ mb, thus $\int \rho_j \Gamma_j d^3\mathbf{q} \approx \frac{1}{3}$ and higher-order terms in the Taylor expansion of the logarithm may be dropped, leaving

$$\chi_{\text{opt}}(\mathbf{b}) = i \sum_{j=1}^{A} \int \rho_j(\mathbf{q}_j) \, \Gamma_j(\mathbf{b} - \mathbf{s}_j) \, d^3\mathbf{q}_j. \tag{B.9}$$

Physically, this approximation is valid because the range of the interaction is small compared to the typical internucleon separation distance.

For a collection of nucleons, there are only two independent scattering functions, Γ_p and Γ_n. As a further simplification, suppose there is a single function Γ that describes the average scattering properties of a target nucleon. This approximation is quite accurate at high energies, where NN scattering is primarily geometric. Defining an average density

$$\rho(\mathbf{q}) \equiv \frac{1}{A} \sum_{j=1}^{A} \rho_j(\mathbf{q}), \tag{B.10}$$

the total phase-shift becomes

$$\begin{aligned}
\chi_{\text{opt}}(\mathbf{b}) &= iA \int \rho(\mathbf{q}) \, \Gamma(\mathbf{b} - \mathbf{s}) \, d^3\mathbf{q} \\
&= iA \int \Gamma(\mathbf{s}) \, d^2\mathbf{s} \int \rho(\mathbf{b}, z) \, dz,
\end{aligned} \tag{B.11}$$

where the components of the average coordinate are denoted $\mathbf{q} \equiv (\mathbf{s}, z)$, and the argument of Γ has been simplified by again dropping terms of order a^2/R^2. Now the Γ-integral is related to the single-particle amplitude via Equation B.1

$$\int \Gamma(\mathbf{s}) \, d^2\mathbf{s} = \frac{2\pi}{ik} f(0), \tag{B.12}$$

thus the total phase-shift is simply

$$\chi_{\text{opt}}(\mathbf{b}) = \frac{2A\pi}{k} f(0) \int \rho(\mathbf{b}, z) \, dz. \tag{B.13}$$

Comparison with Equation B.2 then requires that the optical potential take the form

$$V_{\text{opt}}(r) = -\frac{2A\pi\hbar^2}{M} f(0) \, \rho(r), \tag{B.14}$$

where $r = |\mathbf{r}|$.

A more general two-particle amplitude might include spin dependence

$$\begin{aligned}
f(\mathbf{k}', \mathbf{k}) &= \mathcal{F}(\mathbf{k}', \mathbf{k}) + (\boldsymbol{\sigma} \cdot \hat{\mathbf{n}}) \, \mathcal{G}(\mathbf{k}', \mathbf{k}) \\
&= \mathcal{F}(\theta) + (\boldsymbol{\sigma} \cdot \hat{\mathbf{n}}) \, \mathcal{G}(\theta),
\end{aligned} \tag{B.15}$$

where, by convention,

$$\hat{\mathbf{n}} = \frac{\mathbf{k} \times \mathbf{k}'}{|\mathbf{k} \times \mathbf{k}'|} \qquad \text{and} \qquad \theta = \frac{\mathbf{k} \cdot \mathbf{k}'}{|\mathbf{k}||\mathbf{k}'|}. \tag{B.16}$$

Following the above derivation with this new amplitude yields the spin-dependent optical potential

$$V_{\text{opt}}(r) = \frac{-2\pi A\hbar^2}{M} \left[\mathcal{F}(0) \, \rho(r) + \frac{i}{\hbar k^2} \mathcal{G}'(0) \frac{1}{r} \frac{d\rho}{dr} (\boldsymbol{\sigma} \cdot \mathbf{L}) \right]. \tag{B.17}$$

The derivatives arise from a Taylor-series expansion of the $(\boldsymbol{\sigma} \cdot \hat{\mathbf{n}})$ term.

The two-particle amplitudes must be taken from experiment. A common parameterization [37] is

$$
\begin{aligned}
\mathcal{F}(q) &= \frac{k\sigma^{NN}}{4\pi} \left(i + \alpha^{NN} \right) e^{-q^2 b_{NN}^2} \\
\mathcal{G}(q) &= \frac{k\sigma^{SO}}{4\pi} \left(i + \alpha^{SO} \right) e^{-q^2 b_{SO}^2} \frac{iq}{2M},
\end{aligned} \tag{B.18}
$$

where $\mathbf{q} = \mathbf{k} - \mathbf{k}'$ and $|\mathbf{k}| = |\mathbf{k}'| = k$. This form is convenient since the optical theorem is manifestly satisfied:

$$
\frac{4\pi}{k} \operatorname{Im} f(0) = \frac{4\pi}{k} \operatorname{Im} \mathcal{F}(0) = \sigma^{NN}. \tag{B.19}
$$

The parameters α, b, and σ are taken from fits to NN scattering data [38, 39].

Appendix C
Optical Potential Boundary Conditions

I derive a simple relationship between an optical potential that obeys outgoing spherical-wave boundary conditions and the corresponding potential that obeys incoming spherical-wave conditions.

Mathematically, a potential that arises from a fundamental (two-body) interaction is a real function of spacetime. When an interaction instead takes place between an incident particle and a *system* of target particles, it is convenient to consider the complex generalization of the real potential: the real part describes the scattering of the incident particle into states of different final momentum as before, while the imaginary part describes absorption of the incident flux by the medium. Of course, the incident particle is not physically "absorbed"; the imaginary part of the potential merely accounts for changes in the internal state of the target. For this appendix only, I distinguish these effective, complex potentials from ordinary real potentials by using script $\mathcal{V}$'s for the former.

Whether real or complex, a potential alone does not completely determine the behavior of the solution to a scattering problem; boundary conditions are also required. There are two such scattering boundary conditions: the usual one in which the final state consists of a scattered (outgoing) spherical wave and an unscattered plane wave, denoted (+); and another, relevant to the (e, e′p) reaction, in which the

initial state consists of an incoming spherical wave and an incoming plane wave, denoted (−). A real, two-body potential is insensitive to the difference between the two types of boundary condition, since it is a local operator and boundary conditions depend on the behavior of wavefunctions at infinity. However, the imaginary part of an effective potential does in general depend on the particular boundary conditions employed. While it is false that $\mathcal{V}^{(+)} = \mathcal{V}^{(-)}$, the two are related; in this appendix I show that they are simply complex conjugates. I follow Feshbach's [40] formal derivation of the many-body optical potential $\mathcal{V}^{(+)}$, and modify it as necessary for quasielastic processes.

Consider a system of $A + 1$ nucleons: A nucleons comprise a target nucleus and the final nucleon is taken to be the projectile. The Hamiltonian for this system can be written

$$H = H_A + T_0 + V, \qquad (C.1)$$

where H_A is the Hamiltonian of the nucleus, T_0 is the kinetic energy of the incident proton, and V is the potential energy of the system. Using the eigenstates of the (undisturbed) nucleus as a basis, the wavefunction of the system can be expanded as

$$\Psi = \sum_i \psi_i u_i, \qquad (C.2)$$

where the bound states obey

$$H_A \psi_i = \epsilon_i \psi_i. \qquad (C.3)$$

Matrix elements of the potential between two bound-state configurations are denoted

$$V_{ij} \equiv (\psi_i \,|\, V \,|\, \psi_j), \qquad (C.4)$$

where round brackets indicate that only target degrees of freedom have been integrated out.

I seek to isolate the dynamics of the projectile, that is, to write a Schrödinger equation for u_0 in which only in the potential term depends on the state of the bound nucleons and $\{u_1, u_2, \ldots\}$. Defining the column vector

$$\Phi \equiv \begin{pmatrix} u_1 \\ u_2 \\ \cdot \\ \cdot \\ \cdot \end{pmatrix}, \tag{C.5}$$

and the row vector

$$\mathbf{V_0}^\dagger = (V_{01}, V_{02}, \ldots), \tag{C.6}$$

the Schrödinger equation for the entire system may be re-expressed as a pair of coupled equations

$$[T_0 + V_{00} - E] \, u_0 = -\mathbf{V_0}^\dagger \Phi$$
$$[\mathbf{H} - E \, \mathbf{I}] \, \Phi = -\mathbf{V_0} \, u_0, \tag{C.7}$$

where $\mathbf{H}$ is a matrix with elements $H_{ij} = T_0 \delta_{ij} + V_{ij} + \epsilon_i \delta_{ij}$. Formally eliminating Φ from the system yields the desired Schrödinger equation

$$\left[T_0 + V_{00} + \mathbf{V_0}^\dagger \frac{1}{E^{(\pm)} \mathbf{I} - \mathbf{H}} \mathbf{V_0} \right] u_0 = E^\pm \, u_0, \tag{C.8}$$

where

$$E^{(\pm)} \equiv E \pm i\eta, \qquad \eta \to 0^+ \tag{C.9}$$

insures that appropriate boundary conditions are satisfied. The optical potential I seek is then the sum of the last two terms in the bracketed expression above:

$$\mathcal{V}^{(\pm)} = V_{00} + \mathbf{V_0}^\dagger \frac{1}{E^{(\pm)}\mathbf{I} - \mathbf{H}} \mathbf{V_0}. \qquad (C.10)$$

The identity operator in the space over which $\mathbf{V_0}^\dagger$ acts is

$$\int d\alpha \int_{\varepsilon_0}^{\infty} d\varepsilon' \, |\Phi(\varepsilon', \alpha)\rangle \, \langle \Phi(\varepsilon', \alpha)|, \qquad (C.11)$$

where ε' is an excitation energy (bounded below by ε_0), and α collectively represents any remaining quantum numbers, such as spin. Inserting this operator into the expression for the potential yields

$$\mathcal{V}^{(\pm)} = V_{00} + \int d\alpha \int_{\varepsilon_0}^{\infty} d\varepsilon' \, \mathbf{V_0}^\dagger \, |\Phi(\varepsilon', \alpha)\rangle \, \frac{1}{E^{(\pm)}\mathbf{I} - \mathbf{H}} \, \langle \Phi(\varepsilon', \alpha)| \, \mathbf{V_0}. \qquad (C.12)$$

Care must be taken when performing the ε' integration; there is a pole at $\varepsilon' = E^{(\pm)}$ and the line of the integration must pass on the correct side of the pole in the complex ε' plane. For outgoing spherical-wave boundary conditions, the contour is shown in Figure C.1.

From complex analysis, the imaginary part of the potential is one half the residue at the pole $E^{(+)}$, which is rounded counterclockwise. For the opposite boundary condition, the only change is that the contour passes the pole above the real axis, in a clockwise sense. The sign of the residue is then reversed, so that

$$\mathrm{Im}\left[\mathcal{V}^{(-)}\right] = -\mathrm{Im}\left[\mathcal{V}^{(+)}\right]. \qquad (C.13)$$
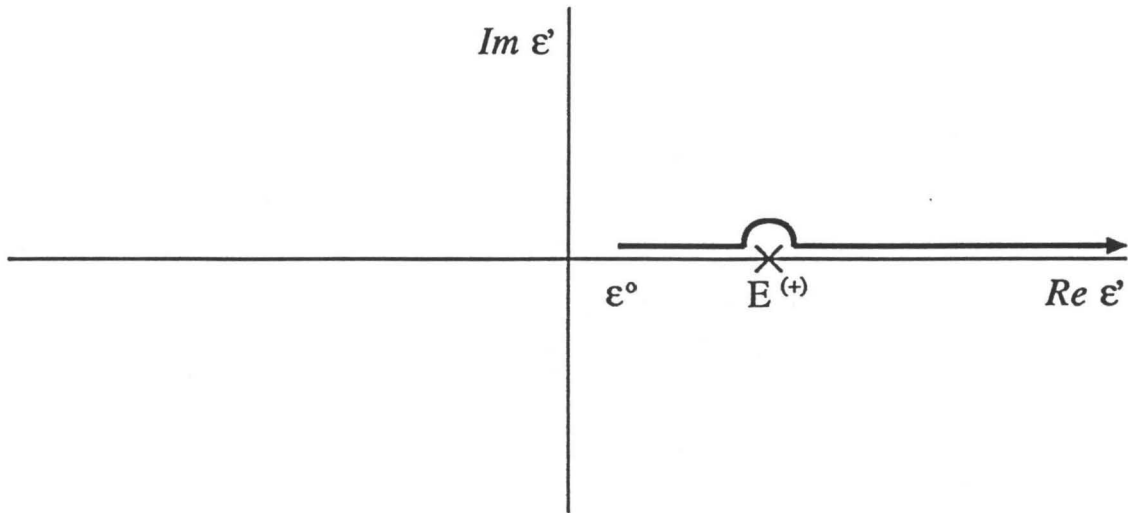
Figure C.1 – Contour of Complex ϵ' Integration

Evidently, the real part is unaffected by the change of boundary conditions, yielding the result

$$\mathcal{V}^{(-)} = \mathcal{V}^{(+)*}. \qquad (C.14)$$

Appendix D
FORTRAN Code

For completeness, I include in this thesis a copy of the FORTRAN 77 code that was used to generate the results presented in Chapters 4 and 5.

```
CPPPPPPPPPPPPPPPPPPPPPPPPPPPPPPPPPPPPPPPPPPPPPPPPPPPPPPPPPPPPPPPPPPPP
C
      PROGRAM RESPONSE
C
C       LATTICE:  R (30) and X (20) and P (300)
C       DISTORTION:  ATTACH FILE WITH SUBROUTINE VOPT
C       COLOR TRANSPARENCY:  MULTIPLIES POTENTIAL ALONG EXIT PATH
C       BOUND STATE:  FROM FURNSTAHL CODE
C
C       COMPUTES THE RESPONSE FUNCTIONS AND TOTAL CROSS SECTION FOR
C       PROTON KNOCKOUT FROM A NUCLEUS
C
C       PHYSICAL INPUTS:
C
C       K        (INPUT,INTEGER)  :  QUANTUM NUMBER OF BOUND STATE
C       TF       (INPUT,REAL)     :  KINETIC ENERGY OF FINAL STATE
C       EI       (INPUT,REAL)     :  TOTAL ENERGY OF INITIAL STATE
C       T2       (INPUT,REAL)     :  AN ARBITRARY REAL NUMBER
C       ETHETA   (INPUT,REAL)     :  ANGLE BTW. INITIAL AND FINAL ELECTRON
C                                    MOMENTUM (SHOULDN'T BE 0.0)
C       PINIT    (INPUT,REAL)     :  MAGNITUDE OF INITIAL ELECTRON MOMENTUM
C       HELICT   (INPUT,REAL)     :  HELICITY OF OUTGOING ELECTRON
C       QSTEP    (INPUT,REAL)     :  INTERVAL FOR Q(PERP)
C       IDIST    (INPUT,INTEGER)  :  0 FOR PLANE WAVES
C                                    1 FOR OPTICAL POTENTIAL (A=40 ONLY)
C                                    2 FOR T-RHO
C
C
C       F (R) , G (R)             :  RADIAL WAVEFUNCTIONS OF BOUND STATE
C                                    GENERATED BY FURNSTAHL QHD CODE
C       VS (R) , VV (R)           :  DIRAC OPTICAL POTENTIALS (SCALAR/VECTOR)
C       PHYSICAL CONSTANTS        :  MASS, MAGNETIC MOMENT OF PROTON
C                                    MASS SCALE IN DIPOLE FORM FACTOR
C
C       NUMERICAL INPUTS:
C
C       NMAX                      :  MAXIMUM NUMBER FOR N OF BOUND STATE
C       RMAX                      :  UPPER LIMIT ON R INTEGRATION
```

```
C         NR                      :  NUMBER OF POINTS IN R INTEGRATION
C         NRV                     :  NUMBER OF POINTS IN POTENTIAL ARRAY
C         NX                      :  NUMBER OF POINTS IN THETA INTEGRATION
C         X(I) , WT(I)            :  GAUSSIAN WEIGHTS, ABSCISSAS (I=1,NX)
C         DELR , DELT             :  USED IN DIFFERENTIAITION
C         DZ                      :  Z STEPSIZE FOR INTEGRATION ALONG EXIT PATH
C         T2                      :  AN ARBITRARY ANGLE, SHOULD NOT BE N*PI/2
C
C         ALL ENERGIES AND MOMENTA ARE INPUT IN MEV AND ALL DISTANCES
C         ARE INPUT IN FERMIS
C
C         ASSUMPTIONS  :
C
C         DISTORTIONS OF FINAL STATE TREATED IN EIKONAL APPROXIMATION
C         DIPOLE FORM FOR PROTON FORM FACTORS
C
      PARAMETER
     *( NR      =    30
     *, NRV     =   300
     *, NX      =    20    )
C
      REAL
     * X       (NX)
     *, WT      (NX)
C
      COMMON /NUMERICS/
     * IR       , DR       , IX
     *, WT       , X        , RMAX
     *, DELR     , DELT     , DZ
     *, QSTEP    , NQS      , DRV
C
      COMPLEX
     * I
C
      COMMON /CONSTANTS/
     * PMASS   , PMU
     *, PKAPPA  , FFS
     *, I       , PI
     *, HC      , ALPHA
     *, IDIST   , ICT
     *, T2
C
      REAL
     * NB      , NS
     *, KZ      , LHADR
C
      COMMON /KINEMATICS/
     * QX       , QZ       , QT
     *, KZ       , E        , P
     *, EI       , K        , L       (2)
     *, J2       , M2       , ML      (2)
     *, MSF      , NB       , NS
     *, TF       , ETHETA   , PINIT
     *, HELICT   , LHADR    , TSHRINK
```

```
      *, IA
C
       COMPLEX
      *  JO         , JX        , JY        , JZ
      *, JOP        , JXP       , JYP       , JZP
      *, JOPP       , JXPP      , JYPP      , JZPP
      *, W01        , W10       , W02       , W20
      *, CRL        , CRP
C
       REAL
      *  KX         , KY
C
       CALL STARTUP
C
       DO 30 II  = 0, NQS
       QX         = II * QSTEP
C
       CALL QXDEPKIN
C
       W00        = 0.0
       W11        = 0.0
       W22        = 0.0
       W01        = (0.0,0.0)
       W10        = (0.0,0.0)
       W02        = (0.0,0.0)
       W20        = (0.0,0.0)
C
       DO 20 M2  = -J2, J2, 2
       DO 10 MSF =  -1,  1, 2
C
       CALL JMU (JO,JX,JY,JZ)
C
       WRITE (8,*) ' QX  = ',QX
       WRITE (8,*) ' M2  = ',M2
       WRITE (8,*) ' MSF = ',MSF
       WRITE (8,*) ' JO  = ',JO
      *,            ' JX  = ',JX
       WRITE (8,*) ' JY  = ',JY
      *,            ' JZ  = ',JZ
C
C         ROTATE J TO NEW FRAME
C
       Q32        = QX**2 + QZ**2
       Q3MAG      = SQRT (Q32)
       Q42        = QT**2 - Q32
       CT1        = QZ / Q3MAG
       ST1        = QX / Q3MAG
       PS         = P / HC
       CT2        = COS (T2)
       ST2        = SIN (T2)
       B          = PI + T2
       CB         = COS (B)
       SB         = SIN (B)
       C2B        = COS (2.0 * B)
```

```
C
C          ROTATE BY T1 ABOUT Y AXIS
C

      JOP          = JO
      JXP          = JX * CT1 - JZ * ST1
      JYP          = JY
      JZP          = JZ * CT1 + JX * ST1
C
C          ROTATE BY T2 ABOUT Z AXIS
C

      JOPP         =  JOP
      JXPP         =  JXP * CT2 - JYP * ST2
      JYPP         =  JYP * CT2 + JXP * ST2
      JZPP         =  JZP
C
C          ADD UP SPIN CONTRIBUTIONS
C

      W00          = W00 + CABS (JOPP) ** 2
      W11          = W11 + CABS (JXPP) ** 2
      W22          = W22 + CABS (JYPP) ** 2
      W01          = W01 + JOPP * CONJG (JXPP)
      W10          = W10 + JXPP * CONJG (JOPP)
      W02          = W02 + JOPP * CONJG (JYPP)
      W20          = W20 + JYPP * CONJG (JOPP)
C
   10 CONTINUE
   20 CONTINUE
C

      SC           = HC ** 3
C

      CRL          = (W02 + W20)
      CRP          = (W10 - W01) * I
C

      RL           =          W00 / (J2 + 1.0)             * SC
      RT           = (W22 + W11) / (J2 + 1.0)              * SC
      RTT          = (W22 - W11) / (J2 + 1.0) / C2B        * SC
      RLT          =  REAL (CRL) / (J2 + 1.0) / SB         * SC
      RLTP         =  REAL (CRP) / (J2 + 1.0) / CB         * SC
C

      IF (ABS(AIMAG(CRL)*SC) .GT. 1E-6)
     *  WRITE (6,*) ' NONZERO IMAG (CRL) = ',AIMAG(CRL)*SC
      IF (ABS(AIMAG(CRP)*SC) .GT. 1E-6)
     *  WRITE (6,*) ' NONZERO IMAG (CRP) = ',AIMAG(CRP)*SC
C

      SMOTT        = ALPHA * COS (ETHETA/2.0)
     *              / (2.0 * PINIT * SIN (ETHETA/2.0) ** 2)
      SMOTT        = SMOTT ** 2
C

      TEMP3        = TAN (ETHETA/2.0)
      TEMP1        = TEMP3 ** 2
      TEMP2        = Q42 / Q32
C

      TEMP4        = (             TEMP2 ** 2.0              ) * RL
     *              + ( TEMP1 - TEMP2   / 2.0               ) * RT
```

```
     *              - (            TEMP2   / 2.0           *  C2B) * RTT
     *              + ((TEMP1 - TEMP2) ** 0.5 * TEMP2 *   SB) * RLT
     *              + (HELICT * TEMP2 * TEMP3            *   CB) * RLTP
C
     STOT       = PMASS * KZ / (2.0 * PI) ** 3 * SMOTT * TEMP4
C
     WRITE (10,*) PS,RL
     WRITE (12,*) PS,RT
     WRITE (14,*) PS,RLT
     WRITE (16,*) PS,RTT
     WRITE (18,*) PS,RLTP
     WRITE (20,*) PS,STOT
C
  30 CONTINUE
     END
C
CSSSSSSSSSSSSSSSSSSSSSSSSSSSSSSSSSSSSSSSSSSSSSSSSSSSSSSSSSSSSSSSSSSSSSSSS
C
     SUBROUTINE STARTUP
C
C      OPENS FILES, WRITES HEADERS, READS INPUT FILES,
C      DOES EVERYTHING THAT ONLY GETS DONE ONCE
C
     PARAMETER
    *( NR      =    30
    *, NRV     =   300
    *, NX      =    20   )
C
     REAL
    * X       (NX)
    *, WT      (NX)
C
     COMMON /NUMERICS/
    * IR       , DR      , IX
    *, WT      , X       , RMAX
    *, DELR    , DELT    , DZ
    *, QSTEP   , NQS     , DRV
C
     COMPLEX
    * I
C
     COMMON /CONSTANTS/
    * PMASS    , PMU
    *, PKAPPA  , FFS
    *, I       , PI
    *, HC      , ALPHA
    *, IDIST   , ICT
    *, T2
C
     REAL
    * NB      , NS
    *, KZ      , LHADR
    *, LHMULT
C
```

```
      COMMON /KINEMATICS/
      *  QX          , QZ        , QT
      *, KZ          , E         , P
      *, EI          , K         , L        (2)
      *, J2          , M2        , ML       (2)
      *, MSF         , NB        , NS
      *, TF          , ETHETA    , PINIT
      *, HELICT      , LHADR     , TSHRINK
      *, IA
C
      REAL
      *  FNK    (0:NR)
      *, GNK    (0:NR)
      *, FSTAR  (2,2,NX)
C
      COMMON /WAVEFN/
      *  FNK      , GNK
      *, FSTAR
C
      REAL
      *  RHO    (0:NRV)
C
      COMMON /DENSITY/
      *  RHO
C
      DATA
      *  PMASS   / 938.27960            /
      *, FFS     / 842.62000            /
      *, HC      / 197.32858            /
      *, PMU     /   2.79000            /
      *, PKAPPA  /   1.79000            /
      *, I       /(  0.00000,  1.00000)/
      *, ALPHA   /   0.0072992701       /
C
      PI        = 4.0 * ATAN (1.0)
C
      IJKL      = 0
C
    5 CONTINUE
C
C        WAIT WHILE FILE BECOMES AVAILABLE
C
      IJKL      = IJKL + 1
      IF (IJKL .GE. 1000) STOP ' CANT OPEN FILE '
      DO IJK    = 1, 100000
      ENDDO
C
C      OPEN FILES
C
      OPEN ( 2,ERR=5     ,STATUS='OLD')
      OPEN ( 4,ERR=5     ,STATUS='OLD')
      OPEN ( 8,FILE='eo0',STATUS='NEW')
      OPEN (10,FILE='eo1',STATUS='NEW')
      OPEN (12,FILE='eo2',STATUS='NEW')
```

```
      OPEN (14,FILE='eo3',STATUS='NEW')
      OPEN (16,FILE='eo4',STATUS='NEW')
      OPEN (18,FILE='eo5',STATUS='NEW')
      OPEN (20,FILE='eo6',STATUS='NEW')
C
C        READ INPUT PARAMETERS
C
      READ (5,*) TF,IA,IDIST,ICT
      READ (5,*)
      READ (5,*) QSTEP,NQS,DZ
      READ (5,*)
      READ (5,*) PINIT,ETHETA,DELT,DELR
      READ (5,*)
      READ (5,*) T2,HELICT,LHMULT
      READ (5,*)
C
C        GAUSSIAN WEIGHTS AND ABSCISSAS
C
      DO 10 JX  = NX/2 + 1, NX
      READ (2,*) X (JX), WT (JX)
  10  CONTINUE
C
      DO 20 JX  = 1, NX/2
      X  (JX)   = - X (NX + 1 - JX)
      WT (JX)   =   WT (NX + 1 - JX)
  20  CONTINUE
C
C        FURNSTAHL WAVEFUNCTION FILE HEADER INFORMATION
C
      READ (4,*)
      READ (4,*)
      READ (4,*) NRDUM,DRDUM
      READ (4,*)
      READ (4,1) K,EI
      READ (4,*)
C
C        SCALE TO RIGHT UNITS (MEV)
C
      IF (MOD (NRDUM,NR ) .NE. 0) STOP ' NR  WRONG '
      IF (MOD (NRDUM,NRV) .NE. 0) STOP ' NRV WRONG '
C
      NSKIP     = NRDUM / NR
      DRDUM     = DRDUM / HC
      DR        = NSKIP * DRDUM
      RMAX      = DR * NR
      DRV       = NRDUM / NRV * DRDUM
C
C        READ FURNSTAHL RADIAL WAVEFUNCTION
C
      DO 50 JR  = 0, NR-1
        READ (4,*) RDUM, GNK (JR), FNK (JR)
        DO 40 ISKIP = 1, NSKIP - 1
        READ (4,*)
  40    CONTINUE
```

```
            GNK (JR) = GNK (JR) * SQRT (HC)
            FNK (JR) = FNK (JR) * SQRT (HC)
   50   CONTINUE
C
        GNK (NR)  = 0.0
        FNK (NR)  = 0.0
C
        CLOSE (2)
        CLOSE (4)
C
C          CHECK NORM OF BOUND STATE
C
        WS          = 4.0
        JR          = 0
C
        GSUM        = GNK (JR) ** 2
        FSUM        = FNK (JR) ** 2
C
        DO 60 JR  = 1, NR-1
C
           GSUM     = GSUM + GNK (JR) ** 2 * WS
           FSUM     = FSUM + FNK (JR) ** 2 * WS
C
           WS       = 6.0 - WS
C
   60   CONTINUE
C
        JR          = NR
C
        GSUM        = (GSUM + GNK (JR) ** 2) * DR / 3.0
        FSUM        = (FSUM + FNK (JR) ** 2) * DR / 3.0
        ANORM       = GSUM + FSUM
C
        WRITE (6,*) ' WAVEFN NORM: ',ANORM
C
C          CHECK NORM OF DENSITY
C
        WS          = 4.0
        JR          = 0
        RDUM        = JR * DRV
        PSUM        = RDUM ** 2 * RHO (JR)
C
        DO 70 JR  = 1, NRV-1
C
           RDUM     = JR * DRV
           PSUM     = PSUM + RDUM ** 2 * RHO (JR) * WS
           WS       = 6.0 - WS
C
   70   CONTINUE
C
        JR          = NRV
        RDUM        = JR * DRV
        PSUM        = (PSUM + RDUM ** 2 * RHO (JR)) * 4.0 * PI * DRV / 3.0
        BNORM       = PSUM
```

```
C
      WRITE (6,*) ' DENSITY NORM: ',BNORM
C
C      THAT KINEMATICS WHICH IS INDEPENDENT OF QX
C      (IF IT DEPENDS ON QX, IT IS DONE IN QXDEPKIN)
C
      EBIND       = PMASS - EI
      QT          = TF + EBIND
      KZ          = SQRT (2.0 * TF * PMASS + TF * TF)
      E           = SQRT (   PMASS * PMASS + KZ * KZ)
      NS          = SQRT ( (E + PMASS) / (2.0 * E) )
      NB          = 1.0
C
C      LHADR IS THE HADRONIZATION LENGTH IN INVERSE MEV
C
      TSHRINK     = 1E6 / KZ / KZ
      LHADR       = KZ / PMASS * 0.81 / HC * (1 - TSHRINK)
      LHADR       = LHADR * LHMULT
C
C      BOUND STATE ANGULAR MOMENTUM
C
      J2          = 2 * ABS (K) - 1
C
      IF (K .GT. 0) THEN
        L (1)   =   K
        L (2)   =   K - 1
      ELSEIF (K .LT. 0) THEN
        L (1)   = - (K + 1)
        L (2)   = - K
      ELSE
        STOP ' KAPPA WAS ZERO '
      ENDIF
C
C      WRITE FILE HEADERS
C
      WRITE (6,*) ' K   = ',K
      WRITE (6,*) ' NX  = ',NX
      WRITE (6,*) ' NR  = ',NR
      WRITE (6,*) ' QT  = ',QT
C
      WRITE (8,*) ' K   = ',K
      WRITE (8,*) ' NX  = ',NX
      WRITE (8,*) ' NR  = ',NR
      WRITE (8,*) ' QT  = ',QT
C
      WRITE (10,*) 'TF,IA,K,IDIST,ICT,NQS+1'
      WRITE (12,*) 'TF,IA,K,IDIST,ICT,NQS+1'
      WRITE (14,*) 'TF,IA,K,IDIST,ICT,NQS+1'
      WRITE (16,*) 'TF,IA,K,IDIST,ICT,NQS+1'
      WRITE (18,*) 'TF,IA,K,IDIST,ICT,NQS+1'
      WRITE (20,*) 'TF,IA,K,IDIST,ICT,NQS+1'
C
      WRITE (10,*) TF,IA,K,IDIST,ICT,NQS+1
      WRITE (12,*) TF,IA,K,IDIST,ICT,NQS+1
```

```
      WRITE (14,*) TF,IA,K,IDIST,ICT,NQS+1
      WRITE (16,*) TF,IA,K,IDIST,ICT,NQS+1
      WRITE (18,*) TF,IA,K,IDIST,ICT,NQS+1
      WRITE (20,*) TF,IA,K,IDIST,ICT,NQS+1
C
C         CALCULATE LOOKUP TABLE FOR OPTICAL POTENTIAL
C
      CALL VOPT
C
C         CALCULATE LOOKUP TABLE FOR INTEGRALS OF OPTICAL POTENTIALS
C
      CALL GETFRT
C
      RETURN
C
C         FORMAT
C
    1 FORMAT (15X,I7,2X,F15.5)
C
      END
C
CSSSSSSSSSSSSSSSSSSSSSSSSSSSSSSSSSSSSSSSSSSSSSSSSSSSSSSSSSSSSSSSSSSSSSS
C
      SUBROUTINE GETFRT
C
C         COMPUTES THE FUNCTIONS C(R,TH) AND S(R,TH) (AND THEIR
C         DERIVATIVES) WHICH DEPEND ON THE INTEGRALS OF THE OPTICAL
C         POTENTIALS (AND THEIR DERIVATIVES)
C         THESE FUNCTIONS ARE COMPUTED OVER THE WHOLE NUCLEUS
C
      PARAMETER
     *( NR       =    30
     *, NRV      =   300
     *, NX       =    20    )
C
      REAL
     * X        (NX)
     *, WT       (NX)
C
      COMMON /NUMERICS/
     * IR       , DR       , IX
     *, WT       , X        , RMAX
     *, DELR     , DELT     , DZ
     *, QSTEP    , NQS      , DRV
C
      COMPLEX
     * I
C
      COMMON /CONSTANTS/
     * PMASS    , PMU
     *, PKAPPA   , FFS
     *, I        , PI
     *, HC       , ALPHA
     *, IDIST    , ICT
```

```fortran
     *, T2
C
      REAL
     *  NB        , NS
     *, KZ        , LHADR
C
      COMMON /KINEMATICS/
     *  QX        , QZ        , QT
     *, KZ        , E         , P
     *, EI        , K         , L        (2)
     *, J2        , M2        , ML       (2)
     *, MSF       , NB        , NS
     *, TF        , ETHETA    , PINIT
     *, HELICT    , LHADR     , TSHRINK
     *, IA
C
      COMPLEX
     *  FRT       (0:NR,NX,6)
C
      COMMON /SPACEFUNC/
     *  FRT
C
      COMPLEX
     *  S1        , S2
     *, S1A       , S2A
     *, S1B       , S2B
     *, S1C       , S2C
     *, S1D       , S2D
     *, DRS1      , DRS2
     *, DTS1      , DTS2
     *, CRT       , SRT
C
C        LOOP OVER SPACE LATTICE
C
      DO 10 IR  = 0, NR
      DO 10 IX  = 1, NX
C
      R         = IR * DR
      TH        = ACOS (X(IX))
      CT        = COS (TH)
      ST        = SIN (TH)
      B         = R * ST
      Z         = R * CT
C
      IF     (R .EQ.  0.0) THEN
        RA      = R + DELR / HC
        RB      = R
        DDR     = DELR / HC
      ELSEIF (R .EQ. RMAX) THEN
        RA      = R
        RB      = R - DELR / HC
        DDR     = DELR / HC
      ELSE
        RA      = R + DELR / HC
```

```
      RB        = R - DELR / HC
      DDR       = DELR / HC * 2.0
      ENDIF
C
      THC       = TH + DELT
      THD       = TH - DELT
C
      IF (RA .LT. 0.0 .OR. RB .LT. 0) STOP ' ERROR IN DS/DR '
C
      CALL S12_LATPT (R ,TH ,S1 ,S2 )
      CALL S12_NOTLP (RA,TH ,S1A,S2A)
      CALL S12_NOTLP (RB,TH ,S1B,S2B)
      CALL S12_NOTLP (R ,THC,S1C,S2C)
      CALL S12_NOTLP (R ,THD,S1D,S2D)
C
      DRS1      = (S1A - S1B) / DDR
      DRS2      = (S2A - S2B) / DDR
      DTS1      = (S1C - S1D) / 2.0 / DELT
      DTS2      = (S2C - S2D) / 2.0 / DELT
C
      CRT       = EXP (I * S1) * COS (S2)
      SRT       = EXP (I * S1) * SIN (S2)
C
C        NOW FILL UP THE FRT ARRAY AT THIS POINT
C
      FRT (IR,IX,1)   = CRT
      FRT (IR,IX,2)   = SRT
      FRT (IR,IX,3)   = CRT * I * (DRS1 + KZ * CT)      - SRT * DRS2
      FRT (IR,IX,4)   = SRT * I * (DRS1 + KZ * CT)      + CRT * DRS2
      FRT (IR,IX,5)   = CRT * I * (DTS1 - KZ * ST * R) - SRT * DTS2
      FRT (IR,IX,6)   = SRT * I * (DTS1 - KZ * ST * R) + CRT * DTS2
C
   10 CONTINUE
      RETURN
      END
C
CSSSSSSSSSSSSSSSSSSSSSSSSSSSSSSSSSSSSSSSSSSSSSSSSSSSSSSSSSSSSSSSSSSSSSS
C
      SUBROUTINE S12_LATPT (R,TH,S1,S2)
C
C        INTEGRATES THE EIKONAL PHASE ALONG THE EXIT PATH STARTING
C        ON A POINT ON THE (BIG) INTEGRATION LATTICE.
C        THE EIKONAL PHASE IS A FUNCTION OF THE OPTICAL POTENTIALS
C        V (CENTRAL) AND V (SPIN-ORBIT)
C        CALCULATES THE FUNCTION (E + M + VS - VV) FROM THE
C        INTEGRAL OF THE SPIN-ORBIT POTENTIAL (THIS ALLOWS IT
C        TO INCLUDE COLOR TRANSPARENCY EFFECTS)
C
      PARAMETER
     *( NR      =    30
     *, NRV     =   300
     *, NX      =    20    )
C
      REAL
```

```fortran
      *  X          (NX)
      *, WT         (NX)
C
         COMMON /NUMERICS/
      *  IR        , DR        , IX
      *, WT        , X         , RMAX
      *, DELR      , DELT      , DZ
      *, QSTEP     , NQS       , DRV
C
         COMPLEX
      *  I
C
         COMMON /CONSTANTS/
      *  PMASS     , PMU
      *, PKAPPA    , FFS
      *, I         , PI
      *, HC        , ALPHA
      *, IDIST     , ICT
      *, T2
C
         REAL
      *  NB        , NS
      *, KZ        , LHADR
C
         COMMON /KINEMATICS/
      *  QX        , QZ        , QT
      *, KZ        , E         , P
      *, EI        , K         , L         (2)
      *, J2        , M2        , ML        (2)
      *, MSF       , NB        , NS
      *, TF        , ETHETA    , PINIT
      *, HELICT    , LHADR     , TSHRINK
      *, IA
C
         COMPLEX
      *  VC         (0:NRV+1)
      *, VSO        (0:NRV+1)
      *, DENOM      (0:NR,NX)
C
         COMMON /POTENTIAL/
      *  VC        , VSO
      *, DENOM
C
         COMPLEX
      *  SUM1      , SUM2      , SUM3
      *, S1        , S2        , VCP
      *, VSOP
C
      Z          = R * COS (TH)
      B          = R * SIN (TH)
C
      ZP         = Z
      RP         = R
C
```

```
C         POTENTIAL VALUES FROM TABLE TABLE
C
      JR        = NRV / NR * IR
C
      VCP       = VC  (JR)
      VSOP      = VSO (JR)
C
C         CALCULATE COLOR TRANSPARENCY FUNCTION
C
      IF (ICT .EQ. 0 .OR. TSHRINK .GE. 1.0) THEN
        RZ      = 1.0
      ELSEIF (ZP-Z .LT. LHADR) THEN
        RZ      = ((ZP - Z) / LHADR) ** ICT * (1.0 - TSHRINK) + TSHRINK
      ELSE
        RZ      = 1.0
      ENDIF
C
C         COLOR TRANSPARENCY FUNCTION MULTIPLIES POTENTIALS
C
      VCP       = VCP  * RZ
      VSOP      = VSOP * RZ
C
      SUM1      = VCP
      SUM2      = VSOP * ZP
      SUM3      = VSOP
C
   10 CONTINUE
C
      ZP        = ZP + DZ / HC
      RP        = SQRT (ZP*ZP + B*B)
C
      IF (RP .GE. RMAX) GO TO 20
C
      RS        = RP / DRV
      JR        = INT (RS)
C
      VCP       = VC  (JR) + (RS - JR) * (VC  (JR+1) - VC  (JR))
      VSOP      = VSO (JR) + (RS - JR) * (VSO (JR+1) - VSO (JR))
C
C         COLOR TRANSPARENCY FUNCTION
C
      IF (ICT .EQ. 0 .OR. TSHRINK .GE. 1.0) THEN
        RZ      = 1.0
      ELSEIF (ZP-Z .LT. LHADR) THEN
        RZ      = ((ZP - Z) / LHADR) ** ICT * (1.0 - TSHRINK) + TSHRINK
      ELSE
        RZ      = 1.0
      ENDIF
C
      VCP       = VCP  * RZ
      VSOP      = VSOP * RZ
C
      SUM1      = SUM1 + 2.0 * VCP
      SUM2      = SUM2 + 2.0 * VSOP * ZP
```

```
      SUM3       = SUM3 + 2.0 * VSOP
C
      GO TO 10
   20 CONTINUE
C
      SUM1       = SUM1 * DZ / HC / 2.0
      SUM2       = SUM2 * DZ / HC / 2.0
      SUM3       = SUM3 * DZ / HC / 2.0
C
C        CALCULATE DENOMINATOR FUNCTION
C
      DENOM (IR,IX)
     *           = (E + PMASS) * EXP (2.0 * PMASS * SUM2)
C
C        I HAVE TO DO V* FOR INCOMING WAVE BOUNDARY CONDITIONS
C
      SUM1       = CONJG (SUM1)
      SUM2       = CONJG (SUM2)
      SUM3       = CONJG (SUM3)
C
C        EIKONAL PHASE
C
      IF (IDIST .EQ. 2) SUM2 = (0.0,0.0)
C
      S1         = SUM1 * PMASS / KZ + SUM2 * PMASS * I
      S2         = SUM3 * PMASS *  B
C
      RETURN
      END
C
CSSSSSSSSSSSSSSSSSSSSSSSSSSSSSSSSSSSSSSSSSSSSSSSSSSSSSSSSSSSSSSSSSSSSSSS
C
      SUBROUTINE S12_NOTLP (R,TH,S1,S2)
C
C        INTEGRATES THE EIKONAL PHASE ALONG THE EXIT PATH STARTING
C        ON A POINT ON THE (BIG) INTEGRATION LATTICE.
C        THE EIKONAL PHASE IS A FUNCTION OF THE OPTICAL POTENTIALS
C        V (CENTRAL) AND V (SPIN-ORBIT)
C
      PARAMETER
     *( NR        =     30
     *, NRV       =    300
     *, NX        =     20    )
C
      REAL
     * X         (NX)
     *, WT        (NX)
C
      COMMON /NUMERICS/
     * IR        , DR       , IX
     *, WT        , X        , RMAX
     *, DELR      , DELT     , DZ
     *, QSTEP     , NQS      , DRV
C
```

```
      COMPLEX
     *  I
C
      COMMON /CONSTANTS/
     *  PMASS    , PMU
     *, PKAPPA   , FFS
     *, I        , PI
     *, HC       , ALPHA
     *, IDIST    , ICT
     *, T2
C
      REAL
     *  NB       , NS
     *, KZ       , LHADR
C
      COMMON /KINEMATICS/
     *  QX       , QZ       , QT
     *, KZ       , E        , P
     *, EI       , K        , L        (2)
     *, J2       , M2       , ML       (2)
     *, MSF      , NB       , NS
     *, TF       , ETHETA   , PINIT
     *, HELICT   , LHADR    , TSHRINK
     *, IA
C
      COMPLEX
     *  VC       (0:NRV+1)
     *, VSO      (0:NRV+1)
     *, DENOM    (0:NR,NX)
C
      COMMON /POTENTIAL/
     *  VC       , VSO
     *, DENOM
C
      COMPLEX
     *  SUM1     , SUM2     , SUM3
     *, S1       , S2       , VCP
     *, VSOP
C
      Z          = R * COS (TH)
      B          = R * SIN (TH)
C
      ZP         = Z
      RP         = R
C
      RS         = RP / DRV
      JR         = INT (RS)
C
C         INTERPOLATE BETWEEN POTENTIAL VALUES IN TABLE
C
      VCP        = VC  (JR) + (RS - JR) * (VC  (JR+1) - VC  (JR))
      VSOP       = VSO (JR) + (RS - JR) * (VSO (JR+1) - VSO (JR))
C
C         CALCULATE COLOR TRANSPARENCY FUNCTION
```

```
C
      IF (ICT .EQ. 0 .OR. TSHRINK .GE. 1.0) THEN
        RZ      = 1.0
      ELSEIF (ZP-Z .LT. LHADR) THEN
        RZ      = ((ZP - Z) / LHADR) ** ICT * (1.0 - TSHRINK) + TSHRINK
      ELSE
        RZ      = 1.0
      ENDIF
C
C       COLOR TRANSPARENCY FUNCTION MULTIPLIES POTENTIALS
C
      VCP       = VCP  * RZ
      VSOP      = VSOP * RZ
C
      SUM1      = VCP
      SUM2      = VSOP * ZP
      SUM3      = VSOP
C
   10 CONTINUE
C
      ZP        = ZP + DZ / HC
      RP        = SQRT (ZP*ZP + B*B)
C
      IF (RP .GE. RMAX) GO TO 20
C
      RS        = RP / DRV
      JR        = INT (RS)
C
      VCP       = VC  (JR) + (RS - JR) * (VC  (JR+1) - VC  (JR))
      VSOP      = VSO (JR) + (RS - JR) * (VSO (JR+1) - VSO (JR))
C
C       COLOR TRANSPARENCY FUNCTION
C
      IF (ICT .EQ. 0 .OR. TSHRINK .GE. 1.0) THEN
        RZ      = 1.0
      ELSEIF (ZP-Z .LT. LHADR) THEN
        RZ      = ((ZP - Z) / LHADR) ** ICT * (1.0 - TSHRINK) + TSHRINK
      ELSE
        RZ      = 1.0
      ENDIF
C
      VCP       = VCP  * RZ
      VSOP      = VSOP * RZ
C
      SUM1      = SUM1 + 2.0 * VCP
      SUM2      = SUM2 + 2.0 * VSOP * ZP
      SUM3      = SUM3 + 2.0 * VSOP
C
      GO TO 10
   20 CONTINUE
C
      SUM1      = SUM1 * DZ / HC / 2.0
      SUM2      = SUM2 * DZ / HC / 2.0
      SUM3      = SUM3 * DZ / HC / 2.0
```

```
C
C          I HAVE TO DO V* FOR INCOMING WAVE BOUNDARY CONDITIONS
C
      SUM1        = CONJG (SUM1)
      SUM2        = CONJG (SUM2)
      SUM3        = CONJG (SUM3)
C
C       EIKONAL PHASE
C
      IF (IDIST .EQ. 2) SUM2 = (0.0,0.0)
C
      S1          = SUM1 * PMASS / KZ + SUM2 * PMASS * I
      S2          = SUM3 * PMASS *  B
C
      RETURN
      END
C
CSSSSSSSSSSSSSSSSSSSSSSSSSSSSSSSSSSSSSSSSSSSSSSSSSSSSSSSSSSSSSSSSSSSSSSSS
C
      SUBROUTINE QXDEPKIN
C
C       SETS UP KINEMATICS VARIABLES THAT DEPEND ON THE
C       PERPENDICULAR COMPONENT OF THE MOMENTUM TRANSFER (QX)
C
      COMPLEX
     *  I
C
      COMMON /CONSTANTS/
     *  PMASS    , PMU
     *, PKAPPA   , FFS
     *, I        , PI
     *, HC       , ALPHA
     *, IDIST    , ICT
     *, T2
C
      REAL
     *  NB       , NS
     *, KZ       , LHADR
C
      COMMON /KINEMATICS/
     *  QX       , QZ       , QT
     *, KZ       , E        , P
     *, EI       , K        , L        (2)
     *, J2       , M2       , ML       (2)
     *, MSF      , NB       , NS
     *, TF       , ETHETA   , PINIT
     *, HELICT   , LHADR    , TSHRINK
     *, IA
C
C       QX KINEMATICS
C
      Q3MAG       = SQRT (2.0 * TF * PMASS + TF     * TF     )
      TEMP        =      (          Q3MAG ** 2 - QX    * QX     )
C
```

```
      IF (TEMP .LT. 0.0) THEN
          STOP ' REACHED END OF KINEMATIC RANGE '
      ENDIF
C
      QZ            = SQRT (                            TEMP )
      P             = SQRT ((KZ - QZ) ** 2 + QX     * QX  )
      E             = SQRT (        KZ * KZ + PMASS * PMASS)
C
      RETURN
      END
C
CSSSSSSSSSSSSSSSSSSSSSSSSSSSSSSSSSSSSSSSSSSSSSSSSSSSSSSSSSSSSSSSSSSSSSSS
C
      SUBROUTINE JMU (J0,JX,JY,JZ)
C
C        COMPUTES THE MATRIX ELEMENTS OF THE NUCLEAR CURRENT BETWEEN
C        THE INITIAL BOUND STATE AND THE FINAL DISTORTED PLANE WAVE
C
      PARAMETER
     *( NR       =   30
     *, NRV      =  300
     *, NX       =   20    )
C
      REAL
     * X        (NX)
     *, WT       (NX)
C
      COMMON /NUMERICS/
     * IR        , DR        , IX
     *, WT       , X         , RMAX
     *, DELR     , DELT      , DZ
     *, QSTEP    , NQS       , DRV
C
      COMPLEX
     * I
C
      COMMON /CONSTANTS/
     * PMASS     , PMU
     *, PKAPPA   , FFS
     *, I        , PI
     *, HC       , ALPHA
     *, IDIST    , ICT
     *, T2
C
      REAL
     * NB        , NS
     *, KZ       , LHADR
C
      COMMON /KINEMATICS/
     * QX        , QZ        , QT
     *, KZ       , E         , P
     *, EI       , K         , L         (2)
     *, J2       , M2        , ML        (2)
     *, MSF      , NB        , NS
```

```
      *, TF        , ETHETA   , PINIT
      *, HELICT   , LHADR    , TSHRINK
      *, IA
C
       COMPLEX
      *  TSM      (14,2)
C
       COMMON /THTSUM/
      *  TSM
C
       COMPLEX
      *  SUMO     (2)         , JO
      *, SUMX     (2)         , JX
      *, SUMY     (2)         , JY
      *, SUMZ     (2)         , JZ
      *, QDOTJ
      *, QDOTJ1
      *, QDOTJ2
      *, RSM      (14,2)
C
       REAL
      *  C        (2,2)
C
C        SPIN DEPENDENT STUFF
C
       CALL SETSPIN
C
C        SIMPSON INTEGRATION ALONG R
C
       WS        = 4.0
       IR        = 0
       R         = 0.0
C
       CALL THTINT (R)
C
       DO 10 MM  = 1, 2
       DO 10 NN  = 1, 14
C
          RSM (NN,MM)        = TSM (NN,MM)
C
   10  CONTINUE
C
       DO 30 IR  = 1, NR-1
C
          R         = DR * IR
          CALL THTINT (R)
C
          DO 20 MM = 1, 2
          DO 20 NN = 1, 14
C
             RSM (NN,MM)     = RSM (NN,MM) + WS * TSM (NN,MM)
C
   20     CONTINUE
C
```

```
      WS        = 6.0 - WS
C
  30  CONTINUE
C
      IR        = NR
      R         = NR * DR
C
      CALL THTINT (R)
C
      DO 40 MM  = 1, 2
      DO 40 NN  = 1, 14
C
         RSM (NN,MM)        = (RSM (NN,MM) + TSM (NN,MM)) * DR / 3.0
C
  40  CONTINUE
C
C        FORM FACTORS
C
      CALL FORMFAC (F1,F2)
C
      F2        = F2 / (2.0 * PMASS)
C
C        CG COEFFICIENTS PROJECT OUT GOOD J FOR BOUND STATE
C
      CALL CLEBSCH (C)
C
C        CONSTANTS
C
      DO 50 MS  = 1, 2
C
      SUMO (MS) = RSM ( 1,MS) * F1        * (-I)  *  C (1,MS)
     *           + RSM ( 2,MS) * F1        * (-1)  *  C (2,MS)
     *           + RSM ( 3,MS) * F2 * QX * ( I)  *  C (1,MS)
     *           + RSM ( 5,MS) * F2 * QZ * ( I)  *  C (1,MS)
     *           + RSM ( 6,MS) * F2 * QX * (-1)  *  C (2,MS)
     *           + RSM ( 8,MS) * F2 * QZ * (-1)  *  C (2,MS)
C
      SUMX (MS) = RSM ( 3,MS) * F1        * (-I)  *  C (1,MS)
     *           + RSM ( 6,MS) * F1        * (-1)  *  C (2,MS)
     *           + RSM (10,MS) * F2 * QZ * (-1)  *  C (1,MS)
     *           + RSM (13,MS) * F2 * QZ * (-I)  *  C (2,MS)
     *           + RSM ( 3,MS) * F2 * QT * ( I)  *  C (1,MS)
     *           + RSM ( 6,MS) * F2 * QT * (-1)  *  C (2,MS)
C
      SUMZ (MS) = RSM ( 5,MS) * F1        * (-I)  *  C (1,MS)
     *           + RSM ( 8,MS) * F1        * (-1)  *  C (2,MS)
     *           + RSM (10,MS) * F2 * QX * ( 1)  *  C (1,MS)
     *           + RSM (13,MS) * F2 * QX * ( I)  *  C (2,MS)
     *           + RSM ( 5,MS) * F2 * QT * ( I)  *  C (1,MS)
     *           + RSM ( 8,MS) * F2 * QT * (-1)  *  C (2,MS)
C
      SUMY (MS) = RSM ( 9,MS) * F2 * QZ * ( 1)  *  C (1,MS)
     *           + RSM (11,MS) * F2 * QX * (-1)  *  C (1,MS)
     *           + RSM (12,MS) * F2 * QZ * ( I)  *  C (2,MS)
```

```
     *             + RSM (14,MS) * F2 * QX * (-I)  *  C (2,MS)
     *             + RSM ( 4,MS) * F1       * (-I)  *  C (1,MS)
     *             + RSM ( 7,MS) * F1       * (-1)  *  C (2,MS)
     *             + RSM ( 4,MS) * F2 * QT * ( I)  *  C (1,MS)
     *             + RSM ( 7,MS) * F2 * QT * (-1)  *  C (2,MS)
C
  50  CONTINUE
C
     JO         = NB * NS * (SUMO (1) + SUMO (2))
     JX         = NB * NS * (SUMX (1) + SUMX (2))
     JY         = NB * NS * (SUMY (1) + SUMY (2))
     JZ         = NB * NS * (SUMZ (1) + SUMZ (2))
C
C       CHECK TO SEE WHETHER THE CURRENT IS CONSERVED
C
     QDOTJ1     =   QT * JO
     QDOTJ2     = - QX * JX - QZ * JZ
     QDOTJ      =         QDOTJ1  +         QDOTJ2
C
C       OUTPUT CURRENT CONSERVATION INFORMATION
C
c     WRITE (6,*) QDOTJ,QDOTJ1,QDOTJ2
C
     RETURN
     END
C
CSSSSSSSSSSSSSSSSSSSSSSSSSSSSSSSSSSSSSSSSSSSSSSSSSSSSSSSSSSSSSSSSSSSSSS
C
     SUBROUTINE SETSPIN
C
C       SETS UP PAULI SPIN ALGEBRA AND EVERYTHING THAT DEPENDS
C       ON ANGULAR MOMENTUM
C
     PARAMETER
     *( NR       =    30
     *, NRV      =   300
     *, NX       =    20    )
C
     REAL
     * X        (NX)
     *, WT       (NX)
C
     COMMON /NUMERICS/
     * IR       , DR       , IX
     *, WT       , X        , RMAX
     *, DELR     , DELT     , DZ
     *, QSTEP    , NQS      , DRV
C
     COMPLEX
     * I
C
     COMMON /CONSTANTS/
     * PMASS    , PMU
     *, PKAPPA   , FFS
```

```
      *, I        , PI
      *, HC       , ALPHA
      *, IDIST    , ICT
      *, T2
C
       REAL
      *  NB       , NS
      *, KZ       , LHADR
C
       COMMON /KINEMATICS/
      *  QX       , QZ       , QT
      *, KZ       , E        , P
      *, EI       , K        , L      (2)
      *, J2       , M2       , ML     (2)
      *, MSF      , NB       , NS
      *, TF       , ETHETA   , PINIT
      *, HELICT   , LHADR    , TSHRINK
      *, IA
C
       COMPLEX
      *  SO       (2)
      *, SX       (2)
      *, SY       (2)
      *, SZ       (2)
C
       COMMON /SPINS/
      *  SO       , SX
      *, SY       , SZ
C
       REAL
      *  FNK      (0:NR)
      *, GNK      (0:NR)
      *, FSTAR    (2,2,NX)
C
       COMMON /WAVEFN/
      *  FNK      , GNK
      *, FSTAR
C
       INTEGER
      *  FAC      (-12:12)
C
       DATA
      *  FAC      /    12 * 0,          1,          1
      *,                       2,          6,         24
      *,                     120,        720,       5040
      *,                   40320,     362880,    3628800
      *,                39916800,  479001600                /
C
       REAL
      *  NUM
C
C      (INITIAL PAULI SPINOR) (SIGMA-MU) (FINAL PAULI SPINOR)
C
       IF   (MSF .EQ.  1) THEN
```

```
          SO (1)   =   1.0
          SX (1)   =   0.0
          SY (1)   =   0.0
          SZ (1)   =   1.0
          SO (2)   =   0.0
          SX (2)   =   1.0
          SY (2)   =    I
          SZ (2)   =   0.0
       ELSEIF (MSF .EQ. -1) THEN
          SO (1)   =   0.0
          SX (1)   =   1.0
          SY (1)   = -  I
          SZ (1)   =   0.0
          SO (2)   =   1.0
          SX (2)   =   0.0
          SY (2)   =   0.0
          SZ (2)   =  -1.0
       ENDIF
C
C        BOUND STATE ANGULAR MOMENTUM STUFF
C
       DO 10 MS  = 1, 2
         ML (MS) = (M2 + (-1.0) ** MS) / 2
   10  CONTINUE
C
C        THETA DEPENDENT/PHI INDEPENDENT PART OF THE SPHERICAL
C        HARMONICS (FSTAR)
C
       DO 20 JX          = 1, NX
       DO 20 MS          = 1, 2
       DO 20 MK          = 1, 2
C
          NUM            = FAC (L(MK) - ML(MS)) * (2.0 * L(MK) + 1.0)
          DEN            = FAC (L(MK) + ML(MS)) * (4.0 * PI)
C
          IF (DEN.NE.0.0) THEN
            DEN          = 1.0 / DEN
          ENDIF
C
          FSTAR (MK,MS,JX) = SQRT (NUM * DEN) * PLM(L(MK),ML(MS),X(JX))
C
   20    CONTINUE

       RETURN
       END
C
CFFFFFFFFFFFFFFFFFFFFFFFFFFFFFFFFFFFFFFFFFFFFFFFFFFFFFFFFFFFFFFFFFFFFFFFF
C
       REAL FUNCTION PLM (L,M,X)
C
C        COMPUTES THE ASSOCIATED LEGENDRE POLYNOMIAL PLM(X)
C        FOR M NOT IN [-L,L], THE RESULT IS SET TO ZERO
C
C        RESTRICTIONS:
```

```
C
C         RANGE OF X                   :    [-1,1]
C
      INTEGER
     *  FAC      (-12:12)
C
      DATA
     *  FAC      /    12 * 0,            1,           1
     *,                      2,           6,          24
     *,                    120,         720,        5040
     *,                  40320,      362880,     3628800
     *,              39916800,   479001600                /
C
      N              = ABS (M)
C
      IF (ABS(X) .GT. 1.0) STOP ' PLM - 1'
      IF (N + L  .GT.  12) STOP ' PLM - 2'
C
      IF (N .GT. L) THEN
        PLM          = 0.0
        RETURN
      ENDIF
C
C         COMPUTE PNN
C
      PNN            = 1.0
      TEMP           = SQRT ((1.0-X)*(1.0+X))
      DFAC           = 1.0
C
      DO 10 I        = 1, N
        PNN          = - PNN * DFAC * TEMP
        DFAC         = DFAC + 2.0
  10  CONTINUE
C
      IF (L .EQ. N) THEN
        PLN          = PNN
      ELSE
C
C         COMPUTE P(N+1)N
C
        PNP1N        = X * (2*N + 1) * PNN
        IF (L .EQ. N+1) THEN
          PLN        = PNP1N
        ELSE
C
C         COMPUTE PLN
C
          DO 20 LL   = N+2,L
            PLLN     = (X*(2*LL-1)*PNP1N - (LL+N-1)*PNN)/(LL-N)
            PNN      = PNP1N
            PNP1N    = PLLN
  20      CONTINUE
          PLN        = PLLN
        ENDIF
```

```
      ENDIF
C
C        TAKE CARE OF NEGATIVE M'S
C
      IF (M.GE.0) THEN
        PLM          = PLN
      ELSE
        PLM          = PLN * FAC (L-N) / FAC (L+N) * (-1.0) ** N
      ENDIF
C
      RETURN
      END
C
CSSSSSSSSSSSSSSSSSSSSSSSSSSSSSSSSSSSSSSSSSSSSSSSSSSSSSSSSSSSSSSSSSSSSSSS
C
      SUBROUTINE THTINT (R)
C
C        COMPUTES THETA INTEGRALS VIA GAUSSIAN INTEGRATION
C
      PARAMETER
     *( NR       =    30
     *, NRV      =   300
     *, NX       =    20    )
C
      REAL
     * X        (NX)
     *, WT       (NX)
C
      COMMON /NUMERICS/
     * IR        , DR        , IX
     *, WT        , X         , RMAX
     *, DELR      , DELT      , DZ
     *, QSTEP     , NQS       , DRV
C
      COMPLEX
     * I
C
      COMMON /CONSTANTS/
     * PMASS     , PMU
     *, PKAPPA    , FFS
     *, I         , PI
     *, HC        , ALPHA
     *, IDIST     , ICT
     *, T2
C
      REAL
     * NB        , NS
     *, KZ        , LHADR
C
      COMMON /KINEMATICS/
     * QX        , QZ        , QT
     *, KZ        , E         , P
     *, EI        , K         , L         (2)
     *, J2        , M2        , ML        (2)
```

```
     *, MSF      , NB        , NS
     *, TF       , ETHETA   , PINIT
     *, HELICT   , LHADR    , TSHRINK
     *, IA
C
      COMPLEX
     *  TSM     (14,2)
C
      COMMON /THTSUM/
     *  TSM
C
      COMPLEX
     *  FNC     (14,2)
C
      COMMON /MTERMS/
     *  FNC
C
C        GAUSSIAN INTEGRATION FROM X = -1 TO X = 1
C
      DO 10 MM  = 1, 2
      DO 10 NN  = 1, 14
C
        TSM (NN,MM)       = 0.0
C
  10  CONTINUE
C
      DO 30 IX  = 1, NX
C
        TH       = ACOS (X(IX))
C
        CALL INTEGRND (R,TH)
C
        DO 20 MM= 1, 2
        DO 20 NN= 1, 14
C
          TSM (NN,MM)     = TSM (NN,MM) + WT (IX) * FNC (NN,MM)
C
  20      CONTINUE
C
  30  CONTINUE
      RETURN
      END
C
CSSSSSSSSSSSSSSSSSSSSSSSSSSSSSSSSSSSSSSSSSSSSSSSSSSSSSSSSSSSSSSSSSSSSSSSS
C
      SUBROUTINE INTEGRND (R,TH)
C
C        COMPUTES THE INTEGRAND IN THE MATRIX ELEMENTS
C
C        N,K,M2 (INPUT,INTEGER) :  QUANTUM NUMBERS OF BOUND STATE
C        MSF    (INPUT,INTEGER) :  FINAL PROTON SPIN
C        QX,QZ  (INPUT,REAL)    :  SPACELIKE COMPONENTS OF MOM TRANSFER
C        QT     (INPUT,REAL)    :  TIMELIKE COMPONENT OF MOM TRANSFER
C        KZ     (INPUT,REAL)    :  OUTGOING PROTON MOMENTUM
```

```
C         R,TH    (INPUT,REAL)    :  POSITION COORDINATES
C         MTERMS  (OUTPUT)        :  COMMON BLOCK CONTAINING M.E. TERMS
C
      PARAMETER
     *( NR      =    30
     *, NRV     =   300
     *, NX      =    20    )
C
      REAL
     * X       (NX)
     *, WT      (NX)
C
      COMMON  /NUMERICS/
     * IR       , DR       , IX
     *, WT      , X        , RMAX
     *, DELR    , DELT     , DZ
     *, QSTEP   , NQS      , DRV
C
      COMPLEX
     * I
C
      COMMON  /CONSTANTS/
     * PMASS   , PMU
     *, PKAPPA  , FFS
     *, I       , PI
     *, HC      , ALPHA
     *, IDIST   , ICT
     *, T2
C
      REAL
     * NB      , NS
     *, KZ      , LHADR
C
      COMMON  /KINEMATICS/
     * QX       , QZ       , QT
     *, KZ      , E        , P
     *, EI      , K        , L       (2)
     *, J2      , M2       , ML      (2)
     *, MSF     , NB       , NS
     *, TF      , ETHETA   , PINIT
     *, HELICT  , LHADR    , TSHRINK
     *, IA
C
      COMPLEX
     * SO      (2)
     *, SX      (2)
     *, SY      (2)
     *, SZ      (2)
C
      COMMON  /SPINS/
     * SO      , SX
     *, SY      , SZ
C
      COMPLEX
```

```
     *  VC        (0:NRV+1)
     *, VSO       (0:NRV+1)
     *, DENOM     (0:NR,NX)
C
      COMMON /POTENTIAL/
     *  VC        , VSO
     *, DENOM
C
      REAL
     *  FNK       (0:NR)
     *, GNK       (0:NR)
     *, FSTAR     (2,2,NX)
C
      COMMON /WAVEFN/
     *  FNK       , GNK
     *, FSTAR
C
      COMPLEX
     *  FNC       (14,2)
C
      COMMON /MTERMS/
     *  FNC
C
      COMPLEX
     *  FRT       (0:NR,NX,6)
C
      COMMON /SPACEFUNC/
     *  FRT
C
      COMPLEX
     *  ISO       , ISX
     *, ISY       , ISZ
     *, ISP       , ISQ
     *, ISR       , ISS       , IST
     *, CRT       , SRT
     *, DCR       , DSR
     *, DCT       , DST
     *, SPF       (8,2)
     *, ANG       (5)
     *, ALL
C
C        COORDINATES
C
      CT        = COS (TH)
      ST        = SIN (TH)
C
      IF (ST .EQ. 0.0) THEN
        STOP ' 1 / SIN (TH) IS NOT DEFINED ON AXIS '
      ELSE
        STI = 1.0 / ST
      ENDIF
C
      Z         = R * CT
      B         = R * ST
```

```
C
C         FUNCTIONS THAT ONLY DEPEND ON POSITION
C
      CRT       = FRT (IR,IX,1)
      SRT       = FRT (IR,IX,2)
      DCR       = FRT (IR,IX,3)
      DSR       = FRT (IR,IX,4)
      DCT       = FRT (IR,IX,5)
      DST       = FRT (IR,IX,6)
C
      ALL       = EXP (I * (KZ - QZ) * Z)
C
C        LOOP ON INITIAL SPIN
C
      DO 10 MS  = 1, 2
C
C         PAULI MATRIX ELEMENTS
C
      ISO       = SO (MS)
      ISX       = SX (MS)
      ISY       = SY (MS)
      ISZ       = SZ (MS)
C
C         AZIMUTHAL INTEGRALS
C
      ZZ        = - QX * B
      CALL PHIINT (ML(MS),ZZ,ANG)
C
C         DEFINE CLUSTERS
C
      ISP       =     ISX * ANG (2) + ISY * ANG(3)
      ISQ       =     ISX * ANG (3) + ISY * ANG(2)
      ISR       = I * ISO * ANG (3) - ISZ * ANG(2)
      ISS       = I * ISO * ANG (2) + ISZ * ANG(3)
      IST       =     ISY * ANG (3) - ISX * ANG(2)
C
C       TERMS IN THE INTEGRAND FOR THE MATRIX ELEMENTS
C
      SPF ( 1,MS) =  CRT *  ISO * ANG (1)        * R
     *             + SRT *  ISP                  * R    * I
C
      SPF ( 2,MS) = -SRT * (ISO * ANG (4)        * STI
     *                     +ISZ * ANG (5)        * STI  * I)
     *             + DCT * (ISZ * ANG (1) * ST          * I
     *                     -ISQ               * CT       * I)
     *             + DST * (ISO * ANG (4) * CT
     *                     +ISX * ANG (3) * ST           * I
     *                     -ISY * ANG (2) * ST           * I
     *                     +ISZ * ANG (5) * CT           * I)
     *             - DCR * (ISQ               * ST * R    * I
     *                     +ISZ * ANG (1) * CT * R        * I)
     *             + DSR * (ISO * ANG (4) * ST * R
     *                     -ISX * ANG (3) * CT * R        * I
     *                     +ISY * ANG (2) * CT * R        * I
```

```
      *                         +ISZ * ANG (5) * ST * R    * I)
C
      SPF ( 3,MS) = -SRT * (ISX * ANG (4)         * STI
      *                     +ISY * ANG (5)         * STI    )
      *             +  DCT * (ISY * ANG (1) * ST
      *                      -ISR           * CT             )
      *             +  DST * (ISX * ANG (4) * CT
      *                      +ISO * ANG (3) * ST          * I
      *                      +ISZ * ANG (2) * ST
      *                      +ISY * ANG (5) * CT             )
      *             -  DCR * (ISR           * ST * R
      *                      +ISY * ANG (1) * CT * R         )
      *             +  DSR * (ISX * ANG (4) * ST * R
      *                      -ISO * ANG (3) * CT * R    * I
      *                      -ISZ * ANG (2) * CT * R
      *                      +ISY * ANG (5) * ST * R         )
C
      SPF ( 4,MS) = -SRT * (ISY * ANG (4)         * STI
      *                     -ISX * ANG (5)         * STI    )
      *             -  DCT * (ISX * ANG (1) * ST
      *                      +ISS           * CT             )
      *             +  DST * (ISY * ANG (4) * CT
      *                      +ISZ * ANG (3) * ST
      *                      -ISO * ANG (2) * ST          * I
      *                      -ISX * ANG (5) * CT             )
      *             -  DCR * (ISS           * ST * R
      *                      -ISX * ANG (1) * CT * R         )
      *             +  DSR * (ISY * ANG (4) * ST * R
      *                      -ISZ * ANG (3) * CT * R
      *                      +ISO * ANG (2) * CT * R    * I
      *                      -ISX * ANG (5) * ST * R         )
C
      SPF ( 5,MS) = -SRT * (ISZ * ANG (4)         * STI
      *                     +ISO * ANG (5)         * STI * I)
      *             +  DCT * (ISO * ANG (1) * ST          * I
      *                      +IST           * CT             )
      *             +  DST * (ISZ * ANG (4) * CT
      *                      +ISO * ANG (5) * CT          * I
      *                      -ISP           * ST             )
      *             +  DCR * (IST           * ST * R
      *                      -ISO * ANG (1) * CT * R    * I)
      *             +  DSR * (ISZ * ANG (4) * ST * R
      *                      +ISO * ANG (5) * ST * R    * I
      *                      +ISP           * CT * R         )
C
      SPF ( 6,MS) =  CRT *  ISX * ANG (1)        * R
      *             -  SRT *  ISZ * ANG (3)        * R
      *             +  SRT *  ISO * ANG (2)        * R    * I
C
      SPF ( 7,MS) =  CRT *  ISY * ANG (1)        * R
      *             +  SRT *  ISZ * ANG (2)        * R
      *             +  SRT *  ISO * ANG (3)        * R    * I
C
      SPF ( 8,MS) =  CRT *  ISZ * ANG (1)        * R
```

```
     *                  +  SRT  *  ISX  *  ANG (3)      *  R
     *                  -  SRT  *  ISY  *  ANG (2)      *  R
C
C         PUT IN THE NON-SPIN-DEPENDENT PART
C
      FNC ( 1,MS) = SPF ( 1,MS) * ALL * GNK (IR)
     *              * FSTAR (1,MS,IX)
      FNC ( 2,MS) = SPF ( 2,MS) * ALL * FNK (IR) / DENOM (IR,IX)
     *              * FSTAR (2,MS,IX)
      FNC ( 3,MS) = SPF ( 3,MS) * ALL * GNK (IR) / DENOM (IR,IX)
     *              * FSTAR (1,MS,IX)
      FNC ( 4,MS) = SPF ( 4,MS) * ALL * GNK (IR) / DENOM (IR,IX)
     *              * FSTAR (1,MS,IX)
      FNC ( 5,MS) = SPF ( 5,MS) * ALL * GNK (IR) / DENOM (IR,IX)
     *              * FSTAR (1,MS,IX)
      FNC ( 6,MS) = SPF ( 6,MS) * ALL * FNK (IR)
     *              * FSTAR (2,MS,IX)
      FNC ( 7,MS) = SPF ( 7,MS) * ALL * FNK (IR)
     *              * FSTAR (2,MS,IX)
      FNC ( 8,MS) = SPF ( 8,MS) * ALL * FNK (IR)
     *              * FSTAR (2,MS,IX)
      FNC ( 9,MS) = SPF ( 6,MS) * ALL * GNK (IR)
     *              * FSTAR (1,MS,IX)
      FNC (10,MS) = SPF ( 7,MS) * ALL * GNK (IR)
     *              * FSTAR (1,MS,IX)
      FNC (11,MS) = SPF ( 8,MS) * ALL * GNK (IR)
     *              * FSTAR (1,MS,IX)
      FNC (12,MS) = SPF ( 3,MS) * ALL * FNK (IR) / DENOM (IR,IX)
     *              * FSTAR (2,MS,IX)
      FNC (13,MS) = SPF ( 4,MS) * ALL * FNK (IR) / DENOM (IR,IX)
     *              * FSTAR (2,MS,IX)
      FNC (14,MS) = SPF ( 5,MS) * ALL * FNK (IR) / DENOM (IR,IX)
     *              * FSTAR (2,MS,IX)
C
   10 CONTINUE
C
      RETURN
      END
C
CSSSSSSSSSSSSSSSSSSSSSSSSSSSSSSSSSSSSSSSSSSSSSSSSSSSSSSSSSSSSSSSSSSSSSSS
C
      SUBROUTINE PHIINT (M,Z,ANG)
C
C         COMPUTES PHI INTEGRAL IN MATRIX ELEMENT VIA
C         ANALYTIC EXPRESSIONS INVOLVING BESSEL FUNCTIONS
C
C         M         (INPUT,INTEGER) :  ML FOR BOUND STATE
C         Z         (INPUT,REAL)    :  QX * B
C         ANG (5) (OUTPUT,COMPLEX) :  AN (M,Z)
C
      COMPLEX
     * I
C
      COMMON /CONSTANTS/
```

```
      *  PMASS    , PMU
      *, PKAPPA   , FFS
      *, I        , PI
      *, HC       , ALPHA
      *, IDIST    , ICT
      *, T2
C
       COMPLEX
      *  ANG        (5)
C
       IF (Z .NE. 0.0) THEN
C
          CALL BESS (M  ,Z,BM  ,BMM1,BMP1)
          CALL BESS (M-2,Z,BMM2,DUM ,DUM)
C
          ANG (1) =  2.0 * PI * I ** M * BM
          ANG (2) = -PI * I **  M    * (BMM1 + BMP1)
          ANG (3) =  PI * I ** (M-1) * (BMM1 - BMP1)
          ANG (4) = -PI * I ** (M-1) * (BMM2 - BMP2)
          ANG (5) = -PI * I **  M    * (BMM2 + BMP2)
C
          RETURN
C
       ENDIF
       IF (M .EQ. 0) THEN
C
          ANG (1) = CMPLX (2.0 * PI)
          ANG (2) = (0.0,0.0)
          ANG (3) = (0.0,0.0)
          ANG (4) = (0.0,0.0)
          ANG (5) = (0.0,0.0)
          RETURN
C
       ENDIF
       IF (M .EQ. 1) THEN
C
          ANG (1) = (0.0,0.0)
          ANG (2) = CMPLX(-I * PI)
          ANG (3) = CMPLX(     PI)
          ANG (4) = (0.0,0.0)
          ANG (5) = (0.0,0.0)
          RETURN
C
       ENDIF
       IF (M .EQ. -1) THEN
C
          ANG (1) = (0.0,0.0)
          ANG (2) = CMPLX( I * PI)
          ANG (3) = CMPLX(     PI)
          ANG (4) = (0.0,0.0)
          ANG (5) = (0.0,0.0)
          RETURN
C
       ENDIF
```

```
      IF (M .EQ.  2) THEN
C
         ANG (1) = (0.0,0.0)
         ANG (2) = (0.0,0.0)
         ANG (3) = (0.0,0.0)
         ANG (4) = CMPLX(-I * PI)
         ANG (5) = CMPLX(     PI)
         RETURN
C
      ENDIF
      IF (M .EQ. -2) THEN
C
         ANG (1) = (0.0,0.0)
         ANG (2) = (0.0,0.0)
         ANG (3) = (0.0,0.0)
         ANG (4) = CMPLX( I * PI)
         ANG (5) = CMPLX(     PI)
         RETURN
C
      ENDIF
C
      ANG (1) = (0.0,0.0)
      ANG (2) = (0.0,0.0)
      ANG (3) = (0.0,0.0)
      ANG (4) = (0.0,0.0)
      ANG (5) = (0.0,0.0)
      RETURN
C
      END
C
CSSSSSSSSSSSSSSSSSSSSSSSSSSSSSSSSSSSSSSSSSSSSSSSSSSSSSSSSSSSSSSSSSSSSSSSS
C
      SUBROUTINE BESS (N,Z,JN,JNM1,JNP1)
C
C        RETURNS THE BESSEL FUNCTION SEQUENCE J(N,Z),J(N-1,Z),J(N+1,Z)
C
C        N       (INPUT,INTEGER)  :  ORDER OF THE BESSEL FUNCTION
C        Z       (INPUT,REAL)     :  ARGUMENT OF THE BESSEL FUNCTION
C        JN      (OUTPUT,REAL)    :  J(N,Z)
C        JNM1    (OUTPUT,REAL)    :  J(N-1,Z)
C        JNP1    (OUTPUT,REAL)    :  J(N+1,Z)
C
      PARAMETER
     * (MLMAX   = 20 )
C
      REAL
     * JN      , JNM1
     *, JNP1
C
      REAL
     * B       (0:MLMAX)
C
      IF (N .EQ. 0) THEN
C
```

```
      JNM1      = - BESJ1 (Z)
      JN        =   BESJ0 (Z)
      JNP1      =   BESJ1 (Z)
C
      RETURN
      ENDIF
C
      X         = ABS (Z)
      A         = 0.0
      NMAX      = N / ABS (N) * (ABS (N) + 1)
      ND        = 7
C
      CALL BSJA (X,A,NMAX,ND,B)
C
      JNM1      = B (ABS(N-1))
      JN        = B (ABS(N) )
      JNP1      = B (ABS(N+1))
C
      IF (Z .LT. 0.0) THEN
C
C        TAKE CARE OF NEGATIVE ARGUMENTS
C
      JNM1      = JNM1 * (-1.0) ** (N-1)
      JN        = JN   * (-1.0) ** (N )
      JNP1      = JNP1 * (-1.0) ** (N+1)
C
      ENDIF
C
      RETURN
      END
C
CSSSSSSSSSSSSSSSSSSSSSSSSSSSSSSSSSSSSSSSSSSSSSSSSSSSSSSSSSSSSSSSSSSSSSSS
C
      SUBROUTINE FORMFAC (F1,F2)
C
C        COMPUTES PROTON FORM FACTORS F1(Q**2) AND F2(Q**2) ACCORDING
C        TO THE DIPOLE FORMULA
C
C        QX,QZ   (INPUT,REAL)    :  SPACELIKE COMPONENT OF MOM TRANSFER
C        QT      (INPUT,REAL)    :  TIMELIKE COMPONENT OF MOM TRANSFER
C        F1      (OUTPUT,REAL)   :  F1 FORM FACTOR
C        F2      (OUTPUT,REAL)   :  F2 FORM FACTOR
C
C        ALSO USED ARE PROTON MASS AND MAGNETIC MOMENT FROM /PROTON/
C
      COMPLEX
     *  I
C
      COMMON /CONSTANTS/
     *  PMASS    , PMU
     *, PKAPPA   , FFS
     *, I        , PI
     *, HC       , ALPHA
     *, IDIST    , ICT
```

```
     *, T2
C
      REAL
     *  NB         , NS
     *, KZ         , LHADR
C
      COMMON /KINEMATICS/
     *  QX         , QZ        , QT
     *, KZ         , E         , P
     *, EI         , K         , L          (2)
     *, J2         , M2        , ML         (2)
     *, MSF        , NB        , NS
     *, TF         , ETHETA    , PINIT
     *, HELICT     , LHADR     , TSHRINK
     *, IA
C
      Q2           = QT*QT - QX*QX - QZ*QZ
      P2           = PMASS*PMASS
      A2           = FFS*FFS
C
      DENOM        = (A2 - Q2) ** 2 * (4 * P2 - Q2)
      F1           = - A2*A2 * (PMU * Q2 - 4 * P2) / DENOM
      F2           = - A2*A2 * P2 * 4 * (1 - PMU) / DENOM
C
      RETURN
      END
C
CSSSSSSSSSSSSSSSSSSSSSSSSSSSSSSSSSSSSSSSSSSSSSSSSSSSSSSSSSSSSSSSSSSSSSSS
C
      SUBROUTINE CLEBSCH (C)
C
C        COMPUTES THE CLEBSCH-GORDAN COEFFICIENTS
C
C        C (1,1) = <1/2  1/2 L(1) M-1/2 | J M>
C        C (1,2) = <1/2 -1/2 L(1) M+1/2 | J M>
C        C (2,1) = <1/2  1/2 L(2) M-1/2 | J M>
C        C (2,2) = <1/2 -1/2 L(2) M+1/2 | J M>
C
C        K,J,M2 (INPUT,INTEGER)  :  ANG MOMENTUM QUANTUM NUMBERS OF BS
C        C      (OUTPUT,REAL)     :  CLEBSCH-GORDAN COEFFICIENTS
C
      REAL
     *  NB         , NS
     *, KZ         , LHADR
C
      COMMON /KINEMATICS/
     *  QX         , QZ        , QT
     *, KZ         , E         , P
     *, EI         , K         , L          (2)
     *, J2         , M2        , ML         (2)
     *, MSF        , NB        , NS
     *, TF         , ETHETA    , PINIT
     *, HELICT     , LHADR     , TSHRINK
     *, IA
```

```
C
      REAL
     * L2         , C          (2,2)
C
      L2           = FLOAT (2 * L(1))
C
      IF (K .LT. 0) THEN
        C (1,1) =  SQRT ((L2 + M2 + 1.0) / 2.0 / (L2 + 1.0))
        C (1,2) =  SQRT ((L2 - M2 + 1.0) / 2.0 / (L2 + 1.0))
      ELSEIF (K .GT. 0) THEN
        C (1,1) = -SQRT ((L2 - M2 + 1.0) / 2.0 / (L2 + 1.0))
        C (1,2) =  SQRT ((L2 + M2 + 1.0) / 2.0 / (L2 + 1.0))
      ENDIF
C
      L2           = FLOAT (2 * L(2))
C
      IF (K .GT. 0) THEN
        C (2,1) =  SQRT ((L2 + M2 + 1.0) / 2.0 / (L2 + 1.0))
        C (2,2) =  SQRT ((L2 - M2 + 1.0) / 2.0 / (L2 + 1.0))
      ELSEIF (K .LT. 0) THEN
        C (2,1) = -SQRT ((L2 - M2 + 1.0) / 2.0 / (L2 + 1.0))
        C (2,2) =  SQRT ((L2 + M2 + 1.0) / 2.0 / (L2 + 1.0))
      ENDIF
C
      IF (ABS (ML (1)) .GT. L (1)) C (1,1) = 0.0
      IF (ABS (ML (2)) .GT. L (1)) C (1,2) = 0.0
      IF (ABS (ML (1)) .GT. L (2)) C (2,1) = 0.0
      IF (ABS (ML (2)) .GT. L (2)) C (2,2) = 0.0
C
      RETURN
      END
CSSSSSSSSSSSSSSSSSSSSSSSSSSSSSSSSSSSSSSSSSSSSSSSSSSSSSSSSSSSSSSSSSSSSSSS
C
      SUBROUTINE VOPT
C
C         CALCULATE LOOKUP TABLE (1-D) FOR OPTICAL POTENTIAL
C
      PARAMETER
     *( NR       =    30
     *, NRV      =   300
     *, NX       =    20   )
C
      REAL
     * X        (NX)
     *, WT       (NX)
C
      COMMON /NUMERICS/
     * IR        , DR        , IX
     *, WT       , X         , RMAX
     *, DELR     , DELT      , DZ
     *, QSTEP    , NQS       , DRV
C
      COMPLEX
     * I
```

```
C
      COMMON /CONSTANTS/
     *  PMASS    , PMU
     *, PKAPPA   , FFS
     *, I        , PI
     *, HC       , ALPHA
     *, IDIST    , ICT
     *, T2
C
      REAL
     *  NB       , NS
     *, KZ       , LHADR
C
      COMMON /KINEMATICS/
     *  QX       , QZ      , QT
     *, KZ       , E       , P
     *, EI       , K       , L       (2)
     *, J2       , M2      , ML      (2)
     *, MSF      , NB      , NS
     *, TF       , ETHETA  , PINIT
     *, HELICT   , LHADR   , TSHRINK
     *, IA
C
      COMPLEX
     *  VC       (0:NRV+1)
     *, VSO      (0:NRV+1)
     *, DEN      (0:NR,NX)
C
      COMMON /POTENTIAL/
     *  VC       , VSO
     *, DEN
C
      COMPLEX
     *  VS       , VV
C
      REAL
     *  RHO      (0:NRV+1)
C
      IF (IDIST .EQ. 0) THEN
C
C        PLANE WAVES
C
      DO 10 JR  = 0, NRV+1
C
      VC  (JR)  = (0.0,0.0)
      VSO (JR)  = (0.0,0.0)
C
  10  CONTINUE
      RETURN
      ENDIF
C
      IF (IDIST .EQ. 1) THEN
C
C        ONE OF THE PHENOMENOLIGICAL FITS TO SPECIFIC NUCLEI
```

```
C
      IF (IA .EQ. 40) THEN
C
C         CLARK OPTICAL POTENTAIL FOR CALCIUM - 1
C         ENERGY RANGE FOR THIS POTENTIAL
C
      DE        = (TF - 400.0) / 400.0
      A13       = REAL (IA) ** (1.0/3.0)
C
      IF (TF .GT. 1040.0) GOTO 40
C
C         VECTOR POTENTIAL PARAMETERS
C
      CVR       = 0.8894 - 0.3765 * DE + 0.0700 * DE * DE
      RVR       = 1.0159
      AVR       = 0.6678
      CVI       = 1.1446 + 0.1406 * DE - 0.0924 * DE * DE
      RVI       = 1.0842 - 0.0090 * DE - 0.0032 * DE * DE
      AVI       = 0.5702 - 0.0599 * DE + 0.0064 * DE * DE
C
C         SCALAR POTENTIAL PARAMETERS
C
      CSR       = 0.9730 - 0.2170 * DE + 0.0109 * DE * DE
      RSR       = 1.0098
      ASR       = 0.6918
      CSI       = 1.2072 + 0.2324 * DE - 0.2913 * DE * DE
      RSI       = 1.0872 - 0.0090 * DE + 0.0070 * DE * DE
      ASI       = 0.5587 - 0.0452 * DE - 0.0521 * DE * DE
C
C         SCALE FACTORS
C
      CVR       = CVR * ( 300.0)
      CVI       = CVI * (-100.0)
      RVR       = RVR / HC
      AVR       = AVR / HC
      RVI       = RVI / HC
      AVI       = AVI / HC
C
      CSR       = CSR * (-400.0)
      CSI       = CSI * ( 100.0)
      RSR       = RSR / HC
      ASR       = ASR / HC
      RSI       = RSI / HC
      ASI       = ASI / HC
C
C         R-INDEPENDENT EXPONENTIALS
C
      E1VR      = EXP (-RVR * A13 / AVR)
      E1VI      = EXP (-RVI * A13 / AVI)
      E1SR      = EXP (-RSR * A13 / ASR)
      E1SI      = EXP (-RSI * A13 / ASI)
C
      DO 20 JR  = 0, NRV+1
C
```

```fortran
C          R-DEPENDENT EXPONENTIALS
C
      RD          = JR * DRV
C
      E2VR        = EXP (RD / AVR)
      E2VI        = EXP (RD / AVI)
      E2SR        = EXP (RD / ASR)
      E2SI        = EXP (RD / ASI)
C
C          RADIAL DEPENDENCE OF VECTOR/SCALAR REAL/IMAG PARTS
C
      FVR         = (1.0 + E1VR * E2VR) ** (-1.0)
     *            * (1.0 + E1VR / E2VR) ** (-1.0)
      FSR         = (1.0 + E1SR * E2SR) ** (-1.0)
     *            * (1.0 + E1SR / E2SR) ** (-1.0)
      FVI         = (1.0 + E1VI * E2VI) ** (-1.0)
     *            * (1.0 + E1VI / E2VI) ** (-1.0)
      FSI         = (1.0 + E1SI * E2SI) ** (-1.0)
     *            * (1.0 + E1SI / E2SI) ** (-1.0)
C
C          DERIVATIVE TERM FOR SPIN-ORBIT POTENTIAL
C
      IF (RD .EQ. 0.0) THEN
C
      DFVR        = -2.0 * FVR / AVR / AVR * E1VR / (1.0 + E1VR) ** 2
      DFVI        = -2.0 * FVI / AVI / AVI * E1VI / (1.0 + E1VI) ** 2
      DFSR        = -2.0 * FSR / ASR / ASR * E1SR / (1.0 + E1SR) ** 2
      DFSI        = -2.0 * FSI / ASI / ASI * E1SI / (1.0 + E1SI) ** 2
C
      ELSE
C
      DFVR        =(E1VR / E2VR / (1.0 + E1VR / E2VR)
     *            - E1VR * E2VR / (1.0 + E1VR * E2VR))
     *            * FVR / AVR / RD
      DFVI        =(E1VI / E2VI / (1.0 + E1VI / E2VI)
     *            - E1VI * E2VI / (1.0 + E1VI * E2VI))
     *            * FVI / AVI / RD
      DFSR        =(E1SR / E2SR / (1.0 + E1SR / E2SR)
     *            - E1SR * E2SR / (1.0 + E1SR * E2SR))
     *            * FSR / ASR / RD
      DFSI        =(E1SI / E2SI / (1.0 + E1SI / E2SI)
     *            - E1SI * E2SI / (1.0 + E1SI * E2SI))
     *            * FSI / ASI / RD
C
      ENDIF
C
C          VECTOR AND SCALAR POTENTIALS
C
      VV          = CVR * FVR + I * CVI * FVI
      VS          = CSR * FSR + I * CSI * FSI
C
C          SWITCH OVER TO CENTRAL/SPIN ORBIT DESCRIPTION
C
      VC  (JR) = VS + E/PMASS * VV + (VS*VS - VV*VV) / (2.0*PMASS)
```

```
      VSO (JR)  = 1.0 / (2.0 * PMASS * (E + PMASS + VS - VV) )
     *           * (CVR*DFVR + I*CVI*DFVI - CSR*DFSR - I*CSI*DFSI)
C
  20  CONTINUE
      RETURN
C
      ELSEIF (IA .EQ. 16) THEN
C
C        ITALIAN OPTICAL POTENTIAL FOR OXYGEN
C        ENERGY RANGE FOR THIS POTENTIAL
C
      A13       = REAL (IA) ** (1.0/3.0)
      NFIX      = 18
C
      IF (TF .NE. 800.0) GO TO 40
C
C        VECTOR POTENTIAL PARAMETERS
C
      CVR       =   104.20
      RVR       =     1.05
      AVR       =     0.60
      CVI       =   -72.55
      RVI       =     0.98
      AVI       =     0.48
C
C        SCALAR POTENTIAL PARAMETERS
C
      CSR       =  -215.67
      RSR       =     0.99
      ASR       =     0.64
C
C        SCALE FACTORS
C
      RVR       = RVR / HC
      AVR       = AVR / HC
      RVI       = RVI / HC
      AVI       = AVI / HC
      RSR       = RSR / HC
      ASR       = ASR / HC
C
C        R-INDEPENDENT EXPONENTIALS
C
      E1VR      = EXP (-RVR * A13 / AVR)
      E1VI      = EXP (-RVI * A13 / AVI)
      E1SR      = EXP (-RSR * A13 / ASR)
C
      DO 30 JR  = 0, NRV+1
C
C        R-DEPENDENT EXPONENTIALS
C
      RD        = JR * DRV
C
      E2VR      = EXP (RD / AVR)
      E2VI      = EXP (RD / AVI)
```

```
      E2SR        = EXP (RD / ASR)
C
C         RADIAL DEPENDENCE OF VECTOR AND SCALAR REAL PARTS
C         AND VECTOR IMAGINARY PART (R NOT BIG)
C
      FVR         = 1.0 / (1.0 + E1VR * E2VR)
      FSR         = 1.0 / (1.0 + E1SR * E2SR)
      FVI         = 1.0 / (1.0 + E1VI * E2VI)
C
C         DERIVATIVE TERM FOR SPIN-ORBIT POTENTIAL
C
      IF (RD .EQ. 0.0) THEN
C
C         THE ORIGIN WILL BE FIXED UP LATER
C
      DFVR        = 1.0
      DFVI        = 1.0
      DFSR        = 1.0
C
      ELSE
C
      DFVR        = -1.0 / AVR / (1.0 + E1VR * E2VR) ** 2 * E1VR * E2VR
      DFSR        = -1.0 / ASR / (1.0 + E1SR * E2SR) ** 2 * E1SR * E2SR
      DFVI        = -1.0 / AVI / (1.0 + E1VI * E2VI) ** 2 * E1VI * E2VI
      DFVR        = DFVR / RD
      DFSR        = DFSR / RD
      DFVI        = DFVI / RD
C
      ENDIF
C
C         VECTOR AND SCALAR POTENTIALS
C
      VV          = CVR * FVR + I * CVI * FVI
      VS          = CSR * FSR
C
C         SWITCH OVER TO CENTRAL/SPIN ORBIT DESCRIPTION
C
      VC  (JR)  = VS + E/PMASS * VV + (VS*VS - VV*VV) / (2.0*PMASS)
      VSO (JR)  = 1.0 / (2.0 * PMASS * (E + PMASS + VS - VV) )
     *            * (CVR*DFVR + I*CVI*DFVI - CSR*DFSR)
C
  30  CONTINUE
C
C         FIX UP BEHAVIOR NEAR ORIGIN ORIGIN (LINEAR)
C
      DO IF       = 0, NFIX-1
      VSO (IF) = VSO (NFIX)
     *            + FLOAT (NFIX-IF) * (VSO (NFIX) - VSO (NFIX+1))
      ENDDO
C
      RETURN
      ENDIF
      ENDIF
C
```

```
      IF (IDIST .EQ. 2) THEN
C
C          DENSITY DEPENDENT OPTICAL POTENTIAL
C
  40  CONTINUE
      IDIST     = 2
C
C          DENSITY PARAMETERS FROM BARRETT AND JACKSON
C
      IF (IA .EQ. 16) THEN
C
      OMEGA     = -0.051
      RADIUS    =  2.608 / HC
      SKINDP    =  0.513 / HC
      NFIX      = 20
C
      ELSEIF (IA .EQ. 40) THEN
C
      OMEGA     = -0.161
      RADIUS    =  3.766 / HC
      SKINDP    =  0.586 / HC
      NFIX      = 15
C
      ELSEIF (IA .EQ. 208) THEN
C
      OMEGA     =  0.000
      RADIUS    =  6.624 / HC
      SKINDP    =  0.549 / HC
      NFIX      = 15
C
      ELSE
      STOP ' I DONT HAVE DENSITY PARAMETERS FOR THIS NUCLEUS'
      ENDIF
C
C          I GOT FROM THESE NN AMPLITUDE PARAMETERS FROM VARY, ET. AL.
C
      ALPHAA    = -0.2
      ALPHAC    = -1.1
      SIGMAA    =  4.4 / HC / HC
      SIGMAC    =  6.1 / HC / HC
C
C          USE 3-PARAMETER FERMI DISTRIBUTION FOR DENSITIES
C
      DO 50 JR  = 0, NRV+1
C
      RD        = JR * DRV
      RHO (JR)  = (1.0 + OMEGA * RD * RD / RADIUS / RADIUS)
     *            / (1.0 + EXP ((RD - RADIUS) / SKINDP))
C
  50  CONTINUE
C
C          CALCULATE THE NORMALIZATION OF THIS DENSITY
C
      WS        = 4.0
```

```
      JR          = 0
      RDUM        = JR * DRV
      PSUM        = RDUM ** 2 * RHO (JR)
C
      DO 60 JR  = 1, NRV-1
C
         RDUM     = JR * DRV
         PSUM     = PSUM + RDUM ** 2 * RHO (JR) * WS
         WS       = 6.0 - WS
C
  60  CONTINUE
C
      JR          = NRV
      RDUM        = JR * DRV
      PSUM        = (PSUM + RDUM ** 2 * RHO (JR)) * 4.0 * PI * DRV / 3.0
      CNORM       = PSUM
C
      WRITE (6,*) ' DENSITY NORM: ',CNORM
C
C        RESCALE DENSITY SO ITS NORM WILL BE ONE
C
      DO 70 JR  = 0, NRV+1
C
      RHO (JR)  = RHO (JR) / CNORM
C
  70  CONTINUE
C
C        CALCULATE POTENTIALS FROM SCALED DENSITY
C
      DO 80 JR  = 0, NRV+1
C
      RD          = JR * DRV
      XDUM        = (RD - RADIUS) / SKINDP
C
C        SPIN-ORBIT POTENTIAL DEPENDS ON THE DERIVATIVE OF DENSITY
C
      IF (RD .NE. 0.0) THEN
      DRHO        = ((2.0 * OMEGA * RD / RADIUS ** 2) /
     *              (1.0 + EXP (XDUM))
     *            - (1.0 + OMEGA * (RD / RADIUS) ** 2) /
     *              (1.0 + EXP (XDUM)) ** 2.0 *
     *              EXP (XDUM) / SKINDP ) / RD / CNORM
      ELSE
      DRHO        = (2.0 * OMEGA / RADIUS ** 2) / (1.0 + EXP (XDUM))
      DRHO        = DRHO / CNORM
      ENDIF
C
      VC  (JR)  = -IA / PMASS * (I + ALPHAA) / 2.0 * SIGMAA
     *            * KZ * RHO (JR)
      VSO (JR)  = -IA / PMASS * (I + ALPHAC) / 2.0 * SIGMAC
     *            * DRHO / 2.0 / PMASS
C
  80  CONTINUE
C
```

```
C         FIX UP THE BEHAVIOR NEAR THE ORIGIN (LINEAR FIT)
C
      DO 90 IF  = 0, NFIX-1
      VSO (IF)  = VSO (NFIX)
     *            + FLOAT (NFIX-IF) * (VSO (NFIX) - VSO (NFIX+1))
  90  CONTINUE
C
      RETURN
      ENDIF
C
      IF (IDIST .EQ. 3) THEN
C
C         ALTERNATE PARAMETER SET FOR CALCIUM POTENTIAL
C         ENERGY RANGE FOR THIS POTENTIAL
C
      DE        = (TF - 400.0) / 400.0
      A13       = REAL (IA) ** (1.0/3.0)
C
      IF (TF .GT. 1040.0) GOTO 40
      IF (IA .NE. 40) STOP ' IDIST = 3 ONLY FOR IA = 40 '
C
C         VECTOR POTENTIAL PARAMETERS
C
      CVR       = 0.6861 - 0.1618 * DE - 0.0144 * DE * DE
      RVR       = 1.0600
      AVR       = 0.5817
      CVI       = 0.5030 + 0.3274 * DE - 0.0739 * DE * DE
      RVI       = 1.1658 - 0.0882 * DE - 0.0224 * DE * DE
      AVI       = 0.4861 + 0.0603 * DE + 0.0205 * DE * DE
C
C          SCALAR POTENTIAL PARAMETERS
C
      CSR       = 0.6987 - 0.0506 * DE - 0.0336 * DE * DE
      RSR       = 1.0672
      ASR       = 0.6111
      CSI       = 0.3212 + 0.2613 * DE + 0.0969 * DE * DE
      RSI       = 1.2019 - 0.1026 * DE - 0.0681 * DE * DE
      ASI       = 0.4204 + 0.0926 * DE + 0.0282 * DE * DE
C
C          SCALE FACTORS
C
      CVR       = CVR * ( 300.0)
      CVI       = CVI * (-100.0)
      RVR       = RVR / HC
      AVR       = AVR / HC
      RVI       = RVI / HC
      AVI       = AVI / HC
C
      CSR       = CSR * (-400.0)
      CSI       = CSI * ( 100.0)
      RSR       = RSR / HC
      ASR       = ASR / HC
      RSI       = RSI / HC
      ASI       = ASI / HC
```

```
C
C         R-INDEPENDENT EXPONENTIALS
C
      E1VR       = EXP (-RVR * A13 / AVR)
      E1VI       = EXP (-RVI * A13 / AVI)
      E1SR       = EXP (-RSR * A13 / ASR)
      E1SI       = EXP (-RSI * A13 / ASI)
C
      DO 100 JR = 0, NRV+1
C
C         R-DEPENDENT EXPONENTIALS
C
      RD         = JR * DRV
C
      E2VR       = EXP (RD / AVR)
      E2VI       = EXP (RD / AVI)
      E2SR       = EXP (RD / ASR)
      E2SI       = EXP (RD / ASI)
C
C         RADIAL DEPENDENCE OF VECTOR/SCALAR REAL/IMAG PARTS
C
      FVR        = (1.0 + E1VR * E2VR) ** (-1.0)
     *           * (1.0 + E1VR / E2VR) ** (-1.0)
      FSR        = (1.0 + E1SR * E2SR) ** (-1.0)
     *           * (1.0 + E1SR / E2SR) ** (-1.0)
      FVI        = (1.0 + E1VI * E2VI) ** (-1.0)
     *           * (1.0 + E1VI / E2VI) ** (-1.0)
      FSI        = (1.0 + E1SI * E2SI) ** (-1.0)
     *           * (1.0 + E1SI / E2SI) ** (-1.0)
C
C         DERIVATIVE TERM FOR SPIN-ORBIT POTENTIAL
C
      IF (RD .EQ. 0.0) THEN
C
      DFVR       = -2.0 * FVR / AVR / AVR * E1VR / (1.0 + E1VR) ** 2
      DFVI       = -2.0 * FVI / AVI / AVI * E1VI / (1.0 + E1VI) ** 2
      DFSR       = -2.0 * FSR / ASR / ASR * E1SR / (1.0 + E1SR) ** 2
      DFSI       = -2.0 * FSI / ASI / ASI * E1SI / (1.0 + E1SI) ** 2
C
      ELSE
C
      DFVR       =(E1VR / E2VR / (1.0 + E1VR / E2VR)
     *           - E1VR * E2VR / (1.0 + E1VR * E2VR))
     *           * FVR / AVR / RD
      DFVI       =(E1VI / E2VI / (1.0 + E1VI / E2VI)
     *           - E1VI * E2VI / (1.0 + E1VI * E2VI))
     *           * FVI / AVI / RD
      DFSR       =(E1SR / E2SR / (1.0 + E1SR / E2SR)
     *           - E1SR * E2SR / (1.0 + E1SR * E2SR))
     *           * FSR / ASR / RD
      DFSI       =(E1SI / E2SI / (1.0 + E1SI / E2SI)
     *           - E1SI * E2SI / (1.0 + E1SI * E2SI))
     *           * FSI / ASI / RD
C
```

```
      ENDIF
C
C        VECTOR AND SCALAR POTENTIALS
C
      VV        = CVR * FVR + I * CVI * FVI
      VS        = CSR * FSR + I * CSI * FSI
C
C        SWITCH OVER TO CENTRAL/SPIN ORBIT DESCRIPTION
C
      VC  (JR) = VS + E/PMASS * VV + (VS*VS - VV*VV) / (2.0*PMASS)
      VSO (JR) = 1.0 / (2.0 * PMASS * (E + PMASS + VS - VV) )
     *           * (CVR*DFVR + I*CVI*DFVI - CSR*DFSR - I*CSI*DFSI)
C
 100  CONTINUE
      RETURN
      ENDIF
C
      STOP ' OOPS, IDIST OUT OF RANGE '
      END
```

References

[1] See, for example, Table 4.2.

[2] A. Picklesimer, J.W. Van Orden, and S.J. Wallace, Phys. Rev. **C32**, 1312 (1985).

[3] A.H. Mueller in *Proceedings of the Seventeenth Rencontre de Moriund on Elementary Particle Physics*, Les Arcs, France, 1982, ed. J. Tran Thanh Van (Editions Frontieres, Gif-sur-Yvette, France, 1982), and S.J. Brodsky in *Proceedings of the Thirteenth International Symposium on Multiparticle Dynamics*, Volendam, The Netherlands, ed. W. Kittel *et al* (World Scientific, Singapore, 1983).

[4] G. Bertsch *et al*, Phys. Rev. Lett. **47**, 197 (1981).

[5] D.J. Gross and F. Wilczek, Phys. Rev. Lett. **30**, 1343 (1973) and H.D. Politzer, Phys. Rev. Lett. **30**, 1346 (1973).

[6] G.P. LePage and S.J. Brodsky, Phys. Rev. **D22**, 2157 (1980).

[7] S.J. Brodsky and G.R. Farrar, Phys. Rev. Lett. **31**, 1153 (1973).

[8] R.G. Arnold *et al*, Phys. Rev. Lett. **57**, 174 (1976).

[9] G.R. Farrar *et al*, Phys. Rev. Lett. **61**, 686 (1988).

[10] Particle Data Group, Phys. Lett. **B231**, 1 (1990), page III.82.

[11] M.A. Preston and R.K. Bhaduri, *Structure of the Nucleus* (Addision-Wesley, Reading, MA, 1975), pp. 193-4.

[12] R.C. Barrett and D.F. Jackson, *Nuclear Sizes and Structure* (Clarendon Press, Oxford, 1977).

[13] F.E. Low, Phys. Rev. **D12**, 163 (1975).

[14] A.S. Carroll *et al*, Phys. Rev. Lett. **61**, 1698 (1988).

[15] J.P. Ralston and B. Pire, Phys. Rev. Lett. **61**, 1823 (1988).

[16] S.J. Brodsky and G.F. de Teramond, Phys. Rev. Lett. **60**, 1924 (1988).

[17] R.G. Milner, Caltech Preprint OAP-684, March 1988.

[18] A. Picklesimer, J.W. Van Orden, and S.J. Wallace, Phys. Rev. **C32**, 1312 (1985).

[19] T.W. Donnelly in *Proceedings of Workshop on Perspecitves in Nuclear Physics at Intermediate Energies*, Boulder, CO 1958, ed. S. Boffi *et al* (World Scientific, Trieste, 1984); T.W. Donnelly and J.D. Walecka, Ann. Rev. Nucl. Sci. **25**, 329 (1975).

[20] C.J. Horowitz and B.D. Serot, Nucl. Phys. **A368**, 503 (1981), B.C. Clark *et al*, Phys. Rev. Lett. **50**, 1644 (1983), and S. Frullani and J. Mougey, Adv. in Nucl. Phys. **14**, 1 (1984).

[21] E.D. Cooper *et al*, Phys. Rev. **C36**, 2170 (1987).

[22] D.L. Pham and R. De Swiniarsky, Nuovo. Cim. **103**, 375 (1990).

[23] S. Hama *et al*, Phys. Rev. **C41**, 2737 (1990).

[24] R.D. Amado, J. Piekarewicz, D.A. Sparrow, and J.A. McNeil, Phys. Rev. **C28**, 1663 (1983).

[25] R.J. Glauber in *Lectures in Theoretical Physics*, Boulder, CO 1958, ed. W.E. Brittin *et al* (Interscience, New York, 1958).

[26] I note that this detail has been overlooked in the literature, C.J. Horowitz and M.J. Iqbal, Phys. Rev. **C33**, 2059 (1986), Equation 4.

[28] E. Kiritsis and R. Seki, Phys. Rev. Lett. **63**, 953 (1989).

[29] R.J. Furnstahl, C.E. Price, and G.E. Walker, Phys. Rev. **C36**, 2590 (1987).

[30] B.D. Serot and J.D. Walecka, Adv. in Nucl. Phys. **16**, 1 (1986).

[31] D.A. Wasson, *Ph.D. Thesis*, Caltech, 1990.

[32] B.C. Clark *et al*, Phys. Rev. Lett. **50**, 1644 (1983).

[33] Z.E. Meziani *et al*, Phys. Rev. Lett. **52**, 2130 (1984); G.D. Dang and N.V. Giai, Phys. Rev. **C30**, 731 (1984).

[34] See, for example, the optical potential derived in Appendix B.

[35] J.D. Jackson, *Classical Electrodynamics* (John Wiley & Sons, New York, 1962), page 98.

[36] S.E. Koonin, *Computational Physics* (Benjamin-Cummings, Menlo Park, 1986). Gaussian weights and abcissas were taken from M. Abramowitz and I. Stegun, *Handbook of Mathematical Functions* (Dover, New York, 1969), page 98.

[37] J. Bystricky, F. Lehar, and P. Winternitz, Journal de Physique **39**, 1 (1978).

[38] E. Kujawski and J.P. Vary, Phys. Rev. **C12**, 1271 (1975).

[39] C. Ohomori *et al*, Phys. Lett. **B230**, 27 (1989).

[40] H. Feshbach, Ann. Phys. **5**, 357 (1955).